Study of granular temperature in dense fluidized beds by diffusing wave spectroscopy

A Thesis Submitted for the Degree of Doctor of Philosophy

by

Vladimir Zivkovic

School of Engineering and Electronics
The University of Edinburgh
Edinburgh June 2009

Abstract

Diffusing wave spectroscopy (DWS), a non-intrusive multiple scattering technique, can be used to study the fundamentals of particle motion in dynamic dense granular media and measure the mean of the square of the particle velocity fluctuations about their mean, which is related directly to the so-called 'granular temperature' that underpins many theories for dynamic granular processes. An overview of DWS in the context of other techniques for studying the granular temperature and dynamics of particles in granular systems, and its application to a range of fluidized bed configurations is reported in this thesis.

The thesis reports how the granular temperature and particle dynamics varies with the level of forcing for a liquid fluidized bed, and both dry and water-immersed vibro-fluidized beds. This data reveals that the granular temperature scales with, and is of the same order as, the forcing velocity (i.e. superficial velocity or peak vibrational velocity) for all except the water-immersed vibro-fluidized bed where it scales with the peak acceleration. The former appear to be in accord with theory, while no theory as yet has predicted the latter. The experimental data was also deconvoluted to reveal how the solid fraction affects the granular temperature in a liquid fluidized bed, which represents the most detailed experimental study in this regard. For the first time is revealed that vertical profiles of the granular temperature are a consequence of observed concentration stratification in a liquid fluidized bed. By way of example of the results that can be obtained using DWS, we have shown how it has provided a basis for us to hypothesise that particles in vibro-fluidized beds (both dry and water-immersed) rattle around in cages formed by their neighbours until their collective re-arrangement occurs at long time scales.

Declaration

The work presented in this thesis was carried out in the School of Engineering and Electronics, the University of Edinburgh, between September 2005 and March 2009. It is the original work of the author except acknowledged otherwise in the text. The present document has not been submitted for any other degree or professional qualification.

Vladimir Zivkovic

June 2009

Acknowledgement

I would like to thank my supervisors, Dr Don Glass and Professor Mark Biggs, for giving me the opportunity to work in their group, supporting and leading me through my PhD study. I would like to thank them for all their understanding, patience and kindness.

Thanks to all past and present members of the group, especially Dr Alex Buts, Dr Paolo Pagliai and Dr Yassir T. Makkawi for all their help, all the useful discussions and support during the past years. Thanks also to Dr Georgios Petekidis (IESL-FORTH, Crete) for practical introduction to the DWS technique.

I would also like to thank my family in Serbia and Germany, as well as all my friends for all their love and encouragement. Special thanks to Milan, Jovana and Tijana for all their patience and support.

At the end, I would like to thank the Engineering and Physical Sciences Research Council (EPSRC), UK and University of Edinburgh (Principal’s Scholarships) for financial support.

Table of Contents

List of Figures

List of Tables

Nomenclature

A	Amplitude of vibration, m
a_p	Vibrational acceleration, m s^{-2}
A_r	Cross sectional area of bed, m^2
$C_{ext}(t)$	External torque, N m
$C_{ext}(\omega)$	Fourier transform of $C_{ext}(t)$, N m s^{-1}
D	Diffusion coefficient of scatterers, m^2 s^{-1}
D_l	Diffusion coefficient of the light, m^2 s^{-1}
d_p	Particle diameter, m
$E(t)$	Electric field of light, V m^{-1}
$E^*(t)$	Complex conjugate of $E(t)$, V m^{-1}
$f(\phi)$	Function proposed by Batchelor, dimensionless
f	Frequency, Hz
f_d	Frequency of Doppler signal burst, Hz
f_l	Frequency of light, Hz
f_r	Resonant frequency, Hz
g	Gravity acceleration, m s^{-2}
$g_1(t)$	Electric field autocorrelation function (FACF), dimensionless
$g_2(t)$	Intensity autocorrelation function (IACF), dimensionless
Ga	Galileo number, dimensionless

h	Height of bed, m
h_w	Water level height in bed, m
$I(t)$	Intensity of the light, PMT counts/second
$<I>$	Average intensity of light at the detector, PMT counts/second
$<I_p>$	Average intensity of light that has travelled along a light path p, PMT counts/second
$I(L)$	Transmitted light intensity, W
J	Flux of photons, s^{-1} m^{-2}
k_0	Wavevector of the light, m^{-1}
l	Scattering mean free path, m
ΔL	Length of a streak line, m
L	Thickness of sample, m
l^*	Transport mean free path, m
l_R^*	Transport mean free path of reference sample, m
l_a	Absorption length, m
l_{aR}	Absorption length of reference sample, m
m_p	Mass of particles, kg
n	Richardson-Zaki equation parameter
n_c	Number of scattering steps, dimensionless
$P(s)$	Light path probability function, dimensionless
R	Reflection coefficient, dimensionless

$r_0(t)$	Position vector of source, m
$<\Delta r^2(t)>$	Mean square displacement, m^2
R^2	Coefficient of determination, dimensionless
Re	Reynolds number, dimensionless
Re_t	Terminal Reynolds number, dimensionless
$r_i(t)$	Position vector of i^{th} particle, m
Δs	Length scale of DWS measurement, m
$s(t)$	Length of a light path, m
$<s>$	Average light path length, m
$S(\omega)$	Noise power spectral density, $rad^2\ Hz^{-1}$
St	Stokes number, dimensionless
Δt	Time delay; camera exposure time, s
t	Time, s
$T(L)$	Transmission of light through sample, dimensionless
t_{dec}	Estimated decorrelation time, s
T_{eff}	Effective temperature, K
$T_R(L)$	Transmission of light through reference sample, dimensionless
U	Energy density of light, $J\ m^{-3}$
U_0	Superficial velocity, $m\ s^{-1}$
U_{mf}	Minimum fluidization velocity, $m\ s^{-1}$

U_{sv}	Mean slip velocity, m s^{-1}
U_t	Terminal particle velocity, m s^{-1}
v	Velocity of particle, m s^{-1}
δv	Fluctuating particle velocity, m s^{-1}
$<v>$	Mean particle velocity, m s^{-1}
$<\delta v^2>$	Square of the fluctuating velocity, m^2 s^{-2}
$<\delta v^2>^{1/2}$	Experimental particle velocity fluctuation, m s^{-1}
v_l	Speed of light, m s^{-1}
v_p	Peak vibrational velocity, m s^{-1}
v_x	Particle velocity in one direction, m s^{-1}
W	Fluidized bed width, m
Δx	Distance in one dimension, m
x	Horizontal distance, m
y	Vertical distance, m
y_p	Vertical position of vibrational piston, m

Greek letters

β	Constant in Siegert relation, dimensionless
β_R	Reflection parameter, dimensionless
$\chi(\omega)$	Complex susceptibility, rad N^{-1} m^{-1}

δ_f	Fringe spacing, m
ε	Bed voidage, dimensionless
$<\varepsilon>$	Mean bed voidage, dimensionless
ϕ	Solid volume fraction, dimensionless
$\mathit{\Gamma}$	Non-dimensional vibrational acceleration, dimensionless
γ	Scaling factor, dimensionless
φ	Half angle between crossing laser beams, rad
$\varphi(t)$	Angular deflection, rad s^{-1}
$\varphi(\omega)$	Fourier transform of $\theta(t)$, rad s^{-2}
λ	Light wavelength, m
μ	Fluid viscosity, N s m^{-2}
θ	Granular temperature, m^2 s^{-2}
$\mathit{\Delta}\theta_p(t)$	Change in the phase of the light on a light path p, rad
$\theta(t)$	Phase of the light, rad
ρ_f	Fluid density, kg m^{-3}
ρ_p	Particle density, kg m^{-3}
τ_c	Time between particle collisions, s

τ_{dws}	Decorrelation time, s
ω	Angular frequency, rad s^{-1}

List of publication produced from this Thesis

Refereed journal publications in print

1. V. Zivkovic, M. J. Biggs, D. H. Glass, P. Pagliai and A. Buts, Particle dynamics in a dense vibrated fluidized bed as revealed by diffusing wave spectroscopy, *Powder Technology*, 182, 192-201, 2008.
2. V. Zivkovic, M. J. Biggs, D. Glass, P. Pagliai and A. Buts, Granular temperature in a liquid fluidized bed as revealed by diffusing wave spectroscopy. *Chemical Engineering Science*, 64, 1102-1110, 2009.
3. V. Zivkovic, M. J. Biggs, D. Glass and L. Xie, Particle dynamics and granular temperatures in dense fluidized beds as revealed by diffusing wave spectroscopy. *Advanced Powder Technology*, 20, 227-233, 2009.

Conference proceedings

4. M. J. Biggs, V. Zivkovic, D. H. Glass, P. Pagliai and A. Buts, Particle dynamics and granular temperatures in dense fluidized beds as revealed by multiple light scattering techniques, *Proceedings of Chemeca 2008–36th Australasian Chemical Engineering Conference*, Paper #117, 10 pp.

Publications in preparation

5. V. Zivkovic, M. J. Biggs, D. Glass, Granular temperature in a dense water-immersed vibrated bed as revealed by diffusing wave spectroscopy, submitted to *Journal of Physics D.*

Chapter 1 Introduction

1.1 Motivation

Granular materials are ubiquitous in our daily lives. Examples of granular materials are all powders, including rice, salt, sugar, coffee, breakfast cereal, pharmaceutical pills, sand, coal and ball bearings. Almost everything that we eat originated in a granular form. Moreover, they play an important role in many industries, such as chemicals, pharmaceuticals, food processing, mining, agricultural, construction and energy production. The impact of particulate products to the US economy is estimated to be 1 trillion US dollars [1]. Losses of capacity in many industrial plants because of problems with the transport of these materials can be reduced with improvement in our understanding of granular material behaviour. In addition, granular materials are clearly important for geological processes such as landslides, erosion/deposition processes, soil response to seismic events, dune migration and coastal geomorphology. Besides these mundane and terrestrial examples, interstellar dust and planetary rings are examples of granular materials in an astrophysical context.

Dynamic granular materials involve a large collection of discrete solid particles that move relative to each other under external forcing such as shearing, vibration or interstitial fluid flow. This continuous supply of energy is necessary to maintain dynamic granular materials because of inelastic particle-particle and particle-surface collisions that lead to rapid dissipation of the kinetic energy of the particles. Once the external energy supply is stopped, dynamic granular materials get stuck in a solid or glassy configuration, and relative motion will come very rapidly to a virtual or complete halt. In consequence, granular materials demonstrate a rich and complex set of behaviour as they can mimic gas, liquid, solid or glassy behaviour depending on the applied external forcing [2]. From the theoretical point of view, granular dynamics represents a fascinating crossroads of fluid dynamics, nonequilibrium statistical mechanics, complex fluid rheology and the theory of pattern formation [3]. Therefore, it is not strange that the study of granular materials has moved from its previous home in civil and chemical engineering to the forefront of physics, applied mathematics and other disciplines in recent years [4]. Further, there is theoretical and observational evidence that asteroids and comets are not cohesive masses of ice, rock and/or metal but instead a conglomeration of particles that range in size from micrometer-sized dust to kilometre-sized boulders, making granular dynamics relevant in explaining the evolution of asteroids and comets or the growth process of the early Solar System [5]. These facts demonstrate that the scope of granular dynamics is broad and significant in various scientific disciplines.

The dominant mechanism affecting the flow behaviour of granular materials is the random motion of particles resulting from interactive collisions between them. This random motion of particles is quantified by the so-called granular temperature, a quantity first formally defined by Ogawa [6]. The velocity of the particle at any instant in time, v, invariably differs from the average velocity of the particles around it, $<v>$. The fluctuating (or peculiar) velocity of a particle is defined as a difference of these two velocities

$$\delta v = v - \langle v \rangle \tag{1.1}$$

It is practical to define the average of the square of the fluctuating velocity as a measure of the velocity fluctuations. Therefore, it is common to define the granular temperature for a monodisperse three dimensional granular material as

$$\theta = \frac{1}{3}\left\langle \delta v^2 \right\rangle \tag{1.2}$$

This quantity has long underpinned kinetic theories of granular flows (e.g. [7-10]), while it is also playing an increasing role in other contexts such as heat transfer [11], segregation [12], erosion [13], attrition [14] and aggregation [4, 15] in various particle processing technologies. The validation of these theories demands experimental elucidation of the particle dynamics in general and the determination of granular temperature in particular.

Experimental work in granular materials is well known for the problems it causes to the experimenter [4]. It is, therefore, not surprising that many theories in this field are compared to the results of numerical simulations rather than experiment. Obviously, experimental work can not be substituted completely by computational predictions and it is important to acquire more experimental data, particularly granular temperature, to validate theories such as those mentioned above. The main objective of this project is therefore, the study of particle dynamics in general and granular temperature in particular for various dense granular systems. The multiple light scattering technique of diffusing wave spectroscopy has been applied extensively to a variety of dense fluidized bed systems to measure granular temperature. The experimental data obtained is used to validate different theoretical and simulation models. Moreover, some interesting features of glassy dynamics, such as caging dynamics and the jamming transition, are observed and discussed in the thesis.

1.2 Outline of thesis

This thesis presents work using diffusing wave spectroscopy (DWS), a non-intrusive technique, to study experimentally the particle dynamics and granular temperature in a liquid fluidized bed and both dry and slurry vibrated beds. This thesis is organized as follows:

Chapter 2 presents a general introduction of experimental techniques used for granular temperature measurements. Several intrusive and non-intrusive experimental methods are summarized and their advantages and disadvantages are discussed.

Chapter 3 presents a general introduction to the theoretical fundamentals of dynamic light scattering theory. Based on two fundamental approximations, diffusing wave spectroscopy theory and its experimental configurations are introduced. A four-step data analysis process for obtaining the granular temperature is presented and discussed. Further, an overview of the static transmission method for measuring two key parameters, the transport mean free path l^* and the absorption length l_a, is given.

Chapter 4 reports granular temperature and solid fraction measurement results in a thin rectangular three-dimensional rectangular water fluidized bed of 165 μm glass particles. The granular temperature is studied at various heights above the distributor and across the bed width for a wide range of superficial velocities. The experimental data show that the fluctuating velocity is the same order as the superficial velocity and that it may be described solely in terms of the solid volume fraction, ϕ. Results are in accord with both theoretical descriptions and numerical simulation results of others.

Chapter 5 presents granular temperature data and long-time dynamics of mono-disperse 950 μm glass particles in a three-dimensional dense granular bed subject to vertical sinusoidal vibrations over a wide range of vibrational conditions and height above the base of the bed. The granular temperature of the particles was found to scale with the square of the peak vibrational velocity in line with current kinetic theories.

Chapter 6 reports granular temperature data as a function of the vibrational conditions and height above the base of the bed in a dense three-dimensional water-immersed vibro-fluidized bed of 475 μm glass particles. The experimental results show some interesting similarities and interesting differences in granular dynamics between dry and water-immersed vibro-fluidized beds. One of the primary differences is observation that the granular temperature scales with the square of the vibrational acceleration in contrast with a dry vibro-fluidized bed scaling, a result not predicted by current theories.

Finally, Chapter 7 summarizes the work undertaken through the thesis and outline future work.

References

1. Rhodes, M., *Introduction to Particle Technology*. 2nd ed. 2008, Chichester: John Wiley & Sons Ltd.
2. Jaeger, H.M., S.R. Nagel, and R.P. Behringer, *Granular solids, liquids, and gases.* Reviews of Modern Physics, 1996. **68**(4): p. 1259-1273.
3. Aranson, I.S. and L.S. Tsimring, *Patterns and collective behavior in granular media: Theoretical concepts.* Reviews of Modern Physics, 2006. **78**(2): p. 641-692.
4. Goldhirsch, I., *Rapid granular flow.* Annual Review of Fluid Mechanics, 2003. **35**: p. 267-293.
5. Kadish, J., E. Rougier, A. Munjiza, and J.R. Barber, *Granular temperature as an energy dissipation mechanism in bodies of the Solar System.* Proceedings of the Royal Society A, 2007. **463**(2086): p. 2485-2493.
6. Ogawa, S. *Multitemperature theory of granular materials*. in *Proceedings of the US-Japan seminar on continuum mechanical and statistical approaches in the mechanics of granular materials*. 1978. Sendai, Japan: Gakajutsu Bunken Fukyu-Kai: Tokyo, Japan.
7. Jenkins, J.T. and S.B. Savage, *A theory for the rapid flow of identical, smooth, nearly elastic, spherical-particles.* Journal of Fluid Mechanics, 1983. **130**: p. 187-202.
8. Lun, C.K.K. and S.B. Savage, *A simple kinetic theory for granular flow of rough, inelastic, spherical particles.* Journal of Applied Mechanics, 1987. **54**: p. 47-53.
9. Brey, J.J., J.W. Dufty, C.S. Kim, and A. Santos, *Hydrodynamics for granular flow at low density.* Physical Review E, 1998. **58**(4): p. 4638-4653.
10. Sela, N. and I. Goldhirsch, *Hydrodynamic equations for rapid flows of smooth inelastic spheres, to Burnett order.* Journal of Fluid Mechanics, 1998. **361**: p. 41-74.
11. Hunt, M.L., *Discrete element simulations for granular material flows: Effective thermal conductivity and self-diffusivity.* International Journal of Heat and Mass Transfer, 1997. **40**(13): p. 3059-3068.
12. Yang, S.C., *Density effect on mixing and segregation processes in a vibrated binary granular mixture.* Powder Technology, 2006. **164**: p. 65-74.
13. Lyczkowski, R.W. and J.X. Bouillard, *State-of-the-art review of erosion modeling in fluid/solids systems.* Progress in Energy and Combustion Science, 2002. **28**(6): p. 543-602.
14. Campbell, C.S., *Impulse strengths in rapid granular shear flows.* Acta Mechanica, 1994. **104**(1-2): p. 65-90.
15. Tan, H.S., M.J.V. Goldschmidt, R. Boerefijn, M.J. Hounslow, A.D. Salman, and J.A.M. Kuipers, *Building population balance model for fluidized bed melt granulation: lessons from kinetic theory of granular flow.* Powder Technology, 2004. **142**(2-3): p. 103-109.

Chapter 2 Overview of granular temperature measurement techniques

2.1 Introduction

Although the temperature of a fluid can be measured easily using a thermometer, granular temperature measurement is not trivial as there is no known granular thermometer [1]. Therefore, considerable research has been undertaken over the past 15 years and more aimed at developing experimental techniques for its measurement. In principle, the methods used to study granular flows can be divided into two groups: intrusive and non-intrusive techniques. Non-intrusive measurement techniques, which determine properties inside granular flow systems by means of instruments located outside, are highly desirable since in this case the measurement does not interfere with the flow [2]. However, the application of these techniques for measurement of granular temperature is very difficult or even impossible in some cases, especially in many industrial contexts because of the typical dimensions of industrial devices. One possible way to extend the application of these methods is to combine them with intrusive methods, using intrusive probes, for example fiber-optical probes, to obtain experimental data in the interior of large experimental equipment [2]. As this work is primarily focused on experimental measurements of granular temperature in laboratory scale dense fluidized beds, techniques for measurement of the particle velocity and the particle velocity fluctuations in academic research are reviewed here.

2.2 Intrusive techniques

2.2.1 Optical fiber probe technique

The measuring principle of the optical fiber probe technique for determination of local particle motion is detecting reflected light from a single particle in the vicinity of two parallel arranged backscatter (reflective type) sensors placed at a known distance, Δx apart [3, 4]. Figure 2.1 represents a head-on view of a typical probe where the thick solid line represents the trajectory of a particle moving longitudinally. The particle passing by each detector successively produces two similar bell-shaped signals with the difference of only a shift in time. The time delay, Δt, is usually obtained by cross-correlating both signals [3-10], but the peak-to-peak detection technique can be used too [11]. This enables computation of the time-averaged magnitude of the particle velocity vector, although only in one dimension

$$v_x = \frac{\Delta x}{\Delta t} \tag{2.1}$$

Due to random motion of the granular particles in all directions, the one dimensional velocity measurements may often lead to misleading views of the actual phenomena. [4]. This shortcoming can be partially resolved by using a multi-fiber optical probe which enables the velocity vector to be resolved in two dimensions [3, 4] for the plane perpendicular to the probe. The main drawback of this technique is its intrusive nature, but careful design of the probes provides little interference to the granular flow. The technique is only directly applicable in dilute granular flows, while for dense systems the use of tracer particles is necessary [4] which makes statistical processing of the data even more complex and tedious. Another disadvantage is the necessity of calibration. Investigators have employed different calibration procedures such as laser Doppler velocimetry [3], a rotating disk [4-9, 11] or a gravity driven flow [9, 10]. Nevertheless, optical fiber probes are quite popular because they are simple, yield high signal-transmission-to-noise ratios and are also relatively cheap.

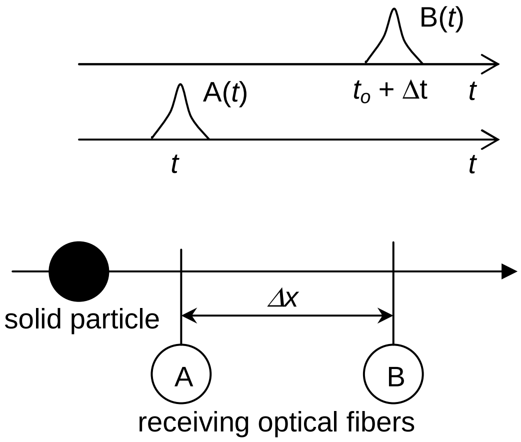

Figure 2.1. Principle of the optical fibre probe technique.

Experimental data obtained by fiber probe measurements provides a basis for calculating the fluctuating velocity by simple statistical procedures. A set of instantaneous particle velocities can be obtained by identifying the peaks in the two signals from the optical sensors corresponding to the passage of an individual particle. By averaging these instantaneous velocities, the ensemble average velocity, $<v>$, and the ensemble-average of the square of the fluctuating velocity, $<\delta v^2>$, can be determined. The analysis described above was used in the early 1990s to measure streamwise velocity fluctuations in three dimensional chute flows [5, 6]. This can be considered as some measure of granular temperature but it only represents one component of the velocity fluctuations. The same velocity distribution method was used for obtaining the velocity fluctuations in a partially filled rotating cylinder [8].

On the other hand, recent studies do not report fluctuating velocity data probably because of the tediousness of the statistical procedure required to obtain it. It can be anticipated that developments in the use of multi-fiber optical probes and the peak-to-peak detection technique should provide improvements to the above described restrictions of methodologies to obtain granular temperature.

2.2.2 Mechanical Spectroscopy

The fluctuation-dissipation theorem [12] provides a fundamental link between two small deviations from thermodynamic equilibrium – the fluctuations of an observable variable in a system at equilibrium and the response function of that observable variable to an external perturbation in its field. Therefore, the effective temperature, T_{eff}, in a simple liquid can be obtained by measuring both the free (fluctuations) and forced (response function) oscillations of an immersed rigid torsion oscillator probe [13]. In the absence of the external torque ($C_{ext}(t) = 0$), the immersed oscillator probe performs an irregular free angular motion, induced by the continuous interaction of the particles with the probe. These fluctuations are defined by the noise power spectral density, $S(\omega)$ obtained from time-series of the angular deflections, $\varphi(t)$. The angular deflections $\varphi(t)$ are detected optically using a mirror fixed on the probe. The complex susceptibility, $\chi(\omega) = \chi'(\omega) - i\chi''(\omega)$, defines the linear response to an externally applied sinusoidal torque $C_{ext}(t) = C_e \sin(\omega t)$. The susceptibility is obtained from $\chi(\omega) = \varphi(\omega) / C_{ext}(\omega)$, where $\varphi(\omega)$ and $C_{ext}(\omega)$ are the Fourier transforms of $\varphi(t)$ and $C_{ext}(t)$ respectively. The effective temperature is defined by the ratio of the noise and the imaginary part of complex susceptibility, $\chi''(\omega)$ [12]

$$\frac{S(\omega)\omega}{4\chi''(\omega)} = k_B T_{eff} \tag{2.2}$$

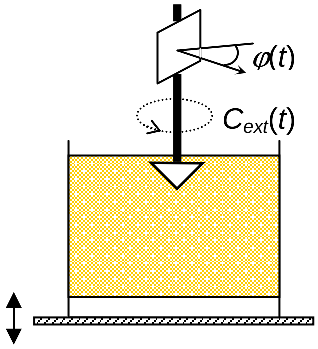

Figure 2.2. Schematic of the torsion oscillator immersed in ‘granular bath’ with mirror fixed on the probe for the angular deflection measurements, $\varphi(t)$. For susceptibility measurements, an external torque $Cext(t)$ can be applied using a permanent magnet fixed on the oscillator and two external coils.

Surprisingly, Mayor and co-workers [13-15] found that this standard equilibrium statistical mechanical relation can be applied to vibro-fluidized granular matter for granular temperature measurement. Therefore, driven granular matter can be considered as a macroscopic ‘thermal bath’ (Figure 2.2), although the analogy is only formal as the granular medium is never in equilibrium in the thermodynamic sense, rather it forms a nonequilibrium steady state. Mechanical spectroscopy is not restricted to dilute systems (applicable in highly dense systems) which is the main asset of the method. However, the main problem of this approach is that the measurements are sensitive to shape and surface roughness of the measuring device, indicating complications that do not occur in simple fluids composed of molecules. Further, the theoretical considerations of Srebro and Levin [16] showed that although the fluctuation-dissipation relation holds, the effective temperature is different from the granular temperature. Thus, more experimental work (in various granular systems) and more theoretical work are necessary in establishing this method. Nonetheless, the measured effective temperature is the same order of magnitude as the mean kinetic energy per particle measured by other methods [13-15].

2.3 Non-intrusive techniques

2.3.1 Particle video imaging techniques

Particle video image processing techniques are the most widely used non-intrusive methods in the study of granular flow. The main asset of these techniques is their whole field nature as they provide velocities across a whole plane in the system at any instant, unlike point measurement techniques. However, the main shortcoming of these techniques is that, even for granular suspensions with a solid fraction greater than a few percent, the optical depth is of the order of a few particle diameters within the bulk. Therefore, image analysis methods are limited to studies of two-dimensional or dilute three-dimensional granular systems. In dense systems their application is restricted to near-wall region studies. Technically, there are basically two primary approaches: recording the long-term trajectories of the particles as they move about the domain (particle tracking velocimetry) or registering particle displacement over short time intervals (particle streak photography and particle image velocimetry).

2.3.1.1 Particle tracking velocimetry (PTV)

PTV has been applied for granular temperature measurements in various granular systems: chute flow [17, 18], vibro-fluidized beds [19-25], sheared granular flow [26, 27], granular flow down inclined planes [28-33] and liquid fluidized beds [34, 35]. In this technique, granular flow is recorded using high speed cameras (in some studies more than 1000 frames per second). The recorded movies are analysed frame by frame to reconstruct long-term trajectories of individual particles by matching particle positions at each successive frame of the movie. Various image analysis methods have been used to obtain the particle position on each frame, such as centroid [17, 20, 23, 28, 30], Hough transform [19, 21], Voronoï imaging [29, 31-35] and autocorrelation analysis method [18, 24, 26, 27]. In the autocorrelation method, use of a subset of coloured tracer particles is necessary which decreases the resolution of the technique. Once the image processing is completed, the particle coordinates form the input to particle-tracking routines which calculate the velocities of particles in all frames.

Granular temperature is computed directly from velocity distribution functions obtained using (usually) the ensemble averaging approach as described in section 2.1.1. [17, 18, 23-29, 31-35] or by fitting it with the Maxwell distribution [19]. Another, more robust, method suitable for granular temperature determination in denser systems is analysis of measured mean square displacement on a short time scale [20-22, 30]. This approach obviates the need for reliable detection of all the collision events. Finally, Spinewine et al. [35] employed a stereoscopic imaging technique using two synchronized cameras and Voronoï tessellation image processing for three-dimensional particle tracking in a liquid fluidized bed. This powerful fluid dynamics technique (3D PTV) enables measurement of all three components of the velocity fluctuations rather than two as in its two-dimensional counterparts employed in all the other studies cited above.

2.3.1.2 Particle streak photography

Gidaspow and collaborators have used the particle streak photography technique to measure granular temperature in circulating [36-40], liquid [38, 41] and gas fluidized beds [42]. In this technique, by exposing particles for a longer camera exposure time , Δt, image streak lines are captured as shown in Figure 2.3. The exposure time (typically of the order of ms) must be carefully selected to obtain a sufficient displacement, but not so large that the particles move out of the field of view. These streak lines represent the distance travelled by the particles in the specified exposure time of the camera. A rotating, coloured transparent disc in front of the light source can be used to determine the direction of flow [39, 40, 42]. The order of the colours on the streak lines indicates the direction of movement. The local particle velocity is measured as the length of a streak, ΔL, divided by the exposure time, Δt

$$v = \frac{\Delta L(x, y)}{\Delta t} \tag{2.3}$$

Thus, only two-dimensional velocity components are determined which is a disadvantage of the technique for application in three-dimensional systems. Granular temperature is computed directly from the velocity distribution functions obtained using an ensemble averaging approach.

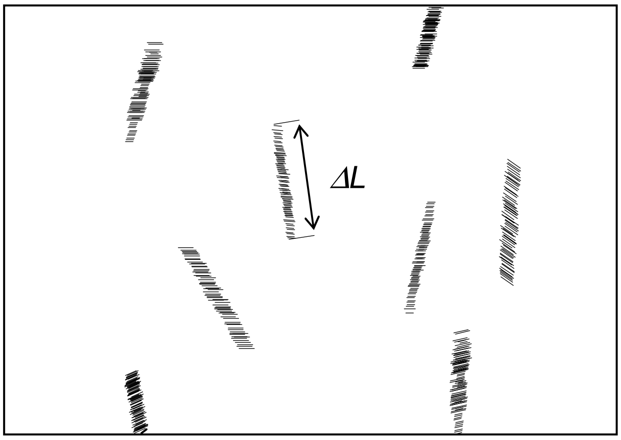

Figure 2.3. Drawing of typical streak lines images.

2.3.1.3 Particle image velocimetry (PIV)

Despite its name, PIV is a technique usually used for accurate measurements of the velocity of the fluid phase at a very large numbers of points simultaneously, using tracer particles [43-45]. Nevertheless, it has been applied in granular systems and there are several studies of velocity fluctuations using this technique. Originally it was applied for studying velocity fluctuations of settling solid particles in a fluid [46-48]. In recent times, the measurement of granular temperature in a liquid [49, 50], a two- dimensional gas spouted bed [51] and a vibro-liquid fluidized bed [52] have been undertaken. All of the referred studies measured the two-dimensional velocity field using planar PIV, although stereo PIV for determining three components of velocity fluctuations is available [44, 53].

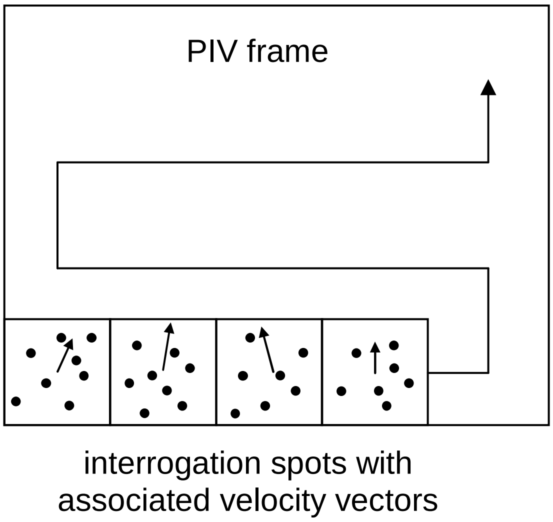

Figure 2.4. Schematic of correlation-based PIV algorithm.

Typical PIV apparatus consists of a camera and a synchronized light source (a laser, usually pulsed, or even a stroboscope) illuminating the system. In contrast to the particle tracking method, PIV does not require the matching of individual particles on successive movie frames [45]. Instead of recording the displacement of individual particles, correlation-based PIV determines the average motion of small groups of particles within small regions known as interrogation spots. The average velocity vector field is found by dividing the frame into interrogation spots and computing sequentially spatial-autocorrelations (single-frame recording), or spatial cross-correlations of the successive frames (multi-frame recording), over all spots, providing one velocity vector per spot (Figure 2.4). In single frame recording, images from several laser (light) pulses are superimposed on the same frame, while several frames are taken during one pulse in multi-frame recording. The autocorrelation technique is applied in single-frame recording but there are two shortcomings of this technique: directional ambiguity of the velocity vector and the impossibility of resolving particle displacements smaller than the particle image diameter [45]. Therefore, the preferred method is spatial cross-correlation of the first frame with the second (double-frame/single pulse recording) without directional ambiguity. Furthermore, even zero displacements can be recorded.

2.3.2 Laser-Doppler velocimetry (LDV)

Like PIV, LDV is a standard technique for measuring velocities in fluid flows where the fluid is seeded with small tracer particles, but turns out to be well adapted to the study of granular flows. However, this optical technique is very difficult to employ even at local solid volume fractions as small as 5 vol % [54]. Nevertheless, due to its high spatial resolution, LDV has become one of the most commonly used experimental techniques in the investigation of flow in dilute granular systems. Furthermore, LDV simultaneously measures the mean and the fluctuating velocity, and the particle diameter. During recent years LDV has been extensively employed for measurement of velocity fluctuations in dilute circulating fluidized beds [55-66], but there are also studies in other granular systems like chute [67] and surface granular flow in a shear cell [68]. In the usual configuration, simultaneous measurements of two velocity components, and indeed velocity fluctuations, in the plane normal to the laser beam are conducted, as explained below. On the other hand, by positioning the LDV probe in two different orientations it is possible to obtain the three velocity components [60]. Recently, Chemloul and Benrabah [69] developed two-phase LDV which is capable of determining the velocity profiles of both the solid particles and the continuous phase.

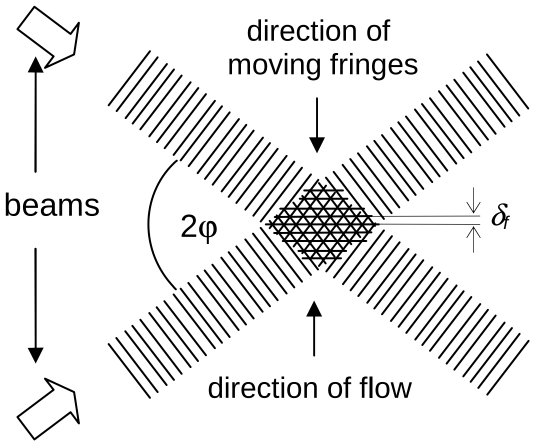

Figure 2.5. Schematic of LDV measuring volume with generated fringe pattern

The LDV technique uses a pattern of interference fringes obtained at the intersection of two laser beams as shown in Figure 2.5. These light and dark fringes generated in the measuring volume are perpendicular to the plane of the two beams. The intensity variation of the scattered light as a particle is passing through the measuring volume is measured with a photo-detector. The velocity of the passing particle is proportional to the frequency of the Doppler signal burst, f_D, and the fringe spacing, δ_f

$$v = f_d \delta_f \tag{2.4}$$

The spacing between the fringes is given by

$$\delta_f = \frac{\lambda}{2\sin\varphi} \tag{2.5}$$

where λ is wavelength of the laser beam and φ is the half-angle between the crossing beams. If a frequency shift of one of the laser beams is introduced [56, 58, 59, 68], the direction of the flow can be obtained.

2.3.3 Radioactive particle tracking (RPT)

Radioactive particle tracking monitoring of a single radioactive labelled particle can reveal detailed solids flow features by determining the instantaneous 3-D Lagrangian trajectory of the tracer and consequently its instantaneous local velocity. Firstly, a minute γ-ray-emitting particle (^{46}Sc) is embedded into a particle of the same properties as other particles. The gamma radiation from the tracer particle is continuously counted by an array of detectors arranged around the fluidized bed as shown in Figure 2.6.

Using an appropriate triangulation procedure these count rates are converted into instantaneous Lagrangian trajectories [70, 71]. On other hand, Limtrakul *et al.* [72] used a calibration procedure to provide a relationship between the distance from each detector to the particle and the intensity count received by the detector. This enabled calculation of the exact position of the tracer particle by using the intensity count received by the detectors and the calibration information provided in the previous step. They termed their approach “computer-aided radioactive particle tracking” (CARPT). Experiments were performed for several hours (6 or more), allowing pseudo whole-field data to be accumulated. Investigators used the ensemble average approach to calculate the spatial distribution of velocity fluctuations.

RPT has been used to measure velocity fluctuations in liquid [70, 72] and gas-liquid [71] fluidized beds. The temporal resolution (30 ms [70, 71] and 20 ms [72]) is a limiting factor for application in a highly dense granular systems.

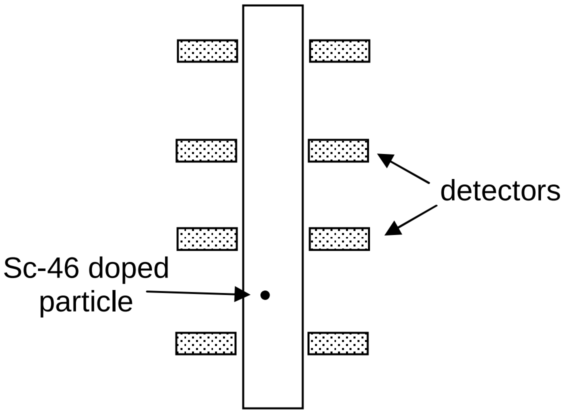

Figure 2.6. Schematic diagram of RPT facility

2.3.4 Positron emission particle tracking (PEPT)

The University of Birmingham Positron Imaging Centre has pioneered and developed the technique of positron emission particle tracking (PEPT) [73-75]. PEPT is a variant of positron emission tomography (PET), widely used in medicine as a functional imaging technique. Whereas measurement of a PET image is relatively slow (some minutes), requiring acquisition of millions of events, in PEPT the location of a single positron-emitting source can be determined very quickly by triangulation of a number of detected events. Three labelling technique have been used to produce a particle tracer with sufficient radioactivity to ensure the tracking efficiency and representative nature of PEPT data [76, 77]. Direct activation of oxygen-containing particles in a cyclotron has been used to produce tracer particles with a size greater than 1mm, with the limitation that the particle must be able to resist a high temperature. For production of tracer particles smaller than 1mm, the ion-exchange method can be used to label strong-base anion exchange resin beads of a size range of 200-600 μm by immersion in a solution of F^{18} ions. The third method, involving surface modification, can be used for other materials. In this way it is possible to label a wide range of materials such as polymers, minerals, coals and metals down to 100 μm in size [77].

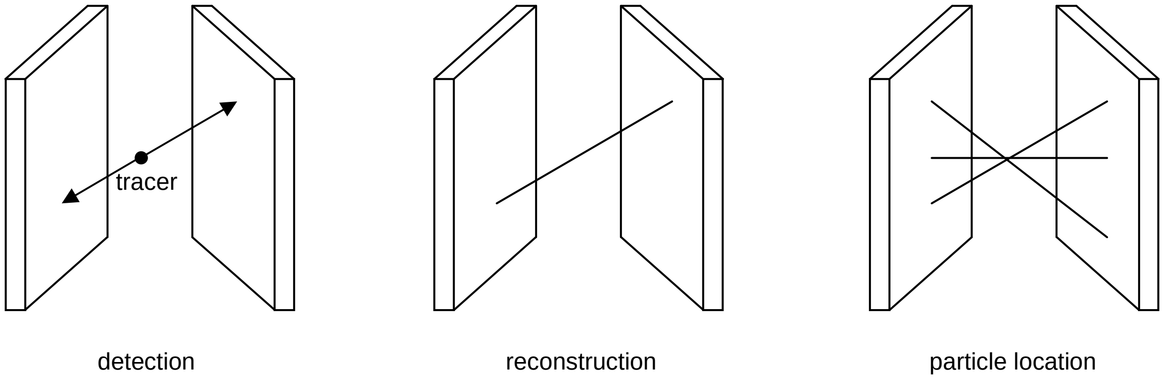

Figure 2.7. The principle of the PEPT technique: coincidence detection of back-to-back γ-rays, reconstruction and determination of tracer location by triangulation.

Positrons emitted from the tracer particle annihilate with free electrons very close to their point of emission, resulting in the formation of two back-to-back γ-rays. The γ-rays are detected by a pair of gamma detectors operated in coincidence, from which a line can be constructed on which the tracer must lie, as schematically represented in Figure 2.7. By using a reconstruction algorithm the position of the particle can be obtained as the intersection point of about 100 reconstructed back-to-back γ-ray lines, although in theory only two such lines are sufficient. This is necessary because in practice many of the detected events are corrupt due to γ-ray scattering or random coincidence. The algorithm employs an iterative scheme to discard corrupt detected events. The automated facility allows experimental data to be logged for a considerable length of time (up to 6 hours), resulting in pseudo whole field data for steady state systems. Under optimum condition, PEPT has a temporal resolution of 2 ms with a spatial accuracy of 1mm [75, 78, 79]. However, spatiotemporal resolution depends on the tracer particle velocity (temporally increasing while spatially decreasing as particle velocity increases [74, 80]) making it suitable for measurement of granular temperature in a highly fluidized granular bed of millimetre sized particles at local solid volume fractions up to 0.15. Wildman and Huntley applied PEPT to measure granular temperature in a three-dimensional monosized vibro-fluidized bed [79, 81], as well as in a binary vibro-fluidized bed [78, 82, 83]. They employed a robust technique of extracting the mean square fluctuation velocity from the ballistic region (short time) of the mean square displacement of the particle.

2.3.5 Nuclear magnetic resonance (NMR)

NMR is now the primary medical imaging technique used to visualize the structure and function of the body using the quantum mechanical magnetic properties of an atom’s nucleus (usually hydrogen nuclei). It has been used for many years by medical scientists and chemists, but in recent years nuclear magnetic resonance imaging has proved to be a useful tool to probe granular dynamics. By using appropriate pulse sequences, measurement of the short-time displacement of the grains in granular systems is possible. NMR techniques have been employed for granular temperature measurements in vibro [84-86] and liquid fluidized beds [87-89]. The main advantage of this technique is its whole field nature and good temporal resolution. The time resolution of applied NMR techniques is of the order of milliseconds. Most NMR acquisition generates signals from a liquid phase such as water or oil within the sample. Usually, in granular studies, mustard or poppy (oil-containing) seeds have been used [85, 86, 88, 89], although oil-filled, hard plastic spherical particles have been employed in one study [87]. However, use of seed grains introduces effects present in practical applications but not usually addressed by simulations: irregular and variable grain sizes, grain rotation, realistic inelastic collisions [85]. In addition, the size of apparatus is limited. The diameter of the apparatus for imaging is constrained by the size of bore of the magnet and the height of the observation window is limited by that of the radio-frequency excitation coil. The current limit is about 50 mm diameter and 50 mm height [90], but it is likely that the size limits will increase as the technique develops.

2.3.6 Acoustic shot noise (ASN)

Acoustic shot noise (ASN) is a non-intrusive probe of average granular temperature at the wall of fluidized bed. The underlying physics of the measurement implies a “white noise” excitation source of the wall vibrational energy by the random impact of the fluidized particles [91-93]. The microsecond impact time of the particles defines random particle impact as an ASN source of wall vibrational energy that is independent of frequency below 300 kHz. In order to obtain granular temperature Cody and collaborators [91-93] utilized power spectral analysis, in particular the theorem of Wiener and Khintchine, which states that for stationary random functions, the power spectrum of a random function is the Fourier transform of its autocorrelation function [94]. This gives quantitative coupling of the ASN excitation of the wall of fluidized bed with the granular temperature at the wall. Thus, the measurement of the steady state fluctuation velocity at the wall, and averaged over the wall, is possible through power spectral analysis of the output of two accelerometers measuring the wall vibrational energy in the 10-20 kHz range dominated by the ASN signal and independent of other excitations of wall vibrational energy in this range.

Cody et al. [91, 93] measured the average granular temperature of a wide range of particles at the wall of a lab scale gas fluidized bed. Time-dependence of the granular temperature under bed collapse has been studied also. Furthermore, the acoustic shot noise probe was used to study particle motion in an industrial scale fluidized bed catalytic crackling unit [92]. The main drawback of the ASN probe method is its limitation to the region near the wall of the fluidized bed because the probes can be mounted only at the wall, but there are two major advantages of the method as it is applicable in highly dense systems as well as on the industrial scale.

2.3.7 Particle pressure-data inversion

Collisional particle pressure, or granular pressure, is the surface force in a granular mixture that is exerted on the containing walls solely by the particle phase due to the motion of particles and their interactions. The pressure that is measured by a standard flush-mounted pressure transducer is the combined pressure of fluid and particle phase. Campbell and Wang [95] developed a probe to isolate the particle pressure by subtraction between the total and the fluid pressure directly at the point of measurement. This particle pressure transducer is very simple and consists of a solid diaphragm flush-mounted into the wall. The face of the diaphragm experiences the combined pressure of fluid and particles, while the rear experiences only fluid forces as particles are prevented from entering through the access holes into a chamber behind the diaphragm. However, this is not the instantaneous particle pressure since the fluid pressure is not balanced out instantaneously: the fluid pressure waves take a finite time to reach the rear of the diaphragm. Thus, the drawback of this approach is that it is only possible to measure time-averaged particle pressure which corresponds to the time-averaged response of the diaphragm. Campbell and collaborators [95-97] measured the particle pressure in gas fluidized beds. Polashensky and Chen measured the particle pressure along with the solid volume fraction in gas [98] and circulating [99] fluidized beds. This experimental data enables calculation of the granular temperature by using constitutive relations from the kinetic theory of granular flow, although it was reported only for gas fluidized beds [98].

Development of a high-frequency-response pressure transducer capable of detecting changes in pressure lasting up to 2 μs [100], allowed measurement of particle pressure from individual particle impacts. Pressure fluctuations below 1 kHz are filtered completely so only the pressure pulses generated by the collisions of particles, typically lasting tens of microseconds, are detected [100-102]. This approach has been used to measure particle pressure in liquid [100, 101], gas-liquid [102] and vibro [103] fluidized beds. Louge and Keast [104] simultaneously measured the particle pressure with solid volume fraction in order to calculate granular temperatures in dense granular flow down inclines. The main asset of the technique is its applicability in highly dense granular systems, but the necessity of solid volume fraction measurement along with the restriction to near-wall measurement are the main disadvantages of the technique.

2.4 Conclusion

Chapter 2 presents a variety of state-of-the-art and other experimental techniques that have been developed, adapted and used over the past 15 or more years to measure granular temperature for a wide range of granular systems. A summary of their advantages and disadvantages discussed in the chapter is given in Table 2.1. As can be seen from the table only few methods can be applied in a highly dense system mainly due to high spatiotemporal requirements. For example, using the time criterion proposed by Breault et al. [66]

$$\tau_c = \frac{d_p}{6\phi\delta v} \tag{2.6}$$

the time between particle collisions for 200 μm particles fluidized in water at a solid volume fraction of 0.4 was estimated to be of the order of 10 ms. Further, inter-particle distance is of the order of particle diameter. Thus, the required spatiotemporal resolution is of the order of milliseconds and tens of micrometers for this case, which makes measurement of granular temperature highly difficult using most of the methods reviewed.

The multiple light scattering based technique of diffusing wave spectroscopy (DWS) [105] is neither intrusive (mechanical spectroscopy) nor restricted to the wall region (acoustic shot noise, particle pressure inversion), yet able to probe length (1-10 nm) and time-scales (10 ns) well below those accessible to NMR, their nearest rival in this regard. This makes DWS more suitable than other non-intrusive techniques for granular temperature studies, especially in a highly dense system. More details of this technique are presented in Chapter 3.

Technique	Advantage	Disadvantage	Temporal resolution
Optical fiber probe	Simple and cheap Good temporal resolution	Intrusive Point measurement technique Plane (2D) results Calibration	25 μs – 10 ms
Mechanical Spectroscopy	Applicable in highly dense systems	Intrusive Point measurement technique Sensitive to the shape of probe	not applicable
Imaging techniques	Non-intrusive Whole-field technique	Near-wall measurements Not applicable in highly dense systems	1 ms – 40 ms
Laser Doppler Velocimetry (LDV)	Non-intrusive High spatial resolution	Applicable only in dilute systems Point-measurement technique	1-10 μs
Radioactive Particle Tracking (RPT)	Non-intrusive Pseudo whole-field technique	Tedious Low temporal resolution	20-30 ms
Positron Emission Particle Tracking (PEPT)	Non-intrusive Pseudo whole-field technique	Tedious Low temporal resolution for slower/denser systems (20 ms)	2 ms - 20 ms
Nuclear Magnetic Resonance (NMR)	Non-intrusive Whole-field technique Applicable in highly dense systems	Limited size of apparatus Irregular and variable grain size	0.5-8 ms
Accoustic Shot Noise (ASN)	Non-intrusive Applicable in highly dense systems Applicable on the industrial scale	Near-wall measurement Averaged over the wall	50 -100 μs
Particle pressure inversion	Non-intrusive Applicable in highly dense systems	Near wall measurement Need for solid volume fraction measurement	2 μs – 1 ms

Table 2.1. Advantages and disadvantages of granular temperature measurement techniques.

References

1. Goldhirsch, I., *Introduction to granular temperature.* Powder Technology, 2008. **182**(2): p. 130.
2. Werther, J., *Measurement techniques in fluidized beds.* Powder Technology, 1999. **102**(1): p. 15.
3. Patrose, B. and H.S. Caram, *Optical fiber probe transit anemometer for particle-velocity measurements in fluidized-beds.* AIChE Journal, 1982. **28**(4): p. 604-609.
4. Tayebi, D., H.F. Svendsen, A. Grislingås, T. Mejdell, and K. Johannessen, *Dynamics of fluidized-bed reactors. Development and application of a new multi-fiber optical probe.* Chemical Engineering Science, 1999. **54**(13-14): p. 2113.
5. Ahn, H., C.E. Brennen, and R.H. Sabersky, *Measurements of velocity, velocity fluctuation, density, and stresses in chute flows of granular-materials.* Journal of Applied Mechanics-Transactions of the ASME, 1991. **58**(3): p. 792-803.
6. Hsiau, S.S. and M.L. Hunt, *Shear-induced particle diffusion and longitudinal velocity fluctuations in a granular-flow mixing layer.* Journal of Fluid Mechanics, 1993. **251**: p. 299-313.
7. Sobocinski, D.A., B.J. Young, and H.I. Delasa, *New fiberoptic method for measuring velocities of strands and solids hold-up in gas-solids downflow reactors.* Powder Technology, 1995. **83**(1): p. 1-11.
8. Boateng, A.A. and P.V. Barr, *Granular flow behaviour in the transverse plane of a partially filled rotating cylinder.* Journal of Fluid Mechanics, 1997. **330**: p. 233-249.
9. Ersoy, L.E., M.R. Golriz, M. Koksal, and F. Hamdullahpur, *Circulating fluidized bed hydrodynamics with air staging: an experimental study.* Powder Technology, 2004. **145**(1): p. 25.
10. Zhu, H., J. Zhu, G. Li, and F. Li, *Detailed measurements of flow structure inside a dense gas-solids fluidized bed.* Powder Technology, 2008. **180**(3): p. 339.
11. Zhu, J.X., G.Z. Li, S.Z. Qin, F.Y. Li, H. Zhang, and Y.L. Yang, *Direct measurements of particle velocities in gas-solids suspension flow using a novel five-fiber optical probe.* Powder Technology, 2001. **115**(2): p. 184.
12. Callen, H.B. and T.A. Welton, *Irreversibility and generalized noise.* Physical Review, 1951. **83**(1): p. 34.
13. Mayor, P., G. D'Anna, G. Gremaud, A. Barrat, and V. Loreto, *Mechanical spectroscopy of vibrated granular matter.* Materials Science and Engineering: A, 2006. **442**(1-2): p. 256.
14. D'Anna, G., P. Mayor, A. Barrat, V. Lotero, and F. Nori, *Observing Brownian motion in vibration-fluidized granular matter.* Nature, 2003. **424**(6951): p. 909.
15. Mayor, P., G. D'Anna, A. Barrat, and V. Loreto, *Observing Brownian motion and measuring temperatures in vibration-fluidized granular matter.* New Journal of Physics, 2005. **7**: p. 28.
16. Srebro, Y. and D. Levine, *Exactly solvable model for driven dissipative systems.* Physical Review Letters, 2004. **93**(24): p. 240601.
17. Drake, T.G., *Granular flow: physical experiments and their implications for microstructural theories.* Journal of Fluid Mechanics, 1991. **225**: p. 121-152.

18. Natarajan, V.V.R., M.L. Hunt, and E.D. Taylor, *Local measurements of velocity fluctuations and diffusion coefficients for a granular material flow.* Journal of Fluid Mechanics, 1995. **304**: p. 1-25.
19. Warr, S., J.M. Huntley, and G.T.H. Jacques, *Fluidization of a two-dimensional granular system: Experimental study and scaling behaviour.* Physical Review E, 1995. **52**(5): p. 5583-5595.
20. Losert, W., D.G. Cooper, J. Delour, A. Kudrolli, and J.P. Gollub, *Velocity statistics in excited granular media.* Chaos, 1999. **9**(3): p. 682-690.
21. Wildman, R.D., J.M. Huntley, and J.P. Hansen, *Self-diffusion of grains in a two-dimensional vibrofluidized bed.* Physical Review E, 1999. **60**(6): p. 7066-7075.
22. Wildman, R.D. and J.M. Huntley, *Novel method for measurements of granular temperature distributions in two-dimensional vibro-fluidised beds.* Powder Technology, 2000. **113**: p. 14-22.
23. Feitosa, K. and N. Menon, *Breakdown of energy equipartition in a 2D binary vibrated granular gas.* Physical Review Letters, 2002. **88**: p. 198301.
24. Tai, C.H. and S.S. Hsiau, *Dynamic behaviors of powders in a vibrating bed.* Powder Technology, 2004. **139**: p. 221-232.
25. Yang, S.C., *Density effect on mixing and segregation processes in a vibrated binary granular mixture.* Powder Technology, 2006. **164**: p. 65-74.
26. Hsiau, S.S. and H.W. Jang, *Measurements of velocity fluctuations of granular materials in a shear cell.* Experimental Thermal and Fluid Science, 1998. **17**(3): p. 202-209.
27. Hsiau, S.-S. and Y.-M. Shieh, *Effect of solid fraction on fluctuations and self-diffusion of sheared granular flows.* Chemical Engineering Science, 2000. **55**(11): p. 1969.
28. Azanza, E., F. Chevoir, and P. Moucheront, *Experimental study of collisional granular flows down an inclined plane.* Journal of Fluid Mechanics, 1999. **400**: p. 199-227.
29. Capart, H., D.L. Young, and Y. Zech, *Voronoï imaging methods for the measurement of granular flows.* Experiments in Fluids, 2002. **V32**(1): p. 121.
30. Blair, D.L. and A. Kudrolli, *Collision statistics of driven granular materials.* Physical Review E, 2003. **67**(4): p. 041301.
31. Armanini, A., H. Capart, L. Fraccarollo, and M. Larcher, *Rheological stratification in experimental free-surface flows of granular-liquid mixtures.* Journal of Fluid Mechanics, 2005. **532**: p. 269-319.
32. Perng, A.T.H., H. Capart, and H.T. Chou, *Granular configurations, motions, and correlations in slow uniform flows driven by an inclined conveyor belt.* Granular Matter, 2006. **8**(1): p. 5-17.
33. Armanini, A., L. Fraccarollo, and M. Larcher, *Liquid-granular channel flow dynamics.* Powder Technology, 2008. **182**(2): p. 218-227.
34. Capart, H., L. Fraccarollo, L. Guarino, A. Armanini, and Y. Zech, *Granular temperature behaviour of loose bed debris-flows.* Debris-Flow Hazards Mitigation: Mechanics, Prediction, and Assessment, 2000: p. 361-368.
35. Spinewine, B., H. Capart, M. Larcher, and Y. Zech, *Three-dimensional Voronoï imaging methods for the measurement of near-wall particulate flows.* Experiments in Fluids, 2003. **V34**(2): p. 227.
36. Gidaspow, D. and H.L. Lu, *Collisional viscosity of FCC particles in a CFB.* AIChE Journal, 1996. **42**(9): p. 2503-2510.

37. Gidaspow, D. and L. Huilin, *Equation of state and radial distribution functions of FCC particles in a CFB.* Aiche Journal, 1998. **44**(2): p. 279-293.
38. Gidaspow, D. and H.L. Lu, *A comparison of gas-solid and liquid-solid fluidization using kinetic theory and statistical mechanics.* Fluidization IX, 1998: p. 661-668.
39. Gidaspow, D. and R. Mostofi, *Maximum carrying capacity and granular temperature of A, B and C particles.* AIChE Journal, 2003. **49**(4): p. 831-843.
40. Tartan, M. and D. Gidaspow, *Measurement of granular temperature and stresses in risers.* AIChE Journal, 2004. **50**(8): p. 1760-1775.
41. Gidaspow, D. and L. Huilin, *Liquid-solid fluidization using kinetic theory of granular flow.* AIChE Symposium series 317, 1997. **93**: p. 12-17.
42. Jung, J., D. Gidaspow, and I.K. Gamwo, *Measurement of two kinds of granular temperatures, stresses, and dispersion in bubbling beds.* Indistrial and Engineering Chemistry Research, 2005. **44**(5): p. 1329-1341.
43. Adrian, R.J., *Particle-imaging techniques for experimental fluid-mechanics.* Annual Review of Fluid Mechanics, 1991. **23**: p. 261-304.
44. Adrian, R.J., *Twenty years of particle image velocimetry.* Experiments in Fluids, 2005. **39**(2): p. 159-169.
45. Prasad, A.K., *Particle image velocimetry.* Current Science, 2000. **79**(1): p. 51-60.
46. Segrè, P.N., E. Herbolzheimer, and P.M. Chaikin, *Long-range correlations in sedimentation.* Physical Review Letters, 1997. **79**(13): p. 2574.
47. Segrè, P.N., F. Liu, P. Umbanhowar, and D.A. Weitz, *An effective gravitational temperature for sedimentation.* Nature, 2001. **409**(6820): p. 594-597.
48. Tee, S.Y., P.J. Mucha, M.P. Brenner, and D.A. Weitz, *Velocity fluctuations of initially stratified sedimenting spheres.* Physics of Fluids, 2007. **19**(11).
49. Segrè, P.N. and J.P. McClymer, *Fluctuations, stratification and stability in a liquid fluidized bed at low Reynolds number.* Journal of Physics-Condensed Matter, 2004. **16**(38): p. S4219-S4230.
50. Tee, S.Y., P.J. Mucha, M.P. Brenner, and D.A. Weitz, *Velocity fluctuations in a low-Reynolds-number fluidized bed.* Journal of Fluid Mechanics, 2008. **596**: p. 467-475.
51. Liu, G.Q., S.Q. Li, X.L. Zhao, and Q. Yao, *Experimental studies of particle flow dynamics in a two-dimensional spouted bed.* Chemical Engineering Science, 2008. **63**(4): p. 1131-1141.
52. Lim, E.W.C., Y.S. Wong, and C.H. Wang, *Particle image velocimetry experiment and discrete-element simulation of voidage wave instability in a vibrated liquid-fluidized bed.* Industrial and Engineering Chemistry Research, 2007. **46**(4): p. 1375.
53. Prasad, A.K., *Stereoscopic particle image velocimetry.* Experiments in Fluids, 2000. **29**(2): p. 103-116.
54. Werther, J., B. Hage, and C. Rudnick, *A comparison of laser Doppler and single-fibre reflection probes for the measurement of the velocity of solids in a gas-solid circulating fluidized bed.* Chemical Engineering and Processing, 1996. **35**(5): p. 381-391.
55. Zhang, Y.F. and H. Arastoopour, *Dilute fluidized cracking catalyst particles - gas-flow behavior in the riser of a circulating fluidized-bed.* Powder Technology, 1995. **84**(3): p. 221-229.

56. Samuelsberg, A. and B.H. Hjertager, *An experimental and numerical study of flow patterns in a circulating fluidized bed reactor.* International Journal of Multiphase Flow, 1996. **22**(3): p. 575-591.
57. Van den Moortel, T., E. Azario, R. Santini, and L. Tadrist, *Experimental analysis of the gas-particle flow in a circulating fluidized bed using a phase Doppler particle analyzer.* Chemical Engineering Science, 1998. **53**(10): p. 1883-1899.
58. Mathiesen, V., T. Solberg, H. Arastoopour, and B.H. Hjertager, *Experimental and computational study of multiphase gas/particle flow in a CFB riser.* AIChE Journal, 1999. **45**(12): p. 2503-2518.
59. Mathiesen, V., T. Solberg, and B.H. Hjertager, *An experimental and computational study of multiphase flow behavior in a circulating fluidized bed.* International Journal of Multiphase Flow, 2000. **26**(3): p. 387-419.
60. Ibsen, C.H., T. Solberg, B.H. Hjertager, and F. Johnsson, *Laser Doppler anemometry measurements in a circulating fluidized bed of metal particles.* Experimental Thermal and Fluid Science, 2002. **26**(6-7): p. 851-859.
61. Pandey, P., R. Turton, P. Yue, and L. Shadle, *Nonintrusive particle motion studies in the near-wall region of a pilot-scale circulating fluidized bed.* Industrial and Engineering Chemistry Research, 2004. **43**(18): p. 5582-5592.
62. Breault, R.W., C.J. Ludlow, and P.C. Yue, *Cluster particle number and granular temperature for cork particles at the wall in the riser of a CFB.* Powder Technology, 2005. **149**(2-3): p. 68.
63. Pandey, P. and R. Turton, *Evaluation of a backscatter imaging LDV system and its application to a pilot-scale circulating fluidized bed.* Particulate Science and Technology, 2006. **24**(1): p. 1-22.
64. Bergenblock, T., B. Leckner, F. Onofri, R. Occelli, and L. Tadrist, *Averaging of particle data from phase Doppler anemometry in unsteady two-phase flow: Validation by numerical simulation.* International Journal of Multiphase Flow, 2006. **32**(2): p. 248-268.
65. Bergenblock, T., F. Onofri, B. Leckner, and L. Tadrist, *Experimental estimation of particle flow fluctuations in dense unsteady two-phase flow using phase Doppler anemometry.* International Journal of Multiphase Flow, 2007. **33**(8): p. 849-872.
66. Breault, R.W., C.P. Guenther, and L.J. Shadle, *Velocity fluctuation interpretation in the near wall region of a dense riser.* Powder Technology, 2008. **182**(2): p. 137.
67. Amarouchene, Y. and H. Kellay, *Speed of sound from shock fronts in granular flows.* Physics of Fluids, 2006. **18**(3).
68. Kellay, H., Y. Amarouchene, and J.F. Boudet, *Intermittency of the velocity fluctuations in a granular surface flow.* Physics of Fluids, 2007. **19**(7).
69. Chemloul, N.S. and O. Benrabah, *Measurement of velocities in two-phase flow by laser velocimetry: Interaction between solid particles' motion and turbulence.* Journal of Fluids Engineering-Transactions of the ASME, 2008. **130**(7).
70. Kiared, K., F. Larachi, M. Cassanello, and J. Chaouki, *Flow structure of the solids in a three-dimensional liquid fluidized bed.* Industrial and Engineering Chemistry Research, 1997. **36**(11): p. 4695-4704.
71. Kiared, K., F. Larachi, J. Chaouki, and C. Guy, *Mean & turbulent particle velocity in the fully developed region of a three-phase fluidized bed.* Chemical Engineering andTechnology, 1999. **22**(8): p. 683-689.

72. Limtrakul, S., J. Chen, P.A. Ramachandran, and M.P. Dudukovic, *Solids motion and holdup profiles in liquid fluidized beds.* Chemical Engineering Science, 2005. **60**(7): p. 1889.
73. Parker, D.J., C.J. Broadbent, P. Fowles, M.R. Hawkesworth, and P. McNeil, *Positron emission particle tracking - a technique for studying flow within engineering equipment.* Nuclear Instruments and Methods in Physics Research Section A, 1993. **326**(3): p. 592-607.
74. Parker, D.J., R.N. Forster, P. Fowles, and P.S. Takhar, *Positron emission particle tracking using the new Birmingham positron camera.* Nuclear Instruments and Methods in Physics Research Section A, 2002. **477**(1-3): p. 540-545.
75. Parker, D.J., T.W. Leadbeater, X. Fan, M.N. Hausard, A. Ingram, and Z. Yang, *Positron imaging techniques for process engineering: recent developments at Birmingham.* Measurement Science and Technology, 2008. **19**(9).
76. Fan, X., D.J. Parker, and M.D. Smith, *Labelling a single particle for positron emission particle tracking using direct activation and ion-exchange techniques.* Nuclear Instruments and Methods in Physics Research Section A, 2006. **562**(1): p. 345-350.
77. Fan, X., D.J. Parker, and M.D. Smith, *Enhancing F-18 uptake in a single particle for positron emission particle tracking through modification of solid surface chemistry.* Nuclear Instruments and Methods in Physics Research Section A, 2006. **558**(2): p. 542-546.
78. Wildman, R.D. and J.M. Huntley, *Scaling exponents for energy transport and dissipation in binary vibro-fluidized granular beds.* Physics of Fluids, 2003. **15**(10): p. 3090.
79. Wildman, R.D., J.M. Huntley, and D.J. Parker, *Granular temperature profiles in three-dimensional vibrofluidized granular beds.* Physical Review E, 2001. **63**(6): p. 061311.
80. Parker, D.J., A.E. Dijkstra, T.W. Martin, and J.P.K. Seville, *Positron emission particle tracking studies of spherical particle motion in rotating drums.* Chemical Engineering Science, 1997. **52**(13): p. 2011-2022.
81. Wildman, R.D., J.M. Huntley, J.P. Hansen, D.J. Parker, and D.A. Allen, *Single-particle motion in three-dimensional vibrofluidized granular beds.* Physical Review E, 2000. **62**(3): p. 3826.
82. Wildman, R.D., J.T. Jenkins, P.E. Krouskop, and J. Talbot, *A comparison of the prediction of a simple kinetic theory with experimental and numerical results for a vibrated granular bed consisting of nearly elastic particles of two sizes.* Physics of Fluids, 2006. **18**: p. 073301.
83. Wildman, R.D. and D.J. Parker, *Coexistence of two granular temperatures in binary vibrofluidized beds.* Physical Review Letters, 2002. **88**(6): p. 064301.
84. Yang, X., C. Huan, D. Candela, R.W. Mair, and R.L. Walsworth, *Measurements of grain motion in a dense, three-dimensional granular fluid.* Physical Review Letters, 2002. **88**(4): p. 044301.
85. Huan, C., X. Yang, D. Candela, R.W. Mair, and R.L. Walsworth, *NMR experiments on a three-dimensional vibrofluidized granular medium.* Physical Review E, 2004. **69**: p. 041302.
86. Huntley, J.M., T.W. Martin, M.D. Mantle, M.D. Shattuck, A.J. Sederman, R.D. Wildman, L.F. Gladden, and N.A. Halliwell, *NMR measurements and hydrodynamic simulations of phase-resolved velocity distributions within a*

three-dimensional vibrofluidized granular bed. Proceedings of the Royal Society A: Mathematical, Physical and Engineering Sciences, 2007. **463**(2086): p. 2519.

87. Lasič, S., J. Stepisnik, A. Mohorič, I. Sersa, and G. Planinsič, *Autocorrelation spectra of an air-fluidized granular system measured by NMR.* Europhysics Letters, 2006. **75**(6): p. 887-893.
88. Muller, C.R., D.J. Holland, A.J. Sederman, S.A. Scott, J.S. Dennis, and L.F. Gladden, *Granular temperature: comparison of magnetic resonance measurements with discrete element model simulations.* Powder Technology, 2008. **184**(2): p. 241-253.
89. Holland, D.J., C.R. Muller, J.S. Dennis, L.F. Gladden, and A.J. Sedennan, *Spatially resolved measurement of anisotropic granular temperature in gas-fluidized beds.* Powder Technology, 2008. **182**(2): p. 171-181.
90. Muller, C.R., D.J. Holland, A.J. Sederman, M.D. Mantle, L.F. Gladden, and J.F. Davidson, *Magnetic resonance imaging of fluidized beds.* Powder Technology, 2008. **183**(1): p. 53-62.
91. Cody, G.D., D.J. Golfarb, G.V. Storch, and A.N. Norris, *Particle granular temperature in gas fluidized beds.* Powder Technology, 1996. **87**: p. 211-232.
92. Cody, G.D., R.J. Bellows, D.J. Goldfarb, H.A. Wolf, and G.V. Storch, *A novel non-intrusive probe of particle motion and gas generation in the feed injection zone of the feed riser of a fluidized bed catalytic cracking unit.* Powder Technology, 2000. **110**(1-2): p. 128-142.
93. Cody, G.D., J. Johri, and D. Goldfarb, *Dependence of particle fluctuation velocity on gas flow, and particle diameter in gas fluidized beds for monodispersed spheres in the Geldart B and A fluidization regimes.* Powder Technology, 2008. **182**(2): p. 146.
94. Newland, D.E., *An introduction to random vibrations and spectral and wavelet analysis*. 3rd ed. 1993, New York: Longman Scientific/Wiley.
95. Campbell, C.S. and D.G. Wang, *Particle pressures in gas-fluidized beds.* Journal of Fluid Mechanics, 1991. **227**: p. 495-508.
96. Campbell, C.S. and K. Rahman, *An improved particle pressure transducer.* Measurement Science and Technology, 1992. **3**(8): p. 709.
97. Rahman, K. and C.S. Campbell, *Particle pressures generated around bubbles in gas-fluidized beds.* Journal of Fluid Mechanics, 2002. **455**: p. 103-127.
98. Polashenski, W. and J.C. Chen, *Normal solid stress in fluidized beds.* Powder Technology, 1997. **90**(1): p. 13-23.
99. Polashenski, W. and J.C. Chen, *Measurement of Particle Phase Stresses in Fast Fluidized Beds.* Industrial and Engineering Chemistry Research, 1999. **38**(3): p. 705-713.
100. Zenit, R., M.L. Hunt, and C.E. Brennen, *Collisional particle pressure measurements in solid-liquid flows.* Journal Of Fluid Mechanics, 1997. **353**: p. 261-283.
101. Zenit, R., M.L. Hunt, and C.E. Brennen, *On the direct and radiated components of the collisional particle pressure in liquid-solid flows.* Applied Scientific Research, 1998. **58**(1-4): p. 305-317.
102. Buffiere, P. and R. Moletta, *Collision frequency and collisional particle pressure in three-phase fluidized beds.* Chemical Engineering Science, 2000. **55**(22): p. 5555-5563.
103. Falcon, E., S. Aumaitre, P. Evesque, F. Palencia, C. Lecoutre-Chabot, S. Fauve, D. Beysens, and Y. Garrabos, *Collision statistics in a dilute granular*

gas fluidized by vibrations in low gravity. Europhysics Letters, 2006. **74**(5): p. 830-836.
104. Louge, M.Y. and S.C. Keast, *On dense granular flows down flat frictional inclines*. Physics of Fluids, 2001. **13**(5): p. 1213.
105. Weitz, D.A. and D.J. Pine, *Diffusing-wave spectroscopy*, in *Dynamic Light Scattering: The Method and Some Application*, W. Brown, Editor. 1993, Clarendon Press: Oxford. p. 652-720.

Chapter 3 Diffusing wave spectroscopy (DWS): theory and data analysis procedure

3.1 Introduction

Diffusing wave spectroscopy, which is described in detail by Weitz and Pine [1], is one of a number of multiple light scattering techniques that has been used extensively to study the dynamics of turbid colloids [2, 3] and, to a much lesser extent, dense granular systems [4-10]. Basically, measurement of the intensity fluctuations of laser light through the transparent particles provides information about the motions of the particles in a fluidized bed. Coherent light from a laser is incident normal to one face of the glass fluidized bed chamber. The light enters the sample, undergoes multiple light scattering events from the glass spheres and emerges from the opposite face where it is collected by an optical detector. The light accumulates phase proportional to the length of the path it travels through the scattering medium. The intensity at a point in space is the square of the sum of the fields from all paths which reach that particular point. For a collection of random scatterers, the interference results in a spatially random pattern with regions of bright and dark spots. These bright and dark spots are called speckles. Using an optical fiber as a light detector guarantees that only a single speckle, called a coherence area, is detected. Motion of the particles changes path lengths. The interference from these changing paths creates a fluctuating speckle pattern. An image of a speckle pattern is shown in Figure 3.1.

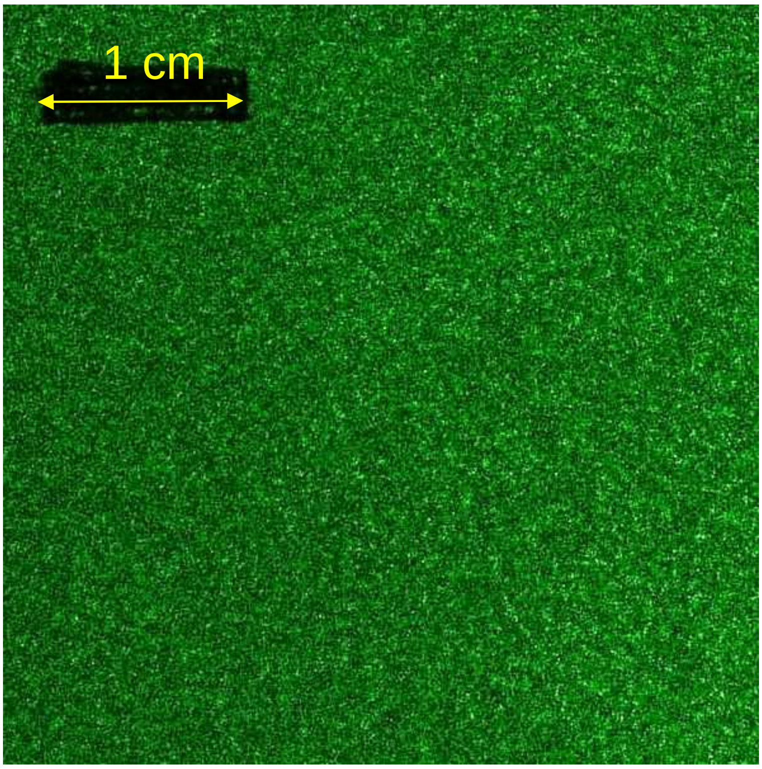

Figure 3.1. Image of a speckle pattern taken half a meter from a randomly packed sample of 165 μm glass particles.

The intensity fluctuations arise when the path length of scattered light changes by one wavelength, λ (the total phase of the light changes by π). The great advantage of multiple light scattering techniques is that they are extremely sensitive to small particle motions. There are typically hundreds of particles involved in the scattering of the light within a fluidized bed. Consequently each particle must only displace a small fraction of the wavelength in order for the entire path length to change by λ. The rate at which the light intensity fluctuates is directly determined by the motion of the particles. Thus, the time evolution of the speckle fluctuations gives a high resolution measurement of particle motion. Diffusing wave spectroscopy utilizes these features for measurement of granular temperature in a dense fluidized bed.

3.2 Theory of Diffusing Wave Spectroscopy (DWS)

As described above, DWS probes small length-scale motions over short time-scales by measurement of the intensity fluctuations of transmitted photons. The intensity fluctuations are characterized by an intensity autocorrelation function (IACF), $g_2(t)$, and the theory of DWS is used to calculate the ensemble averaged mean square displacement (MSD) of the scatterers, $<\Delta r^2(t)>$, from the measured temporal autocorrelation function of the scattered light. The theory of DWS in more detail is given below.

3.2.1 Multiple scattering theory – principle of DWS

The aim of the measurement of scattered light intensity is to relate the motion of the particles to the measured decay of an intensity fluctuation, $g_2(t)$. At given instant in time at the detector, the electric field is the sum of the electric fields of all light paths. This field will change due to changes in scattering paths by the motions of the scatterers and the light intensity will consequently fluctuate. A double sum is necessary in order to calculate the detected field. First, an expression for the phase $\theta(t)$ accumulated by a photon travelling along a light path p of length $s(t)$ as it scatters N times through the dense medium is required. This requires a sum over the positions of particles in the light path. The motion of the particles creates a time-dependent length of the path, $s(t)$, and consequently the phase accumulated in the path acquires time-dependence. The second sum required is a sum over all possible paths from laser source to the detector. This requires expression for the probability that light travels through the medium along a path of length s, denoted as $P(s)$.

Each path of length s will contribute to the decay in the autocorrelation function which can be considered as the characteristic time that the phase accumulated along that path changes by π. If there were only one path in the medium, this would yield an instantaneous decay of the correlation function. However, there are many paths and each contributes a different decay rate to the autocorrelation function. They will contribute in proportion to the relative probability of light travelling on that path, $P(s)$, meaning that paths which are more probable influence the time-scale of the decay more strongly. Thus, the final decay function has to take into account both these contributions. To calculate the path length probability function, $P(s)$, DWS relies on the assumption that the light propagation through a highly scattering medium can be described as a diffusive process. This is due to the fact that each photon is scattered a very large number of times and its path approximates to a random walk.

Within the diffusion approximation, light propagation is parameterized by the diffusion coefficient of light $D_l = v_l l^*/3$, where v_l is the average speed of light in the medium and l^* is the transport mean free path in the medium. This length characterizes the scattering medium itself and it is the total path length a photon must travel before the direction of the light is uncorrelated with its original direction, i.e. completely randomized. This is typically considerably larger than the scattering mean free path, l, i.e. mean distance between scattering events.

3.2.2 Autocorrelation function for multiply-scattered light

This section gives an outline of the calculation of the ensemble averaged MSD from the temporal autocorrelation of scattered light. The derivation in this section follow Weitz and Pine [1]. First, it would be convenient to measure the electric field, $E(t)$, at a measuring point and characterize its fluctuations by the electric-field autocorrelation function (FACF), $g_1(t)$, given by the formula

$$g_1(t) = \frac{\left\langle E(0)E^*(t) \right\rangle}{\left\langle |E|^2 \right\rangle} \tag{3.1}$$

where $E^*(t)$ is the complex conjugate of E(t) and |E| is amplitude of the electric field. However, measuring the electric field in the time domain is very difficult due to the high frequency of visible light, $f_l = v_l/\lambda$, which is of order 10^{15} Hz. Instead, in DWS the intensity of the scattered field, $I(t) \equiv \left\langle E^*(t)E(t) \right\rangle$, is measured in which the rapidly fluctuating $\exp(-i2\pi f_l t)$ component of $E(t)$ has been cancelled [11]. Thus, the average is taken over many cycles of the field oscillations. From the intensity signal, the intensity autocorrelation function (IACF), $g_2(t)$, is obtained

$$g_2(t) = \frac{\left\langle I(t)I(0) \right\rangle}{\left\langle I \right\rangle^2} \tag{3.2}$$

These two temporal autocorrelation functions are related by the Siegert relation

$$g_2(t) \equiv 1 + \beta |g_1(t)|^2 \tag{3.3}$$

where β is a constant determined primarily by the collection optics of the experiment: detection of one coherence area or less yields $\beta = 1$ and $g_2(0) = 2$ for polarized light, while for unpolarized light, $\beta = 0.5$ and $g_2(0) = 1.5$.

A derivation of the expression for $E(t)$ relates the experimentally obtained IACF to the mean square displacement of the particles. As described physically above, the calculated field will be a sum over the paths p which have accumulated phase $\theta(t) = k_0 s$ during the transit time t on a path of total length $s(t)$ through the medium, where $k_0 = 2\pi/\lambda$ is the wave vector of the light. At time t, the electric field at the detector $E(t)$ is the sum over all paths which reach the detector

$$E(t) = \sum_p E_p e^{i\theta_p(t)} \tag{3.4}$$

where E_p is the amplitude of the field from path p. To relate to the experiments, $E(t)$ is inserted into equation 3.1

$$g_1(t) = \frac{1}{\langle I \rangle}\left\langle \left(\sum_p E_p e^{i\theta_p(0)} \right)\left(\sum_{p'} E^*_{p'} e^{-i\theta_{p'}(t)} \right) \right\rangle \tag{3.5}$$

where $\langle I \rangle$ is the total average scattered intensity at the detector. Assuming that photon paths are uncorrelated, equation 3.5 simplifies to

$$g_1(t) = \sum_p \frac{\langle I_p \rangle}{\langle I \rangle} \left\langle e^{i\Delta\theta_p(t)} \right\rangle \tag{3.6}$$

where $\langle I_p \rangle \equiv \left\langle |E_p|^2 \right\rangle$ is the average intensity of the path p.

First, an expression for the change in the phase of the scattered light, $\Delta\theta_p(t)$, resulting from particle motion must be obtained. A single photon passing through the sample undergoes N scattering events as shown on Figure 3.2. The total path length, s, of light which scatters quasi-elastically (all wave vectors have the same magnitude $k_i = k_0$ for all i) N times is

$$s = \sum_{i=0}^{N} \left| r_{i+1} - r_i \right| = \sum_{i=0}^{N} \left(\frac{k_i}{|k_i|} \right) (r_{i+1} - r_i) \tag{3.7}$$

where r_i is the position vector of particle i, r_0 is the position vector of the source (laser) and r_{N+1} is the position vector of the detector.

The total phase shift of the photon for the given path is

$$\theta(t) = \sum_{i=0}^{N} k_i(t) [r_{i+1}(t) - r_i(t)] \tag{3.8}$$

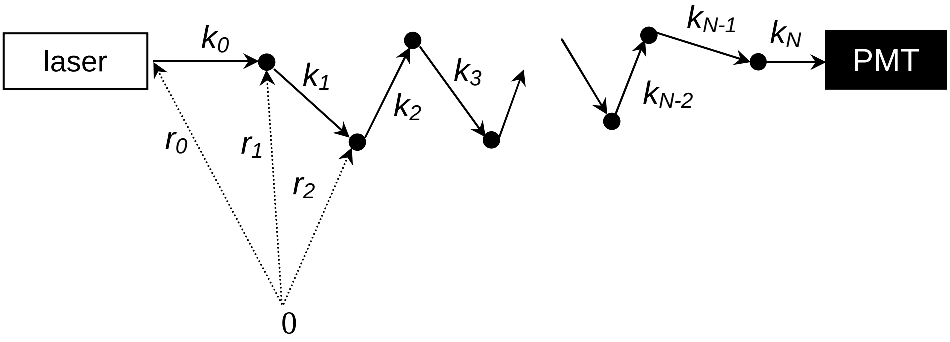

Figure 3.2. A single photon path through a multiple scattering sample. The wavevector k_i have the same magnitude k_0 and vectors r_i gives the instantaneous position of the scattering particles. Note: $r_{i+1} - r_i$ does not equal k_i.

The main result of this derivation [1], obtained after averaging over many particles, is that for a path of total length $s = Nl$ with $N >> 1$ through the sample, the mean squared change in phase for the path is given by

$$\left\langle \Delta\theta_p^2(t) \right\rangle = \frac{2}{3} k_0^2 \left\langle \Delta r^2(t) \right\rangle \frac{s}{l^*} \tag{3.9}$$

This expression relates the mean square phase change of the light to the mean square displacement of the particle motion. Physically it says that phase depends on the path length *s* of the light and not any other path-dependent property. Further it says that the decay time of long light paths will be relatively short and the decay time of short paths will be relatively long. Now we can rewrite equation 3.6 as a sum over path lengths. Further, the fraction of scattered intensity in a path *p*, $\langle I_p \rangle / \langle I \rangle$, is replaced with the fraction of scattered intensity in a paths of length *s*, *P*(*s*), to obtain

$$g_1(t) = \sum_s P(s) \exp\left(-\frac{1}{3} k_0^2 \left\langle \Delta r^2(t) \right\rangle \frac{s}{l^*} \right) \tag{3.10}$$

This relates the decay of FACF to the motion of the scatterers. However, to proceed with the calculation of FACF an expression for the path-length distribution function *P*(*s*) is necessary.

The calculation of the path length distribution *P*(*s*) is where the diffusion approximation is used. Assuming that the light undergoes a large number of scattering events and for length scales much greater than the transport mean free path, l^*, the transport of light is accurately described by the diffusion equation

$$\frac{\partial U}{\partial t} = D_l \nabla^2 U \tag{3.11}$$

where *U* is the energy density of light (number of photons per unit volume) and D_l is the diffusion coefficient of the light. To obtain *P*(*s*) from *U*, consider the following simple thought experiment. An instantaneous pulse of light is incident over some area of the sample. If photons are sent into the sample at time $t = 0$, they will undergo random walks with step size *l*, scatter many times and emerge from the sample some time later. Those photons emerging at time *t* will travelled a distance $s = v_l t$ where v_l is the average speed of light in the medium [12]. The emerging flux of photons, *J*, will be directly proportional to the number of photons which travelled a path of length s, which is equivalent to the probability that a photon should travel that particular distance $P(s)$. Thus to find $P(s)$ we must compute J and this is done using Fick's law [13], $J = D_l \nabla U$. U is obtained by solving equation 3.11 with appropriate boundary conditions.

Clearly a solution to equation 3.11, and consequently $P(s)$, will depend on the geometry of the scattering situations. There are two basic experimental geometries in DWS experiments. The first is backscattering, where the light is incident on one side of the sample and the scattered light is detected from the same side, while in transmission detection is on the opposite side. For example, consider transmission through a very thick sample with sample thickness, L, much larger than l^*. If the sample is thick enough, all of the detected photons will have scattered more or less the same number of times and $P(s)$ can be approximated by a delta function. However in the backscattering geometry, some paths can be short and others long which is taken in account when deriving the expression for the autocorrelation function.

Weitz and Pine [1] solve the diffusion equation 3.11 for a variety of incident light configurations using appropriate boundary conditions. For the case of transmission geometry with planar illumination (laser beam diameter bigger than particle size), the FACF takes the following form

$$g_1(t) = \frac{\dfrac{L/l^* + 4/3}{z_0/l^* + 2/3}\left[\sinh\left(\dfrac{z_0}{l*}\sqrt{\dfrac{6t}{\tau}}\right) + \dfrac{2}{3}\sqrt{\dfrac{6t}{\tau}}\cosh\left(\dfrac{z_0}{l*}\sqrt{\dfrac{6t}{\tau}}\right)\right]}{\left(1+\dfrac{8t}{3\tau}+\dfrac{4l^*}{3l_a}\right)\sinh\left(\dfrac{L}{l^*}\sqrt{\dfrac{6t}{\tau}}\right) + \dfrac{4}{3}\sqrt{\dfrac{6t}{\tau}}\cosh\left(\dfrac{L}{l^*}\sqrt{\dfrac{6t}{\tau}}\right)} \qquad (3.12)$$

where $\dfrac{6t}{\tau} = k_0^2 \left\langle \Delta r^2(t) \right\rangle$, t is time, τ is characteristic time of the scatterers dynamics and $z_o = \gamma l^*$ is the distance over which the incident light is randomized. The scaling factor reflects the distance into the sample that light penetrates before it starts to diffuse. In data analysis the scaling factor γ was set to 1 as the most common value used [1, 7, 8]. Further, in any DWS experiments there will be always some absorption. Besides the heating effect, the effect of absorption is that it alters the distribution of light path lengths, $P(s)$, and in particular attenuates long paths more strongly than short ones. Weitz and Pine [1] showed that the effect of absorption is mathematically the same as a shift in time axis and that the expression for $g_1(t)$ can be adapted to account for absorption simply by making the substitution

$$\frac{t}{\tau} \to \frac{t}{\tau} + \frac{l^*}{2l_a} \tag{3.13}$$

where l_a is the absorption length of the sample. Using this substitution gives the final analytical expression for use in the analysis of my DWS experiments (transmission geometry)

$$g_1(t) = \frac{\dfrac{L/l^* + 4/3}{z_0/l^* + 2/3}\left[\sinh\left(\dfrac{z_0}{l^*}\sqrt{X}\right) + \dfrac{2}{3}\sqrt{X}\cosh\left(\dfrac{z_0}{l^*}\sqrt{X}\right)\right]}{(1+\dfrac{4}{9}X)\sinh\left(\dfrac{L}{l^*}\sqrt{X}\right) + \dfrac{4}{3}\sqrt{X}\cosh\left(\dfrac{L}{l^*}\sqrt{X}\right)} \tag{3.14}$$

where $X = k_0^2\left\langle \Delta r^2(t)\right\rangle + 3l^*/l_a$.

3.2.3 Measurement of parameters

There are two key parameters in equation 3.14 which must me measured. These are the transport free mean path, l^*, or step size in the random walk of photons, and the absorption path length l_a, which accounts for light absorption. In order to determine these parameters the method of static transmission [1, 14] is employed. In principle, measuring the total transmitted light, $T(L)$, as a function of the sample thickness L

determines the parameters l^* and l_a by fitting an appropriate theoretical expression to the experimental data. When the absorption of the sample is negligible, i.e. when absorption length is much greater than sample thickness, transmission [1] is given by

$$T(L) = \frac{5l^* / 3L}{1 + 4l^* / 3L} \tag{3.15}$$

Measuring of the total transmitted light is not trivial, so usually a small portion of the light transmitted in the forward direction is detected and compared with the light transmitted through a reference sample of the same thickness, with a known l^*, measured with the identical optical arrangement. Determination of the transport mean free path is straightforward by normalizing the two measured intensities.

However, we observed that absorption was not negligible for all the dense fluidized beds studied here. In this case the functional form of $T(L)$ is an exponential $\exp(-L/l_a)$ with decay parameter $1/l_a$ [14]. A simple but very good approximation for transmission in the absorption regime is given by

$$T(L) \approx \frac{l^*}{l_a} 2(\beta_R + \gamma) \frac{1}{1 + 2\beta_R l^* / l_a} e^{-L/l_a} \tag{3.16}$$

The parameter β_R accounts for the reflection of the diffusive light at the surface of the sample, i.e. $\beta_R = \frac{2(1+R)}{3(1-R)}$, where R is the diffusive reflection coefficient and the scaling factor γ is expected to be of the order of 1. The absorption path lengths of both the experimental and the reference sample, l_a and l_{aR} respectively, can be reliably determined from the slope of the experimental graph of $T(L)$ vs L, using equation 3.16 which represents the first step in this DWS calibration procedure.

The second step is experimental measurement of the transport mean free path of the reference sample, l_R^*. The reference sample was a dilute colloidal suspension of polystyrene particles in water (vigorously agitated before each measurement to make sure particles were suspended). Therefore, l_R^* can be independently determined by DWS measurement in the weak absorption regime by obtaining the electric-field autocorrelation function, and then inverting the following equation [1]

$$g_1(t) = \frac{\left(\frac{L}{l_R^*} + \frac{4}{3}\right)\sqrt{\frac{6t}{\tau}}}{\left(1 + \frac{8t}{3\tau}\right)\sinh\left(\frac{L}{l_R^*}\sqrt{\frac{6t}{\tau}}\right) + \frac{4}{3}\sqrt{\frac{6t}{\tau}}\cosh\left(\frac{L}{l_R^*}\sqrt{\frac{6t}{\tau}}\right)} \tag{3.17}$$

where $\tau = 1/(Dk_0^2)$ is the characteristic diffusion time of the scatterers. The diffusion coefficient D of the scatterers is calculated from the Stokes-Einstein relation $D = kT/6\pi r\mu$, where r is the particle radius.

Finally in the third step, the transport mean free path of the experimental sample l^* can be determined using

$$\frac{l_a}{l^*} = \frac{l_{aR}}{l_R^*}\left.\frac{T_R(L)}{T(L)}\right|_{L\to 0} + 2\beta_R\left(\left.\frac{T_R(L)}{T(L)}\right|_{L\to 0} - 1\right) \tag{3.18}$$

In order to have better accuracy both quantities l_R^* and l_{aR} should be close to the unknown l^* and l_a. The transport mean free path of the reference sample l_R^* can be changed by changing the concentration of the colloidal suspension, while the absorption length l_{aR} can be adjusted by adding a small amount of absorbing dye.

3.3 DWS experimental set-up

The dynamics of the particles in dense fluidized beds were studied using DWS in transmission mode. A typical DWS apparatus for use in the transmission mode is illustrated in Figure 3.3. The laser used for illuminating was a 400 mW diode pumped solid state linearly polarized laser (Torus 532, Laser Quantum Ltd., Cheshire, UK) operating at a wavelength of 532 nm in single longitudinal mode. A beam of monochromatic light of ~2 mm diameter from the laser was directed normally at the transparent wall of the vessel containing the granular medium. The light passed through the medium, scattering many times before exiting the back of the bed as a diffusion spot of ~ 20 mm diameter for beds of 10-20 mm thickness. The transmitted scattered light was collected over time, t, with a single mode optical fibre (OZ Optics Ltd., Ottawa, Canada). The collected light signal was then divided in a fibre bifurcation and fed into two matched photomultiplier tubes (PMTs) to reduce spurious correlations due to possible after pulsing effects of the detector which can happen if a PMT is subjected to a high intensity light pulse. In this case PMT output exhibits after pulsing, a non-zero residual signal. The intensity outputs $I(t)$ from the PMTs were amplified and fed to a multi-tau digital correlator (Flex 05, Correlator.com, US), which performed a pseudo cross-correlation analysis in real time to give the intensity autocorrelation function, $g_2(t)$. The latter was stored on a PC for further offline analysis as detailed below. In case of a liquid fluidized bed, the bed was fixed on a linear stage whose vertical and horizontal position could be adjusted to permit study along the height and across the width of the bed while leaving the optical arrangements undisturbed. However, this experimental arrangement was not possible in case of vibro-fluidized beds as the air-cooled electromagnetic driven shaker is too heavy. Instead both the laser and the fibre optic detector were mounted on linear stages so that different points above the base of the vibro-FBs could be investigated.

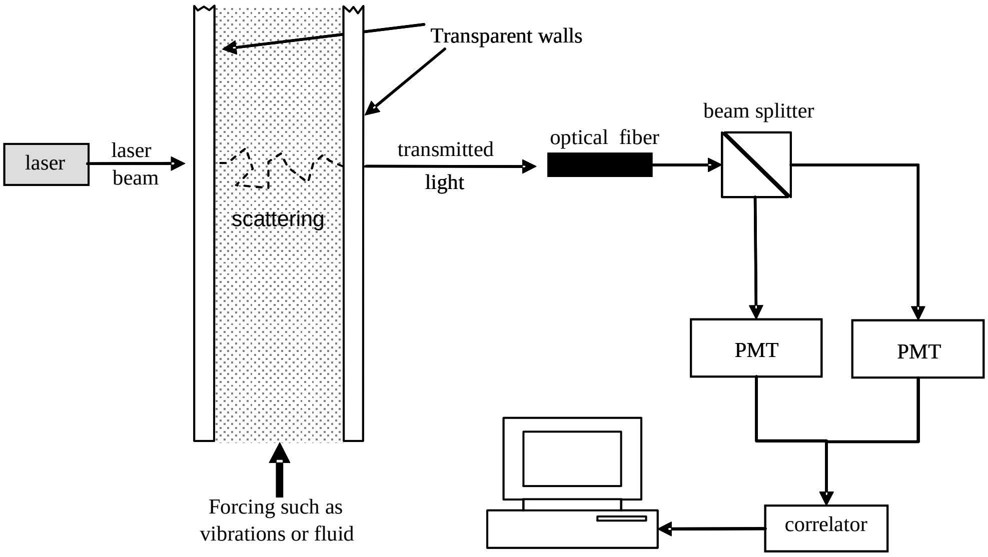

Figure 3.3. Schematic illustrating typical DWS apparatus in transmission geometry.

3.4 DWS data analysis

Output files containing the intensity autocorrelation function, $g_2(t)$, from a multi-tau digital correlator (Flex 05, Correlator.com, US) were then subjected to analysis to determine the velocity fluctuations. Briefly, the analysis involved first determining the normalized electric-field autocorrelation function, $g_1(t)$, from $g_2(t)$ using the Siegert relation, equation 3.3. First, β which is a phenomenological parameter determined primarily by the collection optics of the experiment, is obtained from the intercept of the IACF. Due to the noise at the beginning of the IACF, this free parameter was estimated by averaging of the fluctuating function over the first time steps as shown in Figure 3.4. Since there was no polarizer between the sample and the detector in our experimental set-up, β was always found to be ≈ 0.5 ($g_2(0) = 1.5$), as expected for non-polarized light. This indicates that we have detected only one coherence area and sampled a sufficient number of decorrelation times.

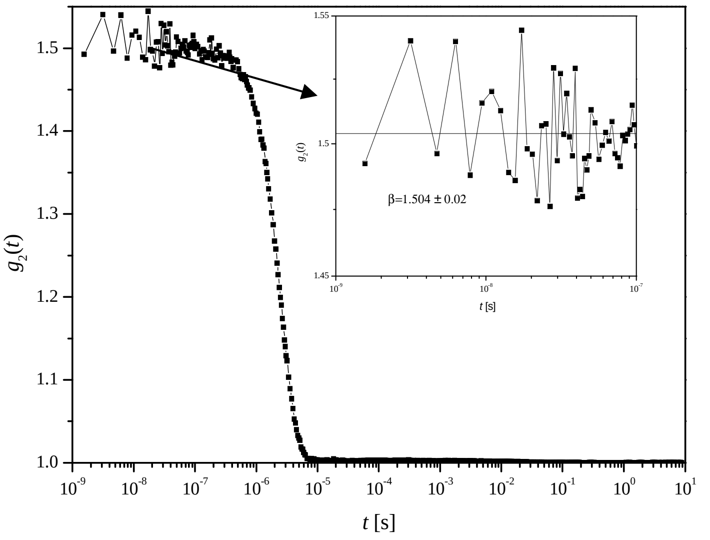

Figure 3.4. Determination of β from intensity autocorrelation function, $g_2(t)$.

Obtaining the FACF using the Siegert relation is the first step in data analysis of DWS experimental data as schematically shown in Figure 3.5. The second step is inverting the appropriate equation, for our DWS experimental set-up equation 3.14, to find the ensemble averaged mean square displacement of particles, $\left\langle \Delta r^2(t) \right\rangle$.The inversion is accomplished using the Matlab built-in root finding technique. Each particle remains in free flight for a short time until a collision with another particle, showing ballistic behaviour and linear dependence on a log-log plot in the short-time region as can be seen on figure 3.5. Therefore, the final step in data analysis is determination of the particle velocity fluctuations from the ballistic region of the MSD by fitting the curve at short time to the formula

$$\left\langle \Delta r^2(t) \right\rangle = \left\langle \delta v^2 \right\rangle t^2 \tag{3.19}$$

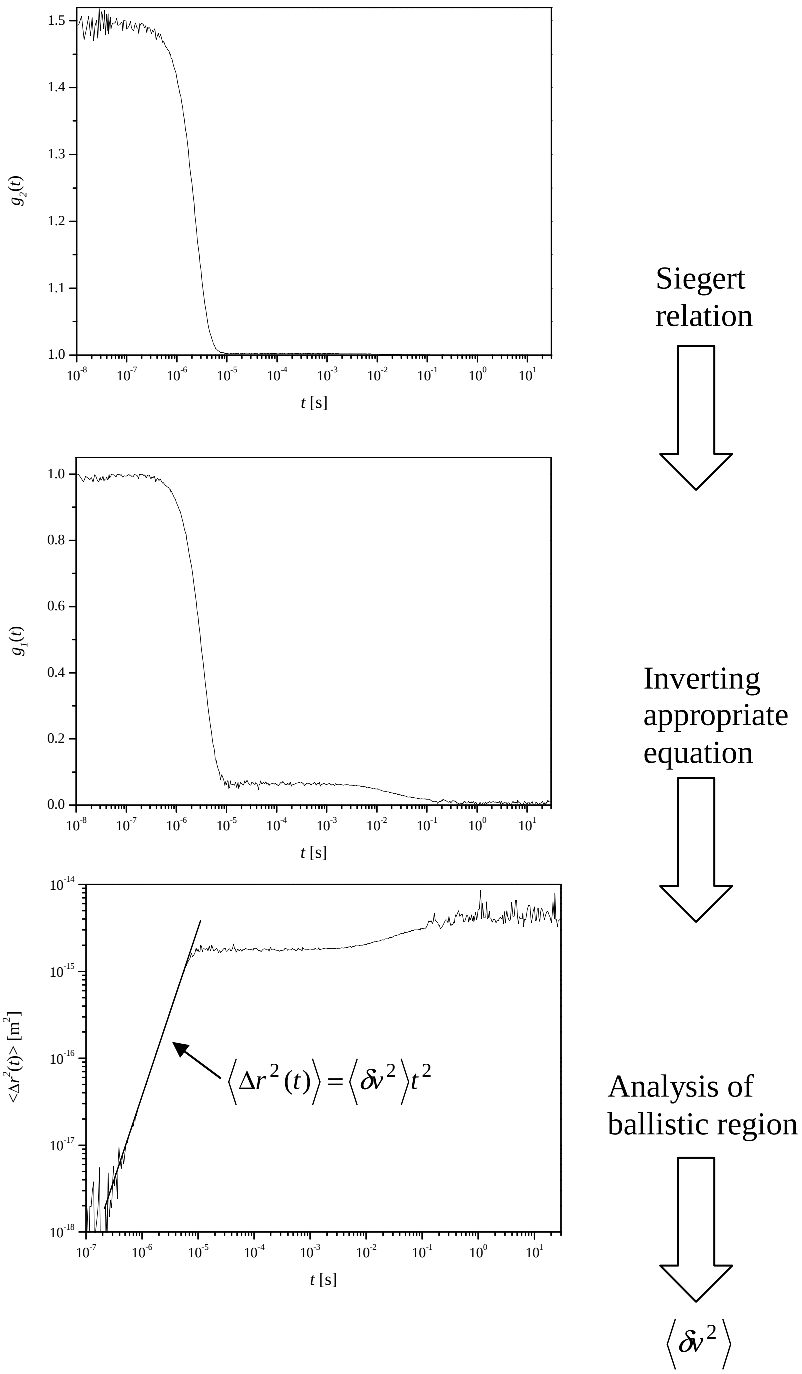

Figure 3.5. DWS experimental data analysis. See text for full explanation.

The ensemble averaged square of the particle velocity fluctuations $\left\langle \delta v^2 \right\rangle$ is the granular temperature averaged over a large volume of the scattering particles and over all three directions. We also fit the experimental data with the purely empirical relation [4, 15]

$$\left\langle \Delta r^2(t) \right\rangle = \frac{\left\langle \delta v^2 \right\rangle t^2}{1+(t/\tau_{dws})^2} \tag{3.20}$$

to obtain a decorrelation time, τ_{dws} which represents the time scale at which we probe the motion of the particles. Further, the product of the particle velocity fluctuations and decorrelation time gives a length scale at which we probe particle dynamics. In our DWS experiments these are the order of microseconds and tens of nanometers respectively.

3.5 DWS limitations

Although it is tempting to report a decorrelation time as a mean time between collisions and the product of granular temperature and decorrelation time as a mean free path of the particles [4, 6-9], the following argument shows that experimenters should be very careful in DWS data interpretation. As already discussed, the IACF decays after some time which is set by the time-scale required for light paths to change by a wavelength or, equivalently, by the time it takes the total phase of a characteristic path to change by ≈ 2π. For thick samples in which every photon undergoes many scattering events, the average photon will undergo $n_c \approx (L/l^*)^2$ scattering steps of length l^* so the average path length is $\langle s \rangle \approx n_c l^*$. Since all photons scatter approximately by the same number of times when in transmission mode, we can use this average path length to estimate a characteristic decay time by substituting into equation 3.9. and equating to $4\pi^2$

$$\left\langle \Delta r^2(t) \right\rangle = \frac{6\pi^2}{k_0^2}\left(l^* / L\right)^2 \tag{3.21}$$

At short time scales the particle moves ballistically such that $\left\langle \Delta r^2(t) \right\rangle = v^2 t^2$, which gives a final form for estimated decorrelation time

$$t_{dec} \approx \frac{\lambda}{v}\left(l^* / L\right)^2 \tag{3.22}$$

Assuming l^* is a tenth of the sample thickness, for a particle moving ballistically at velocity of the order of mm/s, this characteristic time is of the order of microseconds in accordance with our measurements. In this time, the particle will move only tens of nanometres which is only a small fraction of the particle diameter (order of millimetres in our studies) and of the mean particle distance, certainly for systems away from the close-packed limit as discussed in Chapter 4 for example.

Therefore, DWS will only resolve short time-scale and length-scale motion, even with several decay times, because of the experimental limitations of noise. There are other multiple light scattering techniques more suited to probe slower (long time) dynamics like multispeckle DWS [16, 17] and time-resolved correlation spectroscopy [18, 19]. These techniques are sensitive to similar length scales, but increase the timescale over which decorrelation can be accurately measured. To resolve larger length scale motion, the wavelength of the scattering field must be increased and a technique involving ultrasound has been developed – diffusing acoustic wave spectroscopy [15, 20]. This technique was applied to measure granular temperature in a liquid fluidized bed [15].

3.6 Conclusion

Diffusing wave spectroscopy (DWS) can overcome the microscopic limitations in a dense medium by using the principle that the photons scattered by mobile particles carry information about the dynamics of the particles. DWS is a non-intrusive measurement technique based on the light diffusion approximation. Secondly, the effects of the dynamics of the scattering medium are treated with a statistical approximation averaging over all light paths and all scattering events within each light path. These two approximations yield convenient analytical expressions for the autocorrelation function. By measuring the light autocorrelation function, the particle mean square displacement and its velocity fluctuations, i.e. granular temperature can be obtained.

References

1. Weitz, D.A. and D.J. Pine, *Diffusing-wave spectroscopy*, in *Dynamic Light Scattering: The Method and Some Applications*, W. Brown, Editor. 1993, Clarendon Press: Oxford. p. 652-720.
2. Maret, G., *Diffusing-wave spectroscopy*. Current Opinion in Colloid & Interface Science, 1997. **2**(3): p. 251-257.
3. Scheffold, F. and P. Schurtenberger, *Light scattering probes of viscoelastic fluids and solids*. Soft Materials, 2003. **1**(2): p. 139-165.
4. Menon, N. and D.J. Durian, *Diffusing-wave spectroscopy of dynamics in a three-dimensional granular flow*. Science, 1997. **275**: p. 1920-1922.
5. Menon, N. and D.J. Durian, *Particle motions in a gas-fluidized bed of sand*. Phys. Rev. Lett., 1997. **79**(18): p. 3407-3410.
6. You, S.Y. and H.K. Pak, *Study of the short-time dynamics of a thick and highly dense vibro-fluidized granular system by using diffusing wave spectroscopy*. Journal of Korean Physical Society, 2001. **38**(5): p. 577-581.
7. Xie, L., M.J. Biggs, D. Glass, A.S. McLeod, S.U. Egelhaaf, and G. Petekidis, *Granular temperature distribution in a gas fluidized bed of hollow microparticles prior to onset of bubbling*. Europhysics Letters, 2006. **74**(2): p. 268-274.
8. Biggs, M., D. Glass, L. Xie, V. Zivkovic, A. Buts, and M. Curt Koenders, *Granular temperature in a gas fluidized bed*. Granular Matter, 2008. **10**(2): p. 63-73.
9. Zivkovic, V., M.J. Biggs, D.H. Glass, P. Pagliai, and A. Buts, *Particle dynamics in a dense vibrated fluidized bed as revealed by diffusing wave spectroscopy*. Powder Technology, 2008. **182**(2): p. 192-201.
10. Zivkovic, V., M.J. Biggs, D. Glass, P. Pagliai, and A. Buts, *Granular temperature in a liquid fluidized bed as revealed by diffusing wave spectroscopy*. Chemical Engineering Science, 2009. **64**(5): p. 1102.
11. Lemieux, P.A. and D.J. Durian, *Investigating non-Gaussian scattering processes by using nth-order intensity correlation functions*. Journal of the Optical Society of America A, 1999. **16**(7): p. 1651-1664.
12. van Albada, M.P., B.A. van Tiggelen, A. Lagendijk, and A. Tip, *Speed of propagation of classical waves in strongly scattering media*. Physical Review Letters, 1991. **66**(24): p. 3132-3135.
13. Carslaw, H.S. and J.C. Jaeger, *Conduction of heat in solids*. 2nd ed. 1990, Oxford: Clarendon Press.
14. Leutz, W. and J. Rička, *On light propagation through glass bead packings*. Optics Communacation, 1996. **126**: p. 260-268.
15. Cowan, M.L., J.H. Page, and D.A. Weitz, *Velocity fluctuations in fluidized suspensions probed by ultrasonic correlation spectroscopy*. Physical Review Letters, 2000. **85**(2): p. 453-456.
16. Viasnoff, V., F. Lequeux, and D.J. Pine, *Multispeckle diffusing-wave spectroscopy: A tool to study slow relaxation and time-dependent dynamics*. Review Of Scientific Instruments, 2002. **73**(6): p. 2336-2344.

17. Zakharov, P., F. Cardinaux, and F. Scheffold, *Multispeckle diffusing-wave spectroscopy with a single-mode detection scheme.* Physical Review E, 2006. **73**(1): p. 011413.
18. Cipelletti, L., H. Bissig, V. Trappe, P. Ballesta, and S. Mazoyer, *Time-resolved correlation: a new tool for studying temporally heterogeneous dynamics.* Journal Of Physics-Condensed Matter, 2003. **15**(1): p. S257-S262.
19. Duri, A., H. Bissig, V. Trappe, and L. Cipelletti, *Time-resolved-correlation measurements of temporally heterogeneous dynamics.* Physical Review E, 2005. **72**(5): p. 051401.
20. Cowan, M.L., I.P. Jones, J.H. Page, and D.A. Weitz, *Diffusing acoustic wave spectroscopy.* Physical Review E, 2002. **65**(6): p. 066605.

Chapter 4 Granular temperature in a liquid fluidized bed

4.1 Introduction

Much of the available experimentally determined granular temperature data is for gas fluidized beds (see for example Biggs et al. [1] and references therein) due to their extremely wide industrial application. However, liquid fluidized beds are of increasing interest as they find application in hydrometallurgy, food technology, biochemical processing, electrochemical reactions and water treatment [2]. In addition, liquid fluidized beds expand homogenously in contrast to gas fluidized beds, which are usually unstable and give rise to bubbling behaviour. This makes liquid fluidized beds particularly suitable for testing nearly-homogenous two-phase flow models across a wide range of solid fractions [3].

In the last decade, there have been several experimental studies of velocity fluctuations in liquid fluidized beds, although for very limited ranges of experimental conditions. Limtrakul [4], Kiared et al. [5] and Limtrakul et al. [6] used non-invasive radioactive particle tracking techniques to measure velocity fluctuations. Their work was, however, focused on the radial distribution of the granular temperature (amongst other quantities). Segre and McClymer [7] and Tee et al. [8] used particle image velocimetry (PIV) to measure velocity fluctuations in a very dilute system at a mean solid fraction of around 0.1. Gidaspow and Huilin [9] determined velocity fluctuations for a few solid fractions in a two dimensional liquid fluidized bed using a video imaging technique of particle streak photography. Spinewine et al. [10]

employed a stereoscopic particle tracking method and found that the velocity fluctuations decreased monotonically with increasing solid fraction. Using diffusing acoustic wave spectroscopy (DAWS), Cowan et al. [11] observed on the other hand a weak maximum in granular temperature at intermediate solid fractions.

In this chapter a detailed study of the granular temperature in a liquid fluidized bed is reported. Using diffusing wave spectroscopy (DWS), the spatial variation of the granular temperature along with the associated local solid fractions for a thin, rectangular bed of small glass particles fluidized by water across a wide range of superficial velocities (i.e. mean solid volume fractions) is determined. An outline of the experimental set-up and the experimental procedures used is given, followed by presentation of the results obtained and their discussion.

4.2 Experimental section

4.2.1 Experimental set-up

The fluidized bed apparatus is illustrated in Figure 4.1(a). A half metre high rectangular bed of 200 mm by 20 mm cross-section was mounted on a linear stage so that different points of the bed could be investigated with ease. The distributor, which consisted of a stainless steel mesh of 40 μm apertures and a 5 cm deep packed bed of 1.5 mm stainless steel beads, was designed to provide highly uniform and homogeneous fluidization. Water was pumped by a centrifugal pump from a feed reservoir through the bed before being passed back into the reservoir via an overflow at the top of the bed. The water flow rate was measured by a calibrated rotameter (KDG 2000, KDG flowmeters, UK) and the temperature of the water was maintained at 20 ± 0.5° C. As outlined in Chapter 3, typical DWS transmission set-up is used. The bed was fixed on a linear stage whose vertical and horizontal position could be adjusted to permit the study of the bed along its height and across its width as shown in Figure 4.1(b).

The fluidized bed material was made up of SiLibeads type S glass particles (Sigmund Lindner, UK) of density ρ_p = 2500 kg/m^3. The as-supplied particles were carefully sieved between two close meshes to obtain a narrow diameter distribution of $d_p = 165 \pm 15$ µm. The height of material in the fluidized bed when de-fluidized was 75 mm.

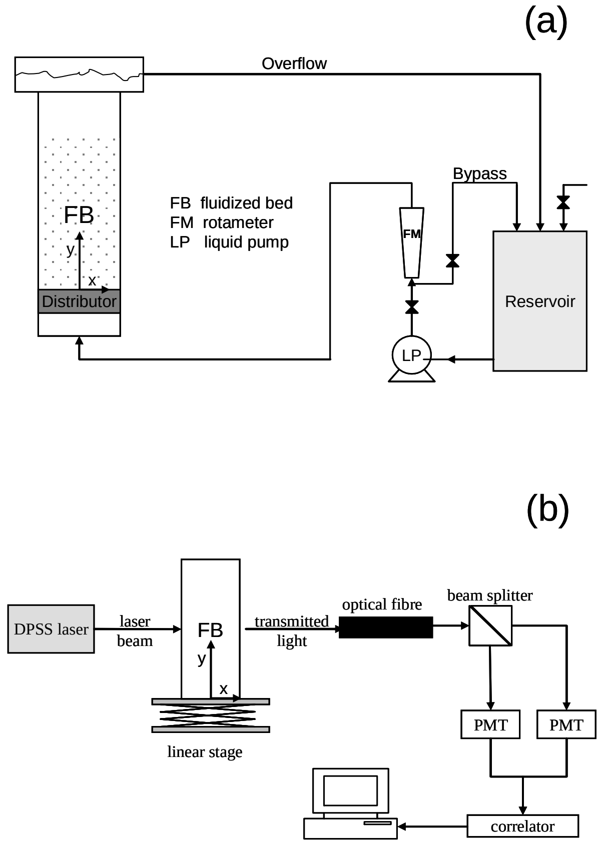

Figure 4.1. Schematic diagram of (a) liquid fluidized bed apparatus and (b) DWS apparatus.

4.2.2 Experimental procedure

The local solids (volume) fraction and granular temperature were determined using the procedures described below at various points across the bed width, x, and above the distributor, y, for superficial velocities in the range of $0.05U_t \leq U_0 \leq 0.49U_t$, where U_t is the particle terminal velocity estimated by fitting the Richardson-Zaki correlation [12] to the bed expansion data; the lower bound of this velocity range is very close to the minimum fluidization velocity, $U_{mf} \approx 0.04U_t$, as estimated by extrapolating the expansion data to a mean solid fraction of $\langle\phi\rangle = 0.55$. Measurements were restricted to points at least 50 mm above the distributor to avoid channelling that occurred under some conditions in the region of $0 \leq y \leq 30$ mm, and 20 mm away from side boundaries to ensure no light paths are cut off at aluminium side-walls.

In a steady-state regime of fluidization, the height of the interface between fluidized particles and clear fluid at the top of the bed, h, was identified and measured with an accuracy of ± 1 mm using a measuring tape attached to the fluidized bed. This height was used to determine the mean bed voidage, $\langle\varepsilon\rangle$, and mean solid fraction, $\langle\phi\rangle$, via

$$\langle\varepsilon\rangle \equiv 1-\langle\phi\rangle = 1-\frac{m_p}{\rho_p A_r h} \tag{4.1}$$

where m_p is the mass of fluidized particles (440 g here) and A_r is the cross-sectional area.

The solid fractions at points in the fluidized bed (i.e. the local solid fractions) were determined by comparing the intensity of the laser light transmitted through the liquid fluidized bed at the points with that transmitted through a reference sample of the same thickness, I/I_r, following the calibration procedure of Duru et al. [13]; this method was found to give slightly better results than a related method of Segre and McClymer [7] and Tee et al. [8]. The light intensity was detected and recorded with a digital optical power meter (Model 815, Newport Corporation, US). The signals were averaged over 60 s, a time much larger than the expected period of any density waves. Figure 4.2 shows height averaged values of light transmission as a function of the mean solid fraction; the curve was described very well by a first-order exponential decay (coefficient of determination $R^2 = 0.99952$).

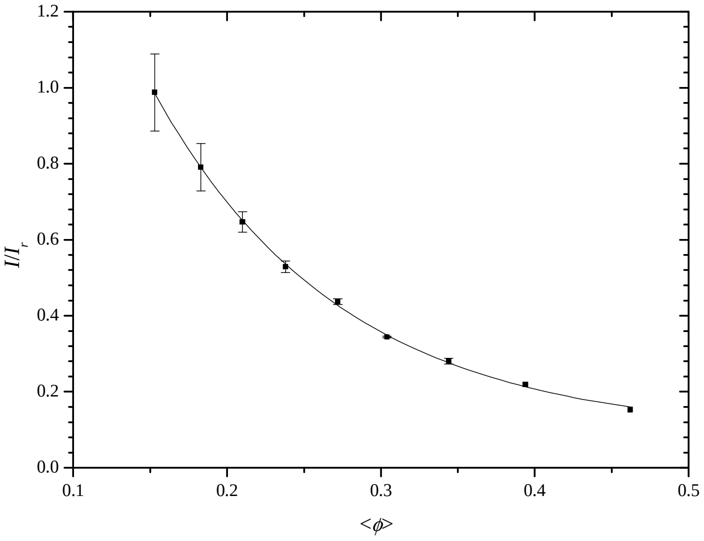

Figure 4.2. Variation of the height averaged normalized transmitted light intensities, I/I_r, with the mean solid fraction, $\langle\phi\rangle$. Error bars are standard deviation of measurements. Solid line corresponds to first order exponential decay function fit.

Intensity autocorrelation functions (IACF) were obtained by collecting and correlating ten blocks of data each 30 s long for each measurement point at each specific flow condition. Each IACF was then subject to the data analysis procedure described in Chapter 3 to obtain the granular temperature.

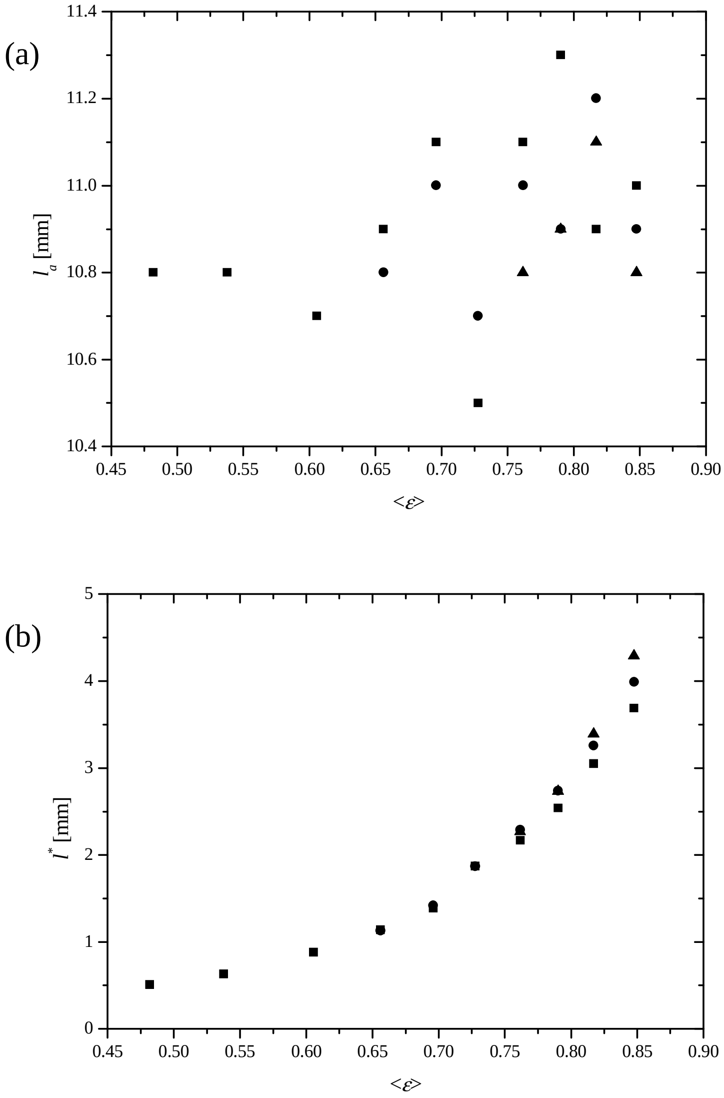

Figure 4.3. Variation of (a) absorption path length and (b) transport mean free path with the overall bed voidage, $\langle\varepsilon\rangle$, for y = 70 mm (square), y = 110 mm (circle) and y = 150 mm (triangles) above the distributor.

Two key parameters, the transport mean free path l^* , or step size in the random walk of photons, and the diffusive absorption length, l_a, which accounts for light absorption, were determined as a function of overall bed voidage and spatial position using the static transmission method [14] as already described in Chapter 3. The reference sample was an 0.1 vol % aqueous suspension of latex spheres (0.6 μm polystyrene, G. Kisker GbR., Germany) whose mean free path and absorption path length obtained from DWS measurement are $l_R^* = 2.30$ mm and $l_{aR} = 11.2 \pm 0.1$ mm respectively. Three beds of thickness $L = 20$, 25 and 30 mm were used for transmission measurement.

Transmitted light intensity was found to vary little across the bed width, indicating that l_a and l^* at a given bed voidage are dependent on height above the distributor only. In line with the results for a gas fluidized bed [1], it was found that l_a varies little with solid fraction and height as figure 4.3(a) shows. It was, therefore, assumed to be an average of the values determined; i.e. $l_a = 10.9 \pm 0.3$ mm.

Figure 4.3(b), which shows variation of the transport mean free path with the overall bed voidage for three heights above the distributor, indicates that l^* increases with the bed voidage and varies with bed height only for the higher voidages. This indicates a non-uniform solid fraction distribution along the bed height in the case of a dilute liquid fluidized bed – we shall return to this point in more detail in section 4.3.3.

4.3 Results and discussion

4.3.1 Fluidized bed expansion

A series of steady-state experiments was conducted to determine the relationship between fluidization superficial velocity, U_0, and overall bed voidage, $\langle\varepsilon\rangle$. The expansion curve, presented in Figure 4.4, is described well (coefficient of determination $R^2 = 0.99877$) by the Richardson-Zaki [12] correlation

$$\frac{U_0}{U_t} = \left\langle \varepsilon \right\rangle^n \tag{4.2}$$

The parameters of above correlations were evaluated using the following correlations proposed by Khan and Richardson [15]

$$\frac{4.8 - n}{n - 2.4} = 0.043 Ga^{0.57} \tag{4.3}$$

$$\mathrm{Re}_t = (2.33 Ga^{0.018} - 1.53 Ga^{-0.016})^{13.3} \tag{4.4}$$

where the Galileo number, Ga, and the terminal Reynolds number, Re_t, are given by

$$Ga = \frac{(\rho_p - \rho_l)\rho_f d_p^3 g}{\mu}; \mathrm{Re}_t = \frac{U_t \rho_f d_p}{\mu} \tag{4.5}$$

Here ρ_f is the fluid density, μ is the fluid viscosity and g is the acceleration due to gravity, while d_p and ρ_p are particle diameter and density respectively. The fitted values of parameters, $n = 4.04 \pm 0.03$ and $U_t = 16.1 \pm 0.2$ mm/s, are very close to values of $n = 4.03$ and $U_t = 17.25$ mm/s predicted using above correlations.

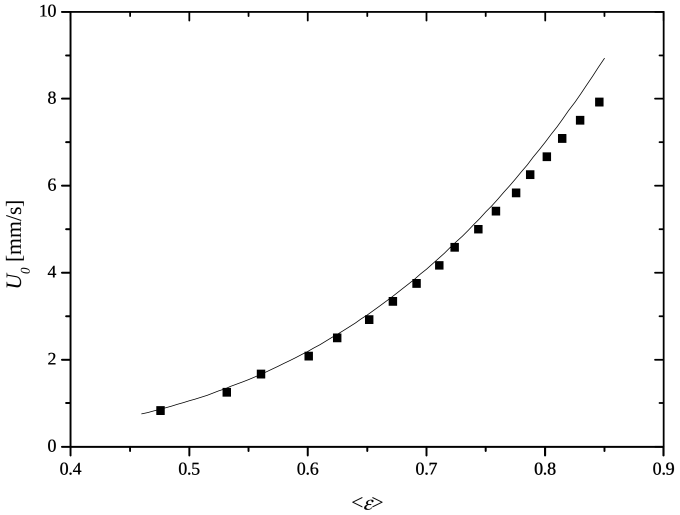

Figure 4.4. Expansion curve of the liquid fluidized bed. Solid line corresponds to Richardson-Zaki equation using Khan-Richardson correlated values.

4.3.2 Autocorrelation functions and particle MSD

The example intensity autocorrelation function (IACF) shown in Figure 4.5(a) first decays over the timescale of 10^{-6} to 10^{-5} s from a plateau of $g_2 \approx 1.5$ to a second plateau of $g_2 \approx 1.002$ before finally decaying to unity at $t \approx 10^{-1}$ s. As the expected dominant frequency for homogenous liquid fluidization is in the region of 4-8 Hz [16], a possible origin of this second decay is light intensity fluctuations arising out of density waves. The timescales seen in the IACF are reflected and enhanced in the normalised electric field autocorrelation function (FACF) obtained from the IACF using the Siegert relationship as shown in figure 4.5(b).

The mean square displacement (MSD) obtained from inversion of equation 3.14 using the FACF is shown in figure 4.5(c). Quantitative analysis of the ballistic region of this MSD using equation 3.19 gives a particle velocity fluctuation of $\langle \delta v^2 \rangle^{1/2}$ =

5.78 mm/s. We also fit the experimental data with the purely empirical relation [17, 18]

$$\left\langle \Delta r^2 \right\rangle = \frac{\left\langle \delta v^2 \right\rangle t^2}{1 + \left(t / \tau_{dws} \right)^2} \tag{4.6}$$

to obtain the same value of the velocity fluctuation and a decorrelation time of τ_{dws} = 7.02 μs.

The product of the granular temperature and decorrelation time obtained from figure 4.5(c) gives a length scale Δs = 40.6 nm at which we probed the particle dynamics. This is only a small fraction of the mean particle diameter and, indeed, the mean inter-particle distance, which is estimated following Wu [19] to be between 50-175 μm for the mean solid fraction here, $\langle \phi \rangle$ = 0.238 , depending on the particle packing type. This clearly indicates that the granular temperature is being measured.

A further check on the validity of our measurements is the time criterion proposed by Breault et al. [20], which requires the temporal sampling resolution to be smaller than the collision time estimate

$$\tau_c = \frac{d_p}{6\phi\delta v} \tag{4.7}$$

For the conditions relevant to figure 4.5, $\tau_c \approx 0.02$ s. As the 2 ns temporal resolution of our DWS apparatus is much less than this time, we certainly can claim measurement of granular temperature. This criterion was satisfied for all the measurements reported here. Therefore, granular temperature was measured rather than turbulent or bulk translational particle kinetic energy [20]. Furthermore, the later type of velocity fluctuations arises from bulk flow, which is not present here as a small mean particle velocity is expected for a liquid fluidized bed (unless bulk solid circulation patterns occurs due to non-uniform liquid distribution which was not the case here).

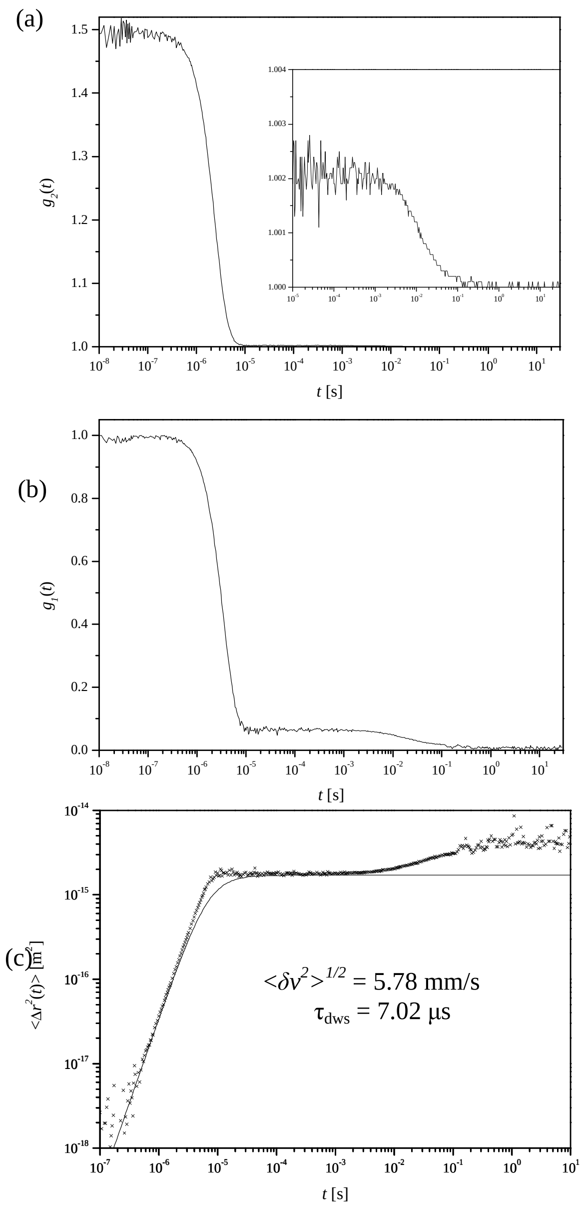

Figure 4.5. (a) The intensity autocorrelation function, g_2, evaluated using transmitted intensity data obtained at a point on the centreline of the bed and y = 70 mm above the bed distributor for a superficial velocity of U_0 = 5.42 mm/s; the insets shows the long-time approach to unity. (b) The normalised electric field autocorrelation function, g_1, obtained from g_2 using the Siegert relationship, equation 3.3. (c) The mean square displacement obtained from g_1 by inverting equation 3.14; the mean fluctuation velocity, $\langle \delta v^2 \rangle^{1/2}$, and decorrelation time, τ_{dws}, are indicated. The solid line is fitted to the empirical equation 4.6.

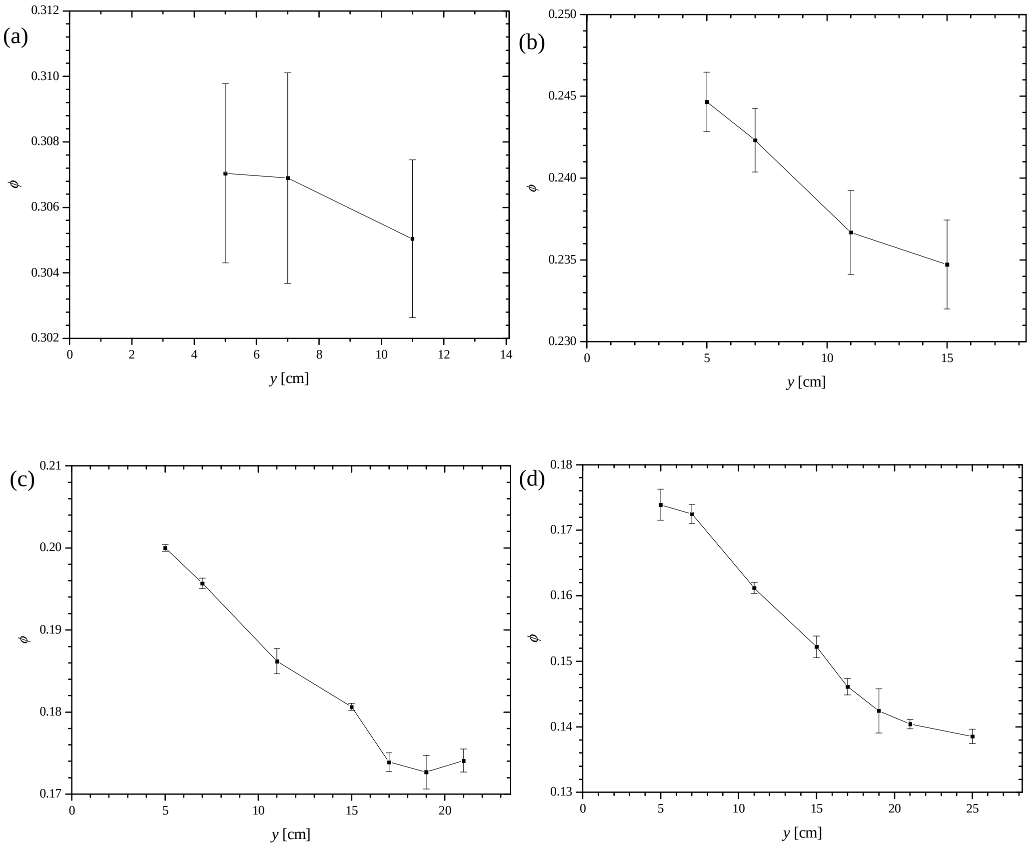

Figure 4.6. Solid fraction, ϕ, as a function of height, y, for four different mean solid fractions: (a) $\langle\phi\rangle = 0.306$ ($U_0 = 0.233U_t$), (b) $\langle\phi\rangle = 0.238$ ($U_0 = 0.336U_t$), (c) $\langle\phi\rangle = 0.183$ ($U_0 = 0.440U_t$), and (d) $\langle\phi\rangle = 0.153$ ($U_0 = 0.492U_t$) measured along the centreline. The right borders of graphs represent the mean fluidized bed heights, h. Error bars are standard deviations of the three experimental runs**.**

4.3.3 Spatial variation of solid volume fraction

Transmission measurements showed no significant variation in the solid fraction across the bed width, *x*, for all superficial velocities considered. We thus assumed the solid fraction to be a function of height above the distributor, *y*, only. As illustrated in figure 4.6(a), the fluidized bed is essentially homogenous at higher mean solid fractions (i.e. lower superficial velocities). However, below mean solid fractions of $\langle \phi \rangle = 0.238$, the local solid fraction, ϕ, decays with height above the distributor with the rate of decay increasing as the mean solid fraction decreases, figure 4.6(b)-(d). The variation of local solids fraction with height above the distributor seen here is in line with the experimental observations of both Segre and McClymer [7] and Tee et al. [8]. The latter workers showed that this variation can be ascribed to particle size polydispersity [8]. However, Segre and McClymer [7] observed little change in the variation of local solids fraction with height when the size polydispersity, σ_d/d_p, was decreased from 0.095, which is similar to that here, to just 0.015. This implies more work is necessary on this subject to find other possible causes for the phenomenon.

4.3.4 Spatial variation of granular temperature

Figures 4.7(a-c) show lateral profiles of the particle velocity fluctuations, $\langle \delta v^2 \rangle^{1/2}$, for three different mean solid fractions at y = 70 mm above distributor; for the mean solid fractions of $\langle \phi \rangle = 0.394$ and $\langle \phi \rangle = 0.238$, this represents the middle part of the bed, while in the third case this point is located in the bottom third of the bed (similar lateral profiles were also observed for the smallest mean solid fraction of $\langle \phi \rangle = 0.153$ in the middle and top parts of the bed). These results strongly suggest that the velocity fluctuations do not vary in any significant way across the bed width. Similarly, previous experimental studies in a cylindrical geometry [4, 5] show no apparent radial variation especially for denser particles such as glass beads. This is in contrast to the experimental finding of Limtrakul et al. [6], who found a higher value of velocity fluctuations close to the wall. One possible reason for this is a larger influence of the outer walls in the cylindrical column used in their study than that of the (quasi-2D) rectangular geometry used here, as pointed out by Cornelissen et al. [21], whose CFD simulations show little variation of velocity fluctuations across the bed width except very close to the wall ($2x/W \geq 0.7$-0.8). Unfortunately, as indicated above, even if such variations do exist, we are unable to detect them in this region due to experimental constraints.

The axial profiles of velocity fluctuations are shown in figures 4.8(a-d). Similarly to the solid fraction, velocity fluctuations vary little with height above the distributor when the mean solid fraction is sufficiently great, figure 4.8(a). Figures 4.8(b)-(d) show, on the other hand, that below a mean solid fraction of $\langle\phi\rangle = 0.238$, the velocity fluctuations do vary with height above the distributor. Although the fluctuations essentially increase with height for $\langle\phi\rangle = 0.238$, figure 4.8(b), there is strong evidence for the velocity fluctuations taking on a maximum in the middle of the bed at lower mean solid fractions, figure 4.8(c)-(d) – we will return to this below.

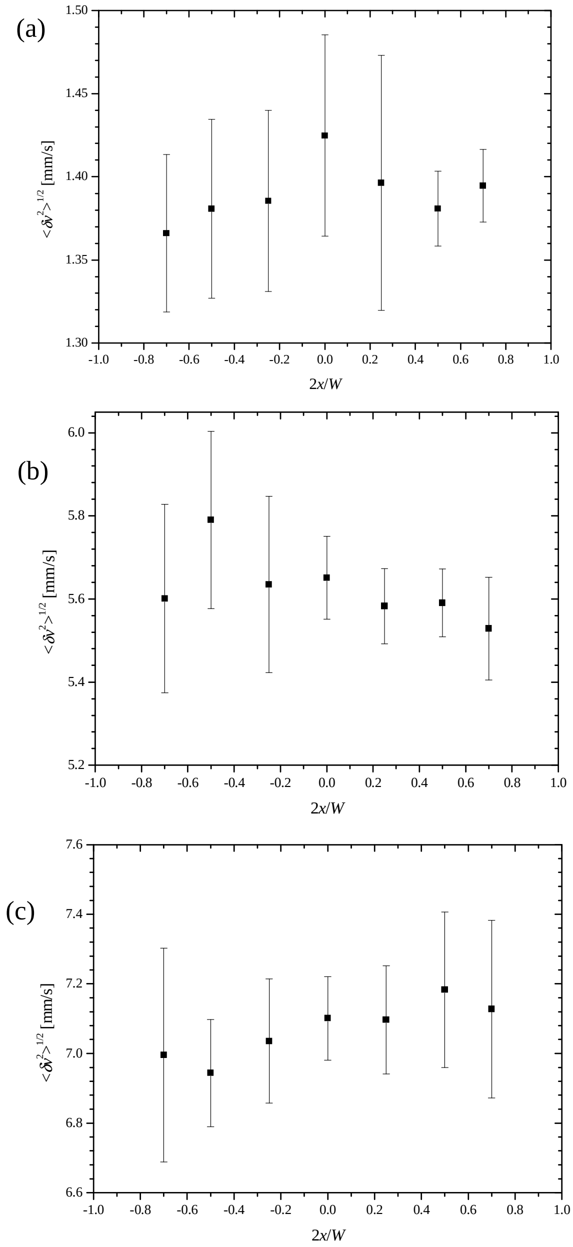

Figure 4.7. The variation of particle velocity fluctuations, $<\delta v^2>^{1/2}$, with dimensionless lateral position $2x/W$ (W is the bed width) for three different mean solid fractions: (a) $\langle \phi \rangle = 0.394$ ($U_0 = 0.129U_t$), (b) $\langle \phi \rangle = 0.238$ ($U_0 = 0.336U_t$), and (c) $\langle \phi \rangle = 0.153$ ($U_0 = 0.492U_t$) measured at $y = 70$ mm above distributor. Error bars are standard deviations of the three experimental runs.

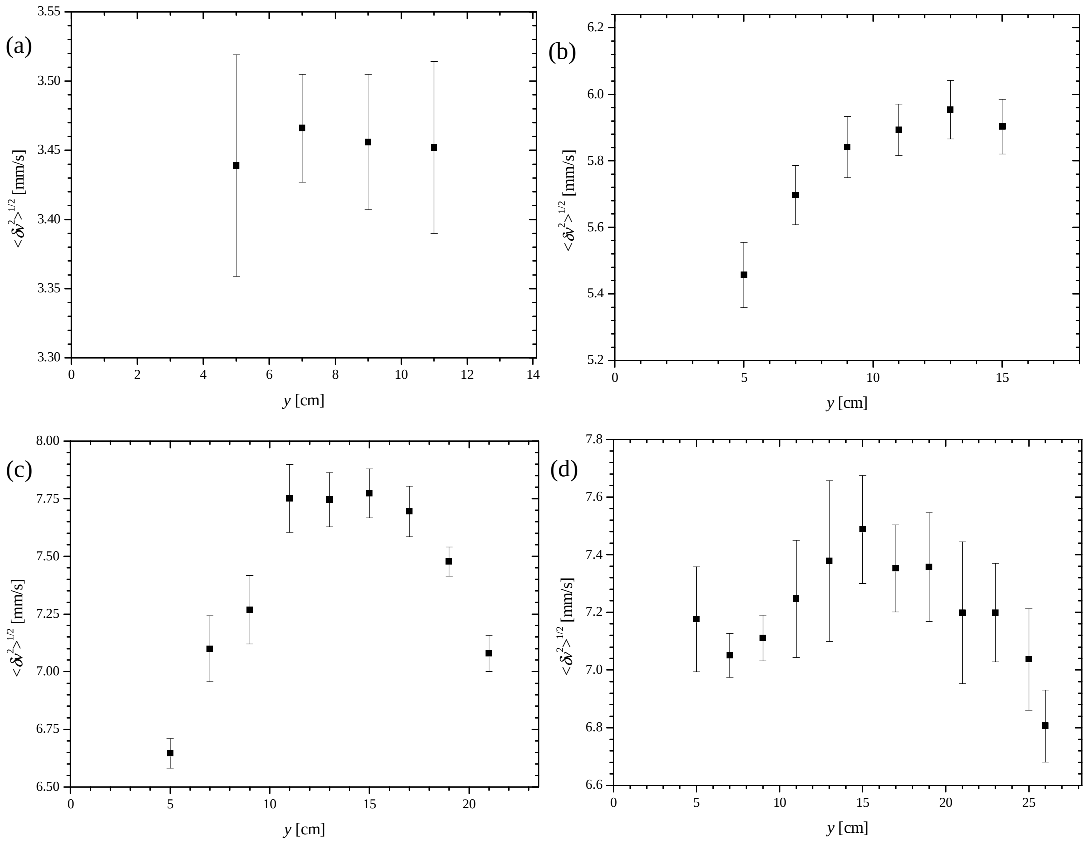

Figure 4.8. The particle velocity fluctuations, $<\delta v^2>^{1/2}$, as a function of measuring height, y, for four different mean solid fractions: (a) $\langle\phi\rangle = 0.306$ ($U_0 = 0.233U_t$), (b) $\langle\phi\rangle = 0.238$ ($U_0 = 0.336U_t$), (c) $\langle\phi\rangle = 0.183$ ($U_0 = 0.440U_t$), and (d) $\langle\phi\rangle = 0.153$ ($U_0 = 0.492U_t$) measured along the centreline. The right borders of graphs represent the mean FB heights, h. Error bars are standard deviations of the three experimental runs.

4.3.5 Relationship between solid fraction and granular temperature

Figure 4.9(a) shows the variation of height averaged values of the velocity fluctuations with superficial velocity. The velocity fluctuations are of the same order of magnitude as the driving velocity and increase with superficial velocity up to a maximum at U_0 = 7.5 mm/s. In order to explain the observed maximum, we re-plot the data to obtain the variation of $\overline{\left\langle \delta v^2 \right\rangle}^{1/2}$ with the mean solid fraction as shown in figure 4.9(b).

This exhibits a maximum at ϕ = 0.175, although there is only one point below this critical solid fraction. Unfortunately, DWS measurements for more dilute cases were impossible due to an increase of *l** which led to a breakage of the diffusion approximation. This is in line with the simulations of Gevrin et al. [3], who observed a maximum in the granular temperature at a solid fraction close to ϕ = 0.2. We failed to fit our experimental data with the semi-empirical scaling law of Gevrin et al. [3]. However, we have found that our data can be well fitted with a log-normal function (coefficient of determination R^2 = 0.9958)

$$\left\langle \delta v^2 \right\rangle^{1/2} = A + \frac{B}{w\phi\sqrt{2\pi}} e^{-\frac{\ln(\phi/\phi_c)^2}{2w^2}} \tag{4.8}$$

where the parameters take the values of A = -0.86251 ± 0.38315, B = 2.20953 ± 0.11422, w = 0.55518 ± 0.04081 and ϕ_c = 0.22496 ± 0.00573. Whilst there is clearly little physical basis for our use of the log-normal function, it does provide an analytical expression that is of ready use to others.

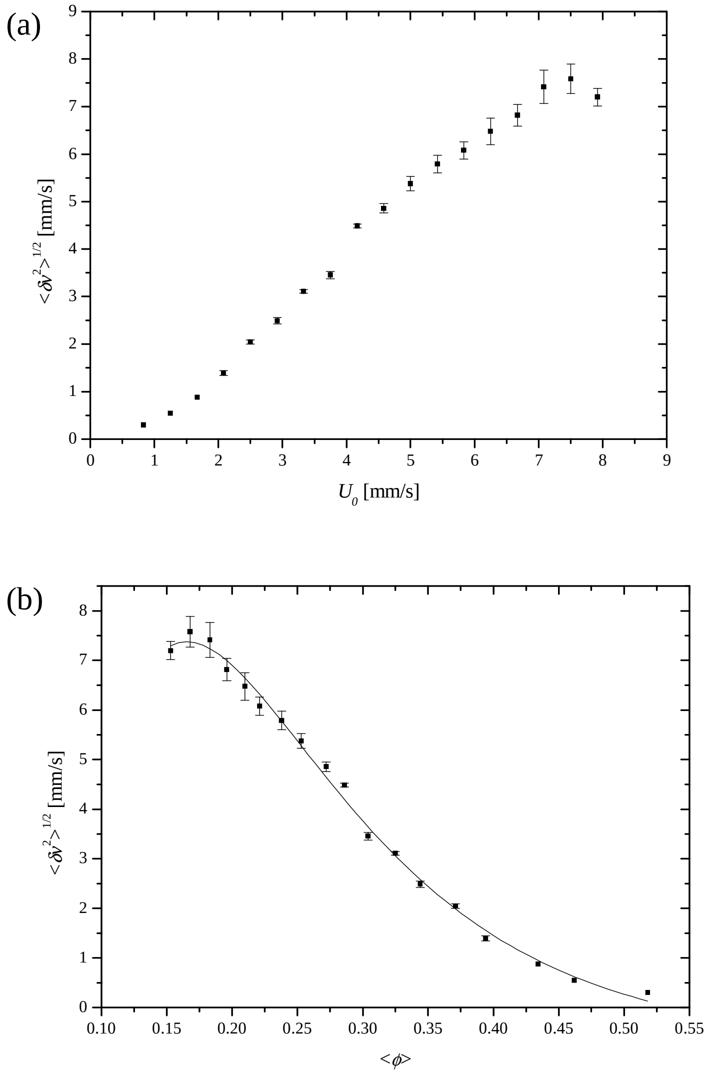

Figure 4.9. The variation of height averaged values of particle velocity fluctuations, $\overline{\langle \delta v^2 \rangle}^{1/2}$ with superficial velocity, U_0 (a) and with the mean solid fraction, $\langle \phi \rangle$, (b). Solid line on graph (b) is the log-normal fit. Error bars are standard deviations of height averaged particle velocity fluctuations.

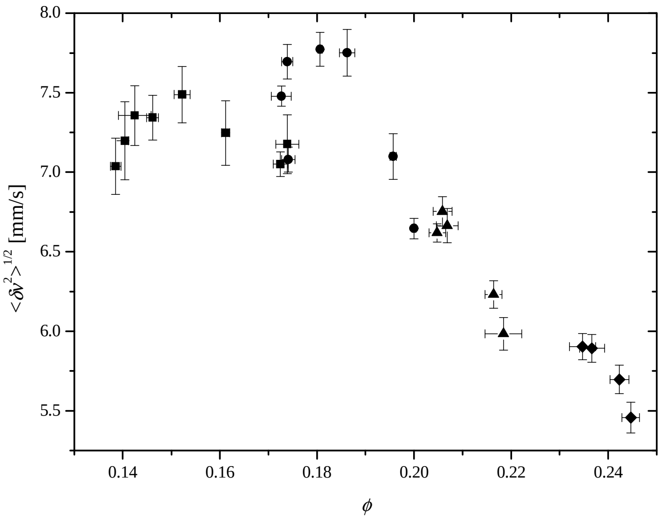

Figure 4.10. The variation of local velocity fluctuations, $<\delta v^2>^{1/2}$, with local values of solid fraction, ϕ. The symbols represent data for different mean solid fractions $\langle \phi \rangle = 0.153$ ($U_0 = 0.492U_t$) (squares), $\langle \phi \rangle = 0.183$ ($U_0 = 0.440U_t$) (circles), $\langle \phi \rangle = 0.210$ ($U_0 = 0.388U_t$) (triangles), and $\langle \phi \rangle = 0.238$ ($U_0 = 0.336U_t$) (diamonds). Error bars are standard deviations of both measured variables. Solid line is fit to the log-normal function.

To further investigate the link between granular temperature and solid fraction, we combined vertical profiles of solid fraction (Figure 4.6) and the velocity fluctuations (Figure 4.8) to yield Figure 4.10, which shows the local velocity fluctuations plotted against the local solid fraction. Although this figure suffers from significant experimental uncertainty, the trends are similar to those seen in figure 4.9, with a maximum occurring at $\phi \approx 0.18$. Comparison now of Figures 4.6(c)-(d) with their counterparts in Figures 4.8(c)-(d) in light of this finding explains the maxima observed in the latter.

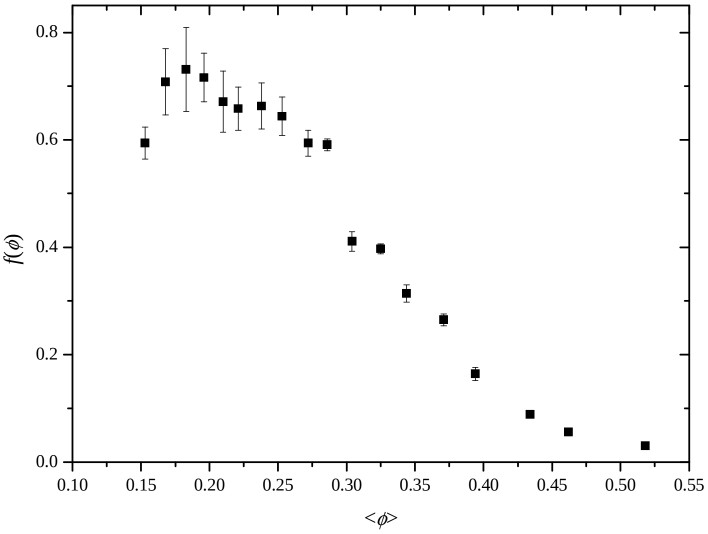

Figure 4.11. Function $f(\phi)$ in equation 4.10 derived from height averaged data shown in figure 4.9. Error bars are standard deviation of derived function.

Batchelor [22] hypothesised that for uniform fluidized bed the mean particle velocity averaged over a cross-section of a uniform fluidized bed, *v*, and the particle velocity fluctuations are related by a function of the solid fraction only

$$\delta v^2 = H(\phi)v^2 \tag{4.9}$$

If we assume that the mean particle velocity, *v*, is proportional to the mean slip velocity, $U_{sv}=U_0/(1-\langle\phi\rangle)$, equation 4.9 can be re-written as [1]

$$\delta v^2 = f(\phi)U_{sv}^2 \tag{4.10}$$

Figure 4.11 shows the function $f(\phi)$ derived from height averaged data shown in figure 4.9 using equation 4.10. Whilst again there are just a few points in the dilute region, the function is very much in line with that described by Batchelor [22] – it increases with solid fraction to a maximum at $\phi \approx 0.18$, reflecting the growing importance of particle-particle collisions, and than decreases to zero as ϕ approaches the close-packed limit where particles are unable to move freely.

4.4 Conclusion

Diffusing wave spectroscopy has been used to measure the particle velocity fluctuations, $\langle \delta v^2 \rangle^{1/2}$, of 165 μm glass particles (ρ_p = 2500 kg/m^3) in a thin, rectangular water fluidized bed. These fluctuations were determined at various heights above the distributor and across the bed width for a wide range of superficial velocities. Our data shows that the velocity fluctuations are of the same order as the superficial velocity. The velocity fluctuations were found to be essentially invariant across the bed width irrespective of the superficial velocity. The velocity fluctuations were also invariant with bed height for superficial velocities below $U_0 = 0.336U_t$, where U_t is the particle terminal velocity estimated by fitting the Richardson-Zaki correlation [12] to the bed expansion data. It was, however, observed to vary with height above the distributor for $U_0 > 0.336U_t$, with a maximum being observed at a point that moved from the bottom to the top of the bed as the superficial velocity increased.

The spatial variation of the solids volume fraction was additionally determined using a light transmission method. As with the velocity fluctuations, the solid fraction was found to be uniform across the bed width irrespective of the superficial velocity, and uniform throughout the bed for $U_0 < 0.336U_t$. It was, however, observed to decrease with height above the distributor for $U_0 \geq 0.336U_t$.

By comparing both the mean and local solid fraction data with the corresponding velocity fluctuation data, it was shown that the latter may be described solely in terms of the solids volume fraction, ϕ. It was found that the velocity fluctuations increase with solid fraction to a maximum at $\phi \approx 0.18$, reflecting the growing importance of particle-particle collisions, before decreasing to zero as ϕ approaches the close-packed limit where particles are unable to move freely. This behaviour is in accord with previous theoretical descriptions [22] and simulation results [3].

References

1. Biggs, M., D. Glass, L. Xie, V. Zivkovic, A. Buts, and M. Curt Koenders, *Granular temperature in a gas fluidized bed.* Granular Matter, 2008. **10**(2): p. 63-73.
2. Fan, L.S., *Summary paper on fluidization and transport phenomena.* Powder Technology, 1996. **88**(3): p. 245-253.
3. Gevrin, F., O. Masbernat, and O. Simonin, *Granular pressure and particle velocity fluctuations prediction in liquid fluidized beds.* Chemical Engineering Science, 2008. **63**(9): p. 2450-2464.
4. Limtrakul, S., *Hydrodynamics of liquid fluidized beds and gas-liquid fluidized beds*. D. Sc. Thesis, Washington University, 1996.
5. Kiared, K., F. Larachi, M. Cassanello, and J. Chaouki, *Flow structure of the solids in a three-dimensional liquid fluidized bed.* Industrial and Engineering Chemistry Research, 1997. **36**(11): p. 4695-4704.
6. Limtrakul, S., J. Chen, P.A. Ramachandran, and M.P. Dudukovic, *Solids motion and holdup profiles in liquid fluidized beds.* Chemical Engineering Science, 2005. **60**(7): p. 1889-1900.
7. Segrè, P.N. and J.P. McClymer, *Fluctuations, stratification and stability in a liquid fluidized bed at low Reynolds number.* Journal of Physics-Condensed Matter, 2004. **16**(38): p. S4219-S4230.
8. Tee, S.Y., P.J. Mucha, M.P. Brenner, and D.A. Weitz, *Velocity fluctuations in a low-Reynolds-number fluidized bed.* Journal of Fluid Mechanics, 2008. **596**: p. 467-475.
9. Gidaspow, D. and L. Huilin, *Liquid-solid fluidization using kinetic theory of granular flow.* AIChE Symposium series 317, 1997. **93**: p. 12-17.
10. Spinewine, B., H. Capart, M. Larcher, and Y. Zech, *Three-dimensional Voronoï imaging methods for the measurement of near-wall particulate flows.* Experiments in Fluids, 2003. **34**(2): p. 227-241.
11. Cowan, M.L., J.H. Page, and D.A. Weitz, *Velocity fluctuations in fluidized suspensions probed by ultrasonic correlation spectroscopy.* Physical Review Letters, 2000. **85**(2): p. 453-456.
12. Richardson, J.F. and W.N. Zaki, *Sedimentation and fluidization: part I.* Transaction of the Institute of Chemical Engineers, 1954. **32**: p. 35-53.
13. Duru, P., M. Nicolas, J. Hinch, and E. Guazzelli, *Constitutive laws in liquid-fluidized beds.* Journal Of Fluid Mechanics, 2002. **452**: p. 371-404.
14. Leutz, W. and J. Rička, *On light propagation through glass bead packings.* Optics Communications, 1996. **126**: p. 260-268.
15. Khan, A.R. and J.F. Richardson, *Pressure gradient and friction factor for sedimentation and fluidisation of uniform spheres in liquids.* Chemical Engineering Science, 1990. **45**(1): p. 255-265.
16. Lettieri, P., R. Di Felice, R. Pacciani, and O. Owoyemi, *CFD modelling of liquid fluidized beds in slugging mode.* Powder Technology, 2006. **167**(2): p. 94-103.
17. Menon, N. and D.J. Durian, *Diffusing-wave spectroscopy of dynamics in a three-dimensional granular flow.* Science, 1997. **275**: p. 1920-1922.

18. Cowan, M.L., I.P. Jones, J.H. Page, and D.A. Weitz, *Diffusing acoustic wave spectroscopy.* Physical Review E, 2002. **65**(6): p. 066605.
19. Wu, S.H., *Phase-Structure And Adhesion In Polymer Blends - A Criterion For Rubber Toughening.* Polymer, 1985. **26**(12): p. 1855-1863.
20. Breault, R.W., C.P. Guenther, and L.J. Shadle, *Velocity fluctuation interpretation in the near wall region of a dense riser.* Powder Technology, 2008. **182**(2): p. 137-145.
21. Cornelissen, J.T., F. Taghipour, R. Escudie, N. Ellis, and J.R. Grace, *CFD modelling of a liquid-solid fluidized bed.* Chemical Engineering Science, 2007. **62**(22): p. 6334-6348.
22. Batchelor, G.K., *A new theory of the instability of a uniform fluidized-bed.* Journal Of Fluid Mechanics, 1988. **193**: p. 75-110.

Chapter 5 Particle dynamics in a dense vibro-fluidized bed

5.1 Introduction

Vibrated granular materials have received much attention over many years because they are a simple example of dissipative non-equilibrium systems that demonstrate rich and complex behaviour [1, 2]. They are, however, also of wide interest across industry. For example, flow of bulk solids from hoppers and silos is often controlled through the application of vibration [3], whilst more recent work has shown that vibration can also improve the fluidization of fine powders [4]. Vibration has long been known to cause segregation in mixtures of different sized particles [5] as well as compaction, whether desired as in the manufacture of sintered products [6] or otherwise [7]. Squires [8] has recently highlighted how vibrated granular systems may lead to improved operation of reactors, combustors and heat exchangers. Finally, vibration of granular materials is important in the construction industry including, for example, the manufacture of building materials [9], soil improvement [10] and soil response to seismic events [11].

Much understanding of the dynamics of particles in vertically vibro-fluidized beds and associated granular temperature data has been accumulated over the past decade or more using video imaging methods [12-21], nuclear magnetic resonance [22, 23], and positron emission particle tracking (PEPT) [24-28]. Various constraints inherent to these methods – multiple light scattering for video methods, small bed-to-particle diameter ratios in NMR, and limited spatial and temporal resolutions – mean they have all been restricted to one particle thick [12-18], relatively shallow [19-21], confined [22, 23] or dilute three-dimensional (3D) [24-28] beds.

A few methods have been (or in principle can be) applied to dense systems not accessible to video-based methods, NMR and PEPT as well as particle pressure data inversion [29], mechanical spectroscopy [30-32], diffusing wave spectroscopy (DWS) [33] and speckle visibility spectroscopy (SVS) [34], which is a modification of DWS. As discussed in Chapter 2, the pressure-data based approach is, however, limited to the wall region, whilst mechanical spectroscopy is an intrusive method that appears to give results that depend on the nature of the probe used. Light scattering methods such as DWS and SVS, on the other hand, are neither intrusive nor restricted to the wall region, yet they are able to probe length and time scales well below those accessible to NMR, their nearest rival in this regard.

The single DWS-based study to date of dense 3D vibro-fluidized beds [33] was very limited in scope, focussing on a single frequency and short time dynamics of the particles. The SVS study [34] was similarly limited, focusing on detailing a new method rather than measuring experimental phenomena. Therefore, I undertook a far more detailed study of the dynamics of particles in a dense 3D vibro-fluidized bed using DWS considering both the short and long-time behaviour of the particles for a wide range of conditions and at various points in the bed – this study is reported in this Chapter. The outline of the experimental details, including those pertaining to the apparatus, the particulate material and the experimental procedures used is given first. This is followed by presentation of the results obtained, which include the particle dynamic regimes observed and the variation of the granular temperature with process conditions and height above the base of the bed, and their discussion.

5.2 Experimental details

5.2.1 Experimental setup

The experimental apparatus is illustrated in figure 5.1. The granular material was held in a rigidly fixed rectangular column constructed from two 500 mm high and 196 mm wide borosilicate glass plates separated by two aluminium edges 14.5 mm thick. The granular material was subject to vertical vibrations at the base of the column by a piston fixed to an air-cooled electromagnetic driven shaker (V721, LDS Ltd., Hertfordshire, UK) controlled by a Dactron COMET USB controller (LDS Ltd.) with feedback from two integrated circuit piezoelectric accelerometers (model 353B03, PCB Piezotronics Inc., NY, US) attached to the piston. The shaker was capable of delivering a range of different vibrational modes at frequencies in the range of 5-4000 Hz, accelerations up to $70g$, and amplitudes as large as 12.7 mm.

The dynamics of the particles in the vibro-fluidized bed were studied using DWS in transmission mode as described in Chapter 3. Both the laser and the fibre optic cable were mounted on linear stages so that different points above the base of the vibro-fluidized bed could be investigated, as can be seen on figure 5.1.

The granular material, which was selected to ensure that all experiments were conducted in the DWS regime, consisted of semi-transparent, strongly light-absorbing, spherical glass particles of diameter $d_p = 0.95 \pm 0.05$ mm. In all cases the vibro-fluidized bed was filled to a depth of 75 mm with the material and subject to at least 10 minutes of vibration at 50 Hz and $4.17g$ before any data was collected so as to ensure, as far as was practically possible, that the bed was in a ‘stationary state’.

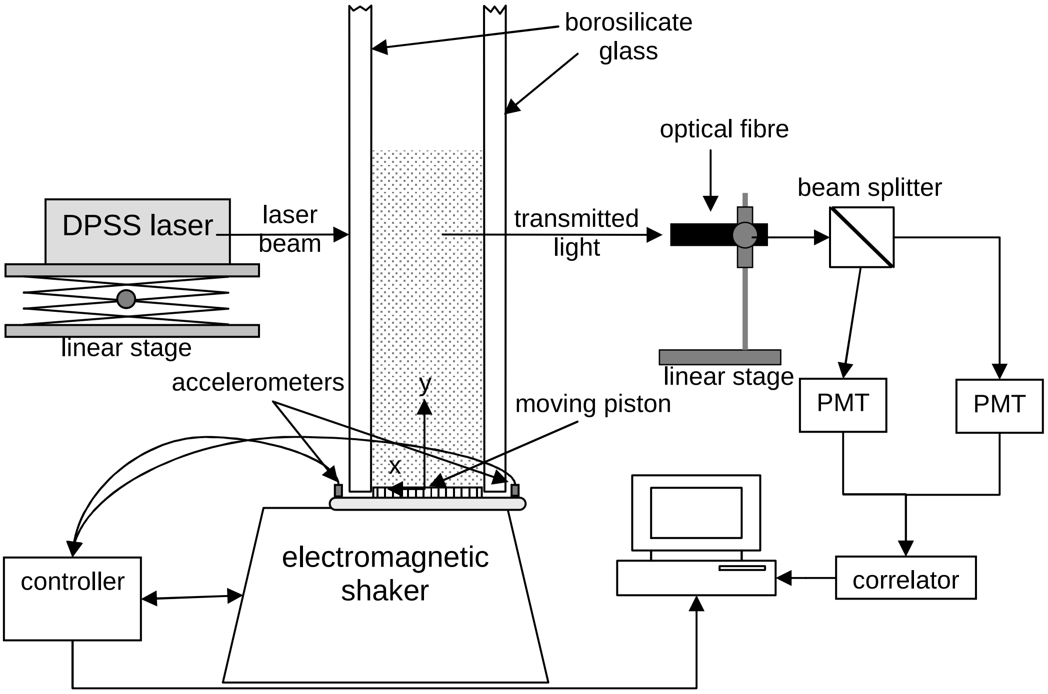

Figure 5.1. Schematic of experimental setup.

5.2.2 Experimental procedure

The vibro-fluidized bed was subject to sinusoidal vibrations in all cases reported here. The vertical position of the piston at time, *t*, for such vibrational motion is governed by

$$y_p = A\sin(\omega t) \tag{5.1}$$

where *A* and $f = \omega/2\pi$ are the amplitude and frequency respectively. The associated peak vibrational velocity and acceleration of the piston are $v_p = \omega A$ and $a_p = \omega^2 A$ respectively; the latter is presented here in the non-dimensional form, $\Gamma = a_p/g$, where *g* is the acceleration due to gravity.

The intensity autocorrelation functions, $g_2(t)$, were determined for the frequency/acceleration combinations indicated in Table 5.1 at three points in the vibro-fluidized bed whose coordinates were $x = 49$ mm and $y = 25$, 40 and 55 mm, where x is the horizontal distance from the centreline of the bed, and y is the distance from the vibrating base of the bed (see figure 5.1). As this table shows, the amplitude of the forcing varied from just under half a particle diameter at $f = 50$ Hz and $\Gamma = 4.170$, to just 1.5% of the particle size at $f = 500$ Hz and $\Gamma = 1.555$. Further inspection of this table also shows that the frequency/acceleration combinations were selected so as to allow systematic study of the effect of peak vibrational velocity and amplitude over wide ranges.

Γ	*f* (Hz)							
	50.00	69.48	96.54	134.14	186.38	258.97	359.84	500.00
1.555	0.1540	0.0798	0.0413	0.0214	0.0111	0.0057	0.0030	0.0015
	48.56	34.95	25.15	18.10	13.03	9.37	6.75	4.86
2.160	0.2145	0.1112	0.0576	0.0298	0.0155	0.0080	0.0041	0.0021
	67.45	48.54	34.93	25.14	18.09	13.02	9.37	6.74
3.000	0.2980	0.1544	0.0800	0.0414	0.0215	0.0111	0.0058	0.0030
	93.68	67.42	48.52	34.92	25.13	18.09	13.02	9.37
4.170	0.4145	0.2147	0.1112	0.0576	0.0298	0.0155	0.0080	0.0041
	130.21	93.71	67.44	48.54	34.93	25.14	18.09	13.02

Table 5.1 Sinusoidal forcing frequency-acceleration combinations considered in this study along with the associated (top) amplitude, A, in mm, and (bottom) peak forcing velocity, v_p, in mm/s. The acceleration and frequency were controlled to a resolution of $0.005g$ and 0.001 Hz respectively.

The transport mean free path, l^*, and absorption path length, l_a, were determined for the positions and conditions considered. Because the experimental set-up meant the incident light intensity could not be measured with ease and only the $L = 14.5$ mm bed described above could be vibrated, a two-stage method based on the static transmission method of Leutz and Rička [35] was used to obtain the transport mean free path and absorption path length data. The reference sample was an 0.1 vol % aqueous suspension of latex spheres (0.6 μm polystyrene, G. Kisker GbR., Germany) whose mean free path is $l_R^* = 2.30$ mm obtained from DWS measurement. A small amount of absorbing dye (Rhodamine B) was then added to the latex solution so as to bring its degree of absorption into line with that of the strongly light-absorbing packed beds used here (see below). The absorption path length of this dyed latex solution was then determined by fitting the equation 3.16 to the transmitted light intensity data, $I(L)$, measured for several different thickness, $L = 15.5$, 20.6 and 24.2 mm, of the dyed solution. A value of $l_{aR} = 5.5 \pm 0.2$ mm was obtained.

The absorption path length of a well tapped packed bed of the particulate material was then determined by fitting equation 3.16 to the transmitted intensity data for beds of thickness $L = 15.5$, 20.6 and 24.2 mm. A value of $l_{aP} = 4.0 \pm 0.2$ was obtained. The transport mean free path of the packed bed was then determined using equation 3.18 where the latex suspension data was identified with l_{aR}, l_R^* and $I_R\left(L\right)$, and the packed bed data with l_a, l^* and $I\left(L\right)$. A value of $l_P^*=1.89 \pm 0.2$ mm was obtained.

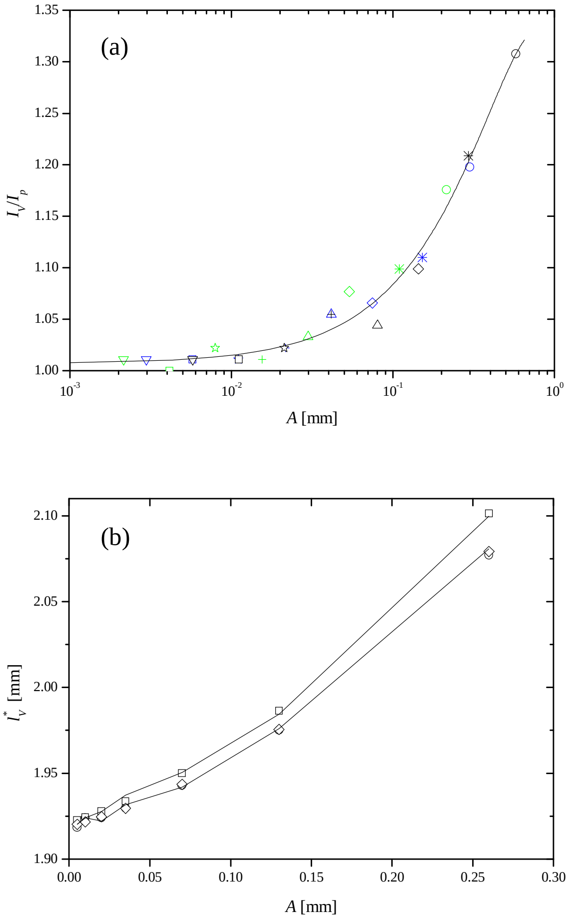

Figure 5.2. (a) Variation of the transmitted light intensity of a vibro-fluidized bed compared to that of a packed bed, I_V/I_P, with vibration amplitude, A, at $x = 49$ mm and $y = 20$ mm for a range of accelerations (2.16g – green, 3.00g – blue, 5.79g – black) and frequencies (50 Hz – circle, 70 Hz – asterisk, 100 Hz – diamond, 134 Hz – triangle, 186 Hz – cross, 260 Hz – star, 360 Hz – square, 500 Hz – inverted triangle). (b) Variation of transport mean free path of the vibro-fluidized bed, l_V^*, with the vibration amplitude, A, at $x = 49$ mm for $y = 25$ mm (circles), $y = 40$ mm (squares) and $y = 55$ mm (diamonds). Lines are a guide for the eye only.

Previous DWS studies on air fluidized beds [36, 37] suggests that the absorption path length in such beds is not particularly sensitive to spatial position or solids density even for large degrees of bed expansion. On this basis and the fact that the degree of expansion experienced in the vibro-fluidized bed considered here was very small, it was assumed here that the value obtained for the packed bed was also valid for all points and conditions in the vibro-fluidized bed; i.e. $l_{aV} = 4.0 \pm 0.2$ mm. Using this assumption, the transport mean free path of the vibro-fluidized bed was determined using equation 3.18 for the points and conditions of interest, where the packed bed data was identified with l_{aR}, l_R^* and $I_R\left(L\right)$, and the vibro-fluidized bed data with l_a, l^* and $I\left(L\right)$.

As figure 5.2(a) shows, the ratios of the transmitted intensities of the vibro-fluidized bed and packed bed, I_V / I_P, were found to correlate very well with the amplitude, A, of the vibrations. Thus, the transport mean free path of the vibro-fluidized bed, l_V^*, was correlated with A as indicated in figure 5.2(b). This figures shows that whilst l_V^* increases with the amplitude of the vibrations and, to a lesser extent, the height above the base of the vibro-fluidized bed, its variation over the range of conditions and positions investigated here is small at ~10-15%.

5.3 Results and discussion

5.3.1 Overview of the particle dynamics observed

Figure 5.3 shows an intensity autocorrelation function (IACF), $g_2(t)$, typical of mid-range frequencies along with the electric field autocorrelation function (FACF), $g_1(t)$, and mean square displacement (MSD), $\left\langle \Delta r^2 \right\rangle$, derived from the analysis outlined in Chapter 3. The IACF decays from $g_2(t) \approx 1.5$ over the timescale of $10^{-6} \sim 10^{-5}$ s to an intermediate plateau of $g_2(t) \approx 1.01$ where it remains before once again decaying over the timescale of $10^{-1} \sim 10^{1}$ s, this time towards unity. A double decay and intervening plateau such as seen here could indicate that the particle dynamics are characterized by two timescales or, alternatively, slow fluctuations in the power of the laser [38]. By applying the same experimental set-up to a dilute emulsion (5.4 % v/v 290 nm PMMA particles in dodecane), the later was ruled by virtue of the fact that IACF possessed only a single decay. I shall return to the origin of this double decay when considering the mean square displacement below.

Figure 5.3(b) shows that the double decay seen in the IACF is clearly reflected in the FACF, as one would expect given the Siegert relationship, equation 3.3. As the height of the intermediate plateau in the FACF is significantly enhanced relative to that of the IACF, it is now possible to see that whilst the second decay may possibly go to $g_1(t) \approx 0$ (i.e. $g_2(t) \approx 1$), poor statistics at long times mean it is not possible to rule out further plateaus and decays. A better picture of this long time behaviour would be obtained using alternative light scattering techniques as discussed in Chapter 3 [39-42].

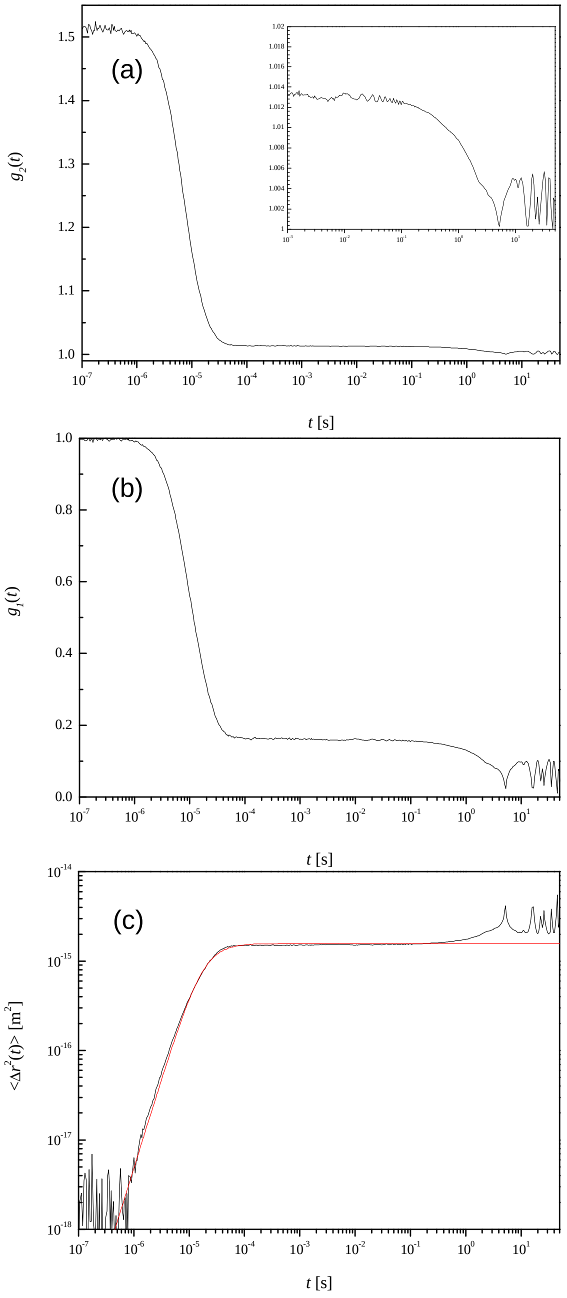

Figure 5.3. (a) The intensity autocorrelation function, $g_2(t)$, for the point $x = 49$ mm and $y = 40$ mm at $\Gamma = 3$ and $f = 96.535$ Hz (corresponding to $v_p = 48.52$ mm/s and $A = 0.08$ mm); the inset shows the long-time approach to unity. (b) The normalised electric field autocorrelation function, $g_1(t)$, obtained from $g_2(t)$ using the Siegert relationship, equation 3.3. (c) The mean square displacement obtained from $g_1(t)$ by inverting equation 3.14. The solid line is fitted to the empirical equation 4.6.

The mean square displacement (MSD) obtained from the inversion of equation 3.14 using the FACF is shown in figure 5.3(c). The MSD is characterised by three well defined regions. The first, which terminates at $t \approx 50$ μs for this case, is associated with the ballistic motion of the particles. Quantitative analysis of this region using equation 3.19 gives a particle velocity fluctuation of $\left\langle \delta v^2 \right\rangle^{1/2} = 3.17$ mm/s. The experimental data was also fitted with the empirical relation, equation 4.6, to obtain the same value of the velocity fluctuation and a decorrelation time of τ_{dws} = 18.1 μs. The product of the two gives a length scale Δs = 57.4 nm at which particle dynamics was probed. Although the granular system is close to the close-packed limit, still this is only a very small fraction of particle diameter and probably of inter-particle distance. Due to the experimental limitations of DWS as discussed in Chapter 3, direct experimental measurements are necessary to validate the attribution of τ_{dws} and Δs to the mean time between collisions and the mean free path respectively as reported in some previous DWS studies [33, 36, 37, 43, 44]. Beyond the ballistic region, the MSD remains unchanged up to $t \approx 0.3$ s, indicating that the particles are in effect moving about a point in space during this period. The third region of the MSD, which is located in this case over the timescale of $t = 0.3 \sim 6$ s, appears to be sub-diffusive where $\left\langle \Delta r^2 \right\rangle \sim t^{\alpha}$ with $\alpha < 1$. Inadequate statistics at long times mean that it is not possible to say if a diffusive region – *i.e.* where $\alpha = 1$ -exists for this or any other condition considered here.

On the basis of video images of a shallow air fluidized bed and MSDs derived for these images, Abate and Durian [20] identified four characteristic regimes: ballistic motion at short times, caged motion at intermediate times where the MSD is largely unchanging as the particles rattle around in cages defined by neighbouring particles, sub-diffusive motion at longer times where particles break free of their cages only to become trapped once again in new cages nearby, and finally at even longer times, diffusive motion. Given the similarities between their MSDs and ours here, it is tempting to draw parallels and ascribe the decays and intervening plateau seen in the ACFs accordingly. However, care needs to be exercised, as DWS is not particularly suited to the study of timescales that are comparable to the forcing dynamics [34], and equation 3.14 is based on certain approximations that may break down to a greater or lesser extent at longer times [45]. As the first decay in the ACFs occurs at a time approximately 10^3 times smaller than the forcing period, it is safe to ascribe it to the ballistic motion of the particles, figure 5.4(a). In order to attribute the intermediate plateau and second decay to caged motion and cage breaking, I appeal to the results of others [39, 46], who have obtained double decays similar to those observed here, albeit for colloidal gels, using light scattering methods that are more appropriate for longer time scales. Both these groups attribute the second decay by implication [39] or explicitly [46] to collective re-arrangement of the colloidal particles following a period of virtually no change at all. On this basis, I believe that despite the potential uncertainties associated with the long time character of the MSDs obtained here, it is reasonable to ascribe the second decay in the ACFs of figure 5.3 and the preceding plateau to particles moving in a collective manner between cages in which they remain trapped for some time, figure 5.4(b) and (c). However, it is not possible to eliminate other possibilities such as density fluctuations.

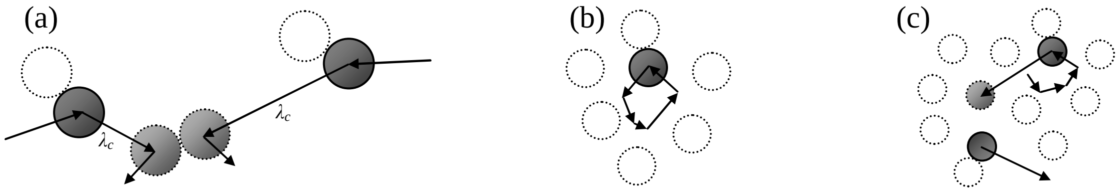

Figure 5.4. A schematic showing the three regimes experienced by the particles in the vibro-fluidized bed studied here: (a) ballistic dynamics at very short times in which the distance travelled between collisions (i.e. free path) is λ_c; (b) 'rattling' around in cages defined by neighbouring particles at intermediate times; and (c) particles moving between cages in a cooperative manner at long times.

Figure 5.5 shows an FACF typical of the higher frequencies considered here. The FACF exhibits an initial decay at short times followed by a finite number of decaying oscillations (or 'echoes' [47]) whose period is identical to that of the forcing (see inset of this figure) and, finally, a gradual decrease in the FACF towards zero. If the amplitude of the echoes were constant, the bed would in effect be oscillating as a single body in tune with the base of the bed [47] implying there is no relative motion of the particles in the scattering volume. Decaying oscillations, on the other hand, indicate that only a fraction of the particles are oscillating in phase with vibrating base, with the remainder undergoing aperiodic motion [47]. This suggests solidlike behaviour of the granular system where the granular viscosity appears to diverge. Kim et al. [48], who also observed this behaviour in a vibro-fluidized bed, likened the behaviour to that of supercooled liquids or dense colloidal suspension near the glass or jamming transition point. The dynamics of the particles that are undergoing non-periodic motion may, therefore, be the same as that depicted in figure 5.4 [49].

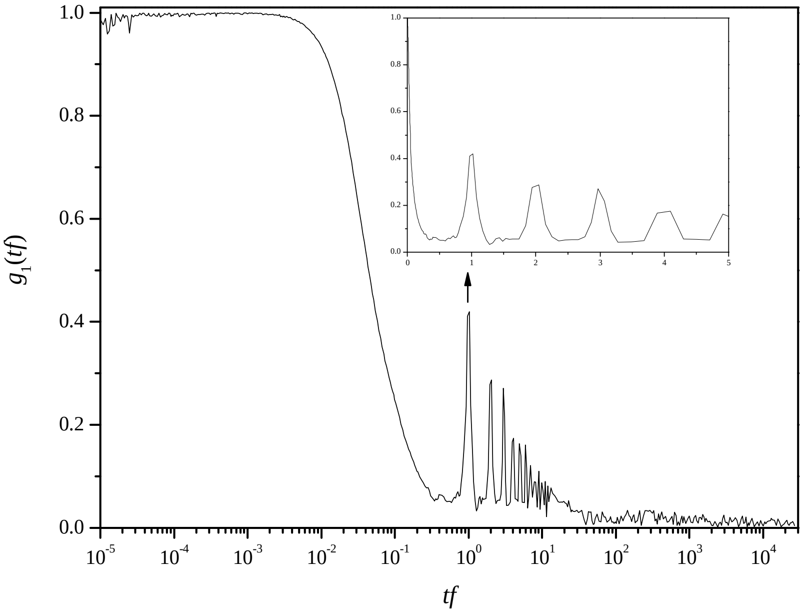

Figure 5.5. The electric field autocorrelation function for the point $x = 49$ mm and $y = 40$ mm at $\Gamma = 2.16$ and $f = 500$ Hz (corresponding to $v_p = 6.74$ mm/s and $A = 0.0021$ mm). Note that the time axes have been non-dimensionalized by the forcing frequency to emphasise the fact that the period of the oscillations is the same as that of the forcing.

Kim et al. [48] observed oscillatory behaviour similar to that of figure 5.5 at 50 Hz for accelerations slightly above 1 *g*. In our experiments oscillations were observed at accelerations up to $\Gamma = 4.17$, 3, 2.16 and 1.555 for $f = 500$ Hz, 359.84 Hz, 258.97 Hz and 186.38 Hz respectively. Our results suggest that the upper limit where oscillations are observed is frequency dependent – both acceleration and frequency are, therefore, important. Figure 5.6 shows that the height of the first echo, $g_1(tf = 1)$, which Kim et al. [48] used as a marker for the presence or otherwise of oscillations, is well correlated by the peak vibrational velocity, whilst no correlation was evident between $g_1(tf=1)$ and the amplitude of forcing – this suggests that energetic rather than geometric factors dictate the behaviour of that fraction of the particles that are undergoing non-periodic motion. Figure 5.6 also shows that the fraction of particles that are undergoing non-periodic motion, which is inversely related to the height of the echoes [47], at a fixed peak vibrational velocity decreases with the distance above the base of the bed – the degree of fluidization in effect increases with height in the bed.

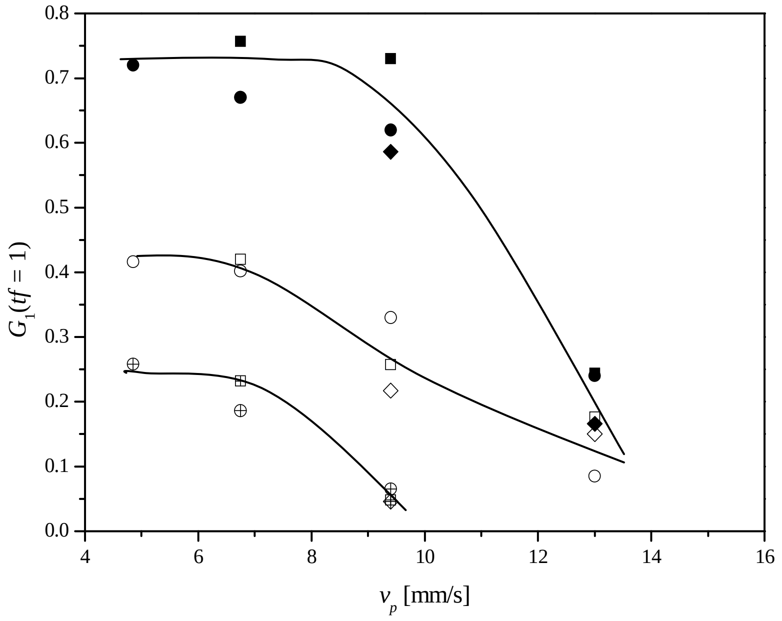

Figure 5.6. Variation of the height of the first echo in the FACF, $g_1(tf=1)$, with peak forcing velocity, v_p, at points $x = 49$ mm and $y = 25$ mm (filled symbols), $y = 40$ mm (open symbols) and $y = 55$ mm (struck through symbols), in the bed for accelerations 1.555*g* (circles), 2.16*g* (squares) and 3*g* (diamonds). Lines are shown as a guide for the eye only.

The FACFs at the lowest frequencies considered here, examples of which are shown in figure 5.7, also include decaying echoes with a period equal to that of the forcing. These echoes, which are superimposed on the intermediate plateau or the second decay depending on the acceleration and frequency of the forcing, are much weaker than those observed at the upper end of the frequency range considered here (compare with figure 5.5). The strength of the oscillations also appears to increase as the acceleration of the forcing increases and its frequency decreases (*i.e.* in effect, they tend to increase with the amplitude and peak vibrational velocity), contrary to the high frequency behaviour. Both this trend and the presence of echoes at 50 Hz for accelerations as high as 4.17g are also in stark contrast to the results of Kim et al. [48], who observed no echoes at 50 Hz for accelerations beyond 1.12g. It is not clear precisely why the behaviour seen here at low frequencies differs from that of Kim et al. [48] in these two respects as well as the higher frequency behaviour observed here, but the differences in apparatus of the two studies suggests two possible causes: (1) the difference in the way the bed is vibrated – Kim and co-workers shake the bed as a whole whilst I ‘pump’ a piston a the base of a column – and the presence of air in our system, which was removed in the experiments of Kim et al. [48], could lead to greater oscillatory driving of the particles at the lower frequencies where amplitudes and peak velocities are significant, and (2) the much smaller amplitude of forcing relative to the particle size here, could lead to less particles being able to take on aperiodic motion for the same energy input.

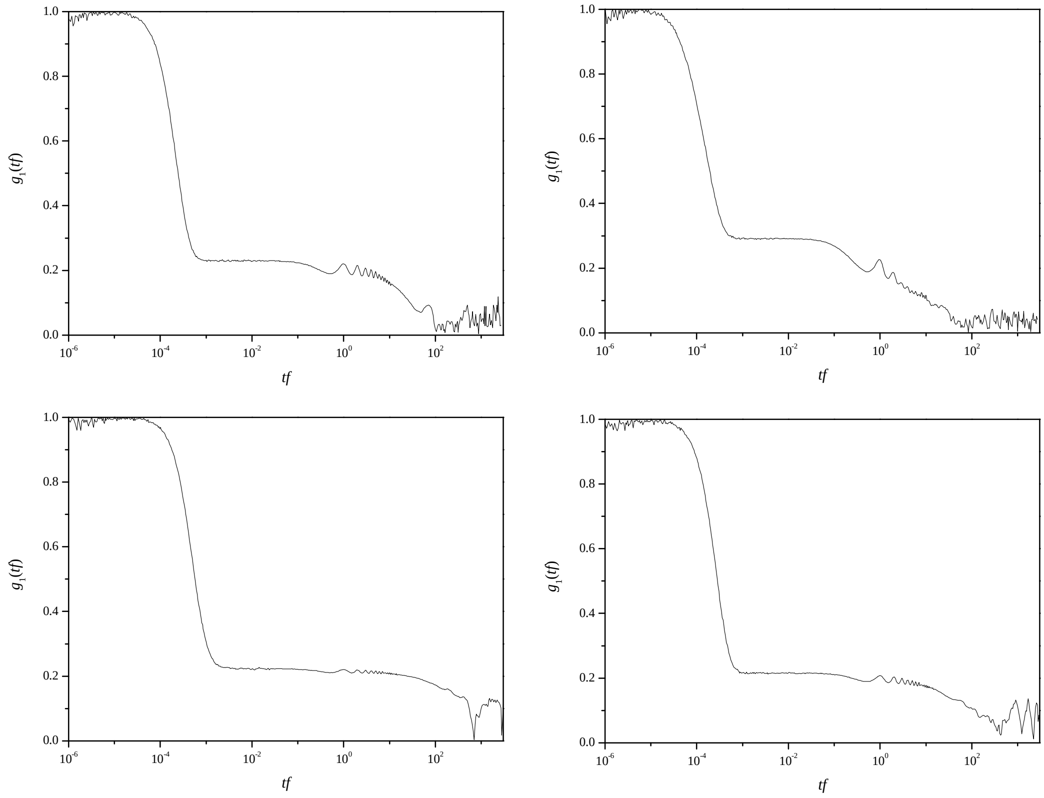

Figure 5.7. The electric field autocorrelation function at the point $x = 49$ mm and $y = 40$ mm for: (a) $\Gamma = 2.16$ and $f = 50$ Hz (corresponding to $v_p = 67.45$ mm/s and $A = 0.2145$ mm), (b) $\Gamma = 4.17$ and $f = 50$ Hz ($v_p = 130.21$ mm/s and $A = 0.4145$ mm), (c) $\Gamma = 2.16$ and $f = 69.48$ Hz ($v_p = 48.54$ mm/s and $A = 0.1112$ mm), (d) $\Gamma = 4.17$ and $f = 69.48$ Hz ($v_p = 93.71$ mm/s and $A = 0.2147$ mm). Note that the time has been nondimensionalized by the forcing frequency to emphasise the fact that the period of the oscillations seen here is the same as that of the forcing.

5.3.2 Granular temperature

Figure 5.8 shows that the granular temperature is correlated very well with the peak vibrational velocity, v_p, whilst there is no correlation with the vibrational acceleration. The data above $v_p = 18$ mm/s appears to be well described by $\left\langle \delta v^2 \right\rangle^{1/2} \sim 0.11 v_p$, a scaling that appears both qualitatively and quantitatively to be very much in line with that obtained by Yang and co-workers [22, 23] using NMR in a relatively confined dense vibro-fluidized bed. The data below $v_p = 18$ mm s^{-1} is also described reasonably well by a linear scaling, $\left\langle \delta v^2 \right\rangle^{1/2} \sim 0.018 v_p$. This crossover point corresponds very well to the point where echoes appear (see the data for $y = 40$ mm in figure 5.6), suggesting that it is near the jamming point [20, 47, 48] where geometrical or kinetic constraints on the possible moves of particles lead to a vanishing particle mobility. Therefore, as the granular system approach the jamming transition, the dynamics slow down dramatically (crossover point) and systems becomes solidlike (echoes).

The data here indicates that the granular temperature scales with the square of the peak vibrational velocity

$$\left\langle \delta v^2 \right\rangle \sim v_p^2 \tag{5.2}$$

This scaling is in line with that obtained experimentally by others for a thin bed [16], a shallow bed [19], a confined bed [22, 23], and a bed similar to ours [33]. This scaling is also in line with a number of theoretical models, including those of Kumaran [50] and Warr et al. [13], who both obtain a scaling exponent of 2, and Martin et al. [51] who obtained a scaling exponent of 1.85 ±0.11 in the absence of significant wall friction. These models are, however, restricted to relatively dilute systems, a point I shall return to further below.

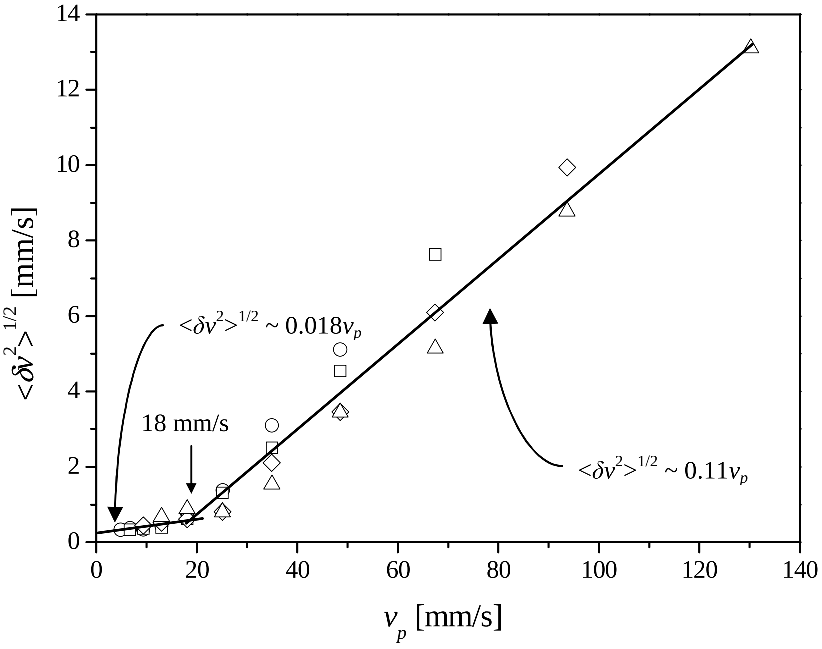

Figure 5.8. Variation of the mean velocity fluctuations about the mean, $\left\langle \delta v^2 \right\rangle^{1/2}$, with peak forcing velocity, v_p, at the point $x = 49$ mm and $y = 40$ mm for accelerations $\Gamma = 1.555$ (circles), $\Gamma = 2.160$ (squares), $\Gamma = 3.000$ (diamonds) and $\Gamma = 4.170$ (triangle). Lines are linear fits to the data and errors are no larger than the symbols.

Figure 5.9, which shows the particle velocity fluctuations as a function of the height above the bed base for three representative frequencies, suggests that the granular temperature varies little with height for the conditions investigated here. This lack of variation is at odds with the experimental data of You and Pak [33], who also studied a dense three-dimensional vibro-FB, where an exponential increase in the granular temperature with height was observed. The reason for this difference is not precisely clear, but the system of You and Pak [33] differed from that used here in a number of potentially important respects including the amplitudes – which were at least 5d_p compared to approximately 0.5d_p here – and the absence of gas in their bed, which You and Pak noted increased the granular temperature. The data of You and Pak [33] also appears to be at odds with that of other studies, albeit for geometries [18] or densities [22-26] that differed from those considered here. In particular, whilst these studies revealed granular temperature can change with height under some conditions, the changes were all far weaker than those observed by You and Pak [33] and were essentially linked to a corresponding variation in the solids density in every case, a variation which is barely seen in You and Pak [33] (~0.02% change across the bed height) or, indeed, here.

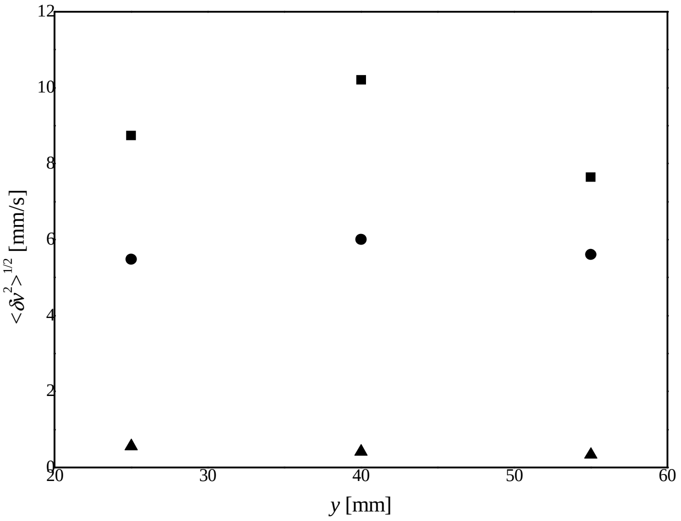

Figure 5.9. Variation of the mean velocity fluctuations about the mean, $\left\langle \delta v^2 \right\rangle^{1/2}$, with height above the vibrating base for accelerations $\Gamma = 3$ at $f = 50$ Hz (square), $f = 70$ Hz (circle), $f = 500$ Hz (triangle). The errors are no larger than the symbols.

5.4 Conclusion

Using diffusing wave spectroscopy, I have elucidated the dynamics of particles in a dense three-dimensional fluidized bed in which the density variations are small, and have determined the granular temperature of particles as a function of the vibrational conditions and height above the base of the bed.

The granular temperature was found to scale very well with the square of the peak vibrational velocity; no correlation was observed between granular temperature and other vibrational variables such as the acceleration or amplitude. The granular temperature was found to vary little with height in the bed, although it was not possible to probe near the top and bottom of the bed where variations may be expected, due to limitations with the experimental apparatus and data analysis procedures adopted.

The longer time dynamics of the particles, which are depicted in figure 5.4, indicates that in systems such as those investigated here, macroscopic particle motion in the bed is governed by the collective motion of particles between cavities in the bed, possibly by acquiring fluctuating velocities that are substantially greater than the local mean of the velocity fluctuations. This suggests that any model that seeks to describe dense vibrated granular systems in which the density fluctuations are small must account for the distribution of fluctuating velocities, not just the mean, and must include spatial correlations. If this is the case, the standard kinetic theory of granular systems [52, 53] may not be appropriate for dense vibro-fluidized beds such as those investigated here without significant development.

References

1. Aranson, I.S. and L.S. Tsimring, *Patterns and collective behavior in granular media: Theoretical concepts.* Reviews of Modern Physics, 2006. **78**(2): p. 641-692.
2. Kadanoff, L.P., *Built upon sand: Theoretical ideas inspired by granular flows.* Reviews of Modern Physics, 1999. **71**(1): p. 435-444.
3. Poncet, J.C., *Total flow - maximizing storage in bins, hoppers, bunkers, and silos by the use of novel correctly applied vibrations*, in *From Powder to Bulk.* 2000, IMechE Conference Transactions. p. 169-184.
4. Xu, C.B. and J. Zhu, *Parametric study of fine particle fluidization under mechanical vibration.* Powder Technology, 2006. **161**(2): p. 135-144.
5. Kudrolli, A., *Size separation in vibrated granular matter.* Reports on Progress in Physics, 2004. **67**: p. 209-247.
6. Linemann, R., J. Runge, M. Sommerfeld, and U. Weissguttel, *Compaction of powders due to vibrations and shocks.* Particle & Particle Systems Characterization, 2004. **21**(4): p. 261-267.
7. Maynard, E.P. *Practical solutions for solving bulk solids flow problems.* in *Proceedings of the 46th Annual Cement Industry Technical Conference.* 2004. New York: IEEE, p. 139-147.
8. Squires, A.M., *Chemical process opportunities for vibrated powders 2. In the field.* Powder Technology, 2004. **147**(1-3): p. 10-19.
9. Safawi, M.I., I. Iwaki, and T. Miura, *A study on the applicability of vibration in fresh high fluidity concrete.* Cement and Concrete Research, 2005. **35**(9): p. 1834-1845.
10. Massarsch, K.R., *Deep compaction of granular soils.* A look Back for Future Geotechnics, ed. S. Wu, W. Zhang, and R.D. Woods. 2001, Rotterdam: A.A. Balkema, p.181-223.
11. Ishihara, K., *Ground behavior during earthquake and its effect on foundation piles.* A look Back for Future Geotechnics, ed. S. Wu, W. Zhang, and R.D. Woods. 2001, Rotterdam: A.A. Balkema, p.15-91.
12. Warr, S., G.T.H. Jacques, and J.M. Huntley, *Tracking the translational and rotational motion of granular particles: Use of high-speed photography and image processing.* Powder Technology, 1994. **81**(1): p. 41.
13. Warr, S., J.M. Huntley, and G.T.H. Jacques, *Fluidization of a two-dimensional granular system: Experimental study and scaling behaviour.* Physical Review E, 1995. **52**(5): p. 5583-5595.
14. Wildman, R.D., J.M. Huntley, and J.P. Hansen, *Self-diffusion of grains in a two-dimensional vibrofluidized bed.* Physical Review E, 1999. **60**(6): p. 7066-7075.
15. Wildman, R.D. and J.M. Huntley, *Novel method for measurements of granular temperature distributions in two-dimensional vibro-fluidised beds.* Powder Technology, 2000. **113**: p. 14-22.
16. Feitosa, K. and N. Menon, *Breakdown of energy equipartition in a 2D binary vibrated granular gas.* Physical Review Letters, 2002. **88**: p. 198301.

17. Tai, C.H. and S.S. Hsiau, *Dynamic behaviors of powders in a vibrating bed.* Powder Technology, 2004. **139**: p. 221-232.
18. Yang, S.C., *Density effect on mixing and segregation processes in a vibrated binary granular mixture.* Powder Technology, 2006. **164**: p. 65-74.
19. Losert, W., D.G. Cooper, J. Delour, A. Kudrolli, and J.P. Gollub, *Velocity statistics in excited granular media.* Chaos, 1999. **9**(3): p. 682-690.
20. Abate, A.R. and D.J. Durian, *Approach to jamming in an air-fluidized granular bed.* Physical Review E, 2006. **74**: p. 031308.
21. Baxter, G.W. and J.S. Olafsen, *The temperature of a vibrated granular gas.* Granular Matter, 2007. **9**(1-2): p. 135-139.
22. Yang, X., C. Huan, D. Candela, R.W. Mair, and R.L. Walsworth, *Measurements of grain motion in a dense, three-dimensional granular fluid.* Physical Review Letters, 2002. **88**(4): p. 044301.
23. Huan, C., X. Yang, D. Candela, R.W. Mair, and R.L. Walsworth, *NMR experiments on a three-dimensional vibrofluidized granular medium.* Physical Review E, 2004. **69**: p. 041302.
24. Wildman, R.D., J.M. Huntley, J.P. Hansen, D.J. Parker, and D.A. Allen, *Single-particle motion in three-dimensional vibrofluidized granular beds.* Physical Review E, 2000. **62**(3): p. 3826.
25. Wildman, R.D., J.M. Huntley, and D.J. Parker, *Granular temperature profiles in three-dimensional vibrofluidized granular beds.* Physical Review E, 2001. **63**(6): p. 061311.
26. Wildman, R.D. and D.J. Parker, *Coexistence of two granular temperatures in binary vibrofluidized beds.* Physical Review Letters, 2002. **88**(6): p. 064301.
27. Wildman, R.D. and J.M. Huntley, *Scaling exponents for energy transport and dissipation in binary vibro-fluidized granular beds.* Physics of Fluids, 2003. **15**(10): p. 3090.
28. Wildman, R.D., J.T. Jenkins, P.E. Krouskop, and J. Talbot, *A comparison of the prediction of a simple kinetic theory with experimental and numerical results for a vibrated granular bed consisting of nearly elastic particles of two sizes.* Physics of Fluids, 2006. **18**: p. 073301.
29. Falcon, E., S. Aumaitre, P. Evesque, F. Palencia, C. Lecoutre-Chabot, S. Fauve, D. Beysens, and Y. Garrabos, *Collision statistics in a dilute granular gas fluidized by vibrations in low gravity.* Europhysics Letters, 2006. **74**(5): p. 830-836.
30. D'Anna, G., P. Mayor, A. Barrat, V. Lotero, and F. Nori, *Observing Brownian motion in vibration-fluidized granular matter.* Nature, 2003. **424**(6951): p. 909.
31. Mayor, P., G. D'Anna, A. Barrat, and V. Loreto, *Observing Brownian motion and measuring temperatures in vibration-fluidized granular matter.* New Journal of Physics, 2005. **7**: p. 28.
32. Mayor, P., G. D'Anna, G. Gremaud, A. Barrat, and V. Loreto, *Mechanical spectroscopy of vibrated granular matter.* Materials Science and Engineering: A, 2006. **442**(1-2): p. 256-262.
33. You, S.Y. and H.K. Pak, *Study of the short-time dynamics of a thick and highly dense vibro-fluidized granular system by using diffusing wave spectroscopy.* Journal of Korean Physical Society, 2001. **38**(5): p. 577-581.

34. Dixon, P.K. and D.J. Durian, *Speckle Visibility Spectroscopy and Variable Granular Fluidization*. Physical Review Letters, 2003. **90**(18): p. 184302.
35. Leutz, W. and J. Rička, *On light propagation through glass bead packings*. Optics Communications, 1996. **126**: p. 260-268.
36. Biggs, M., D. Glass, L. Xie, V. Zivkovic, A. Buts, and M. Curt Koenders, *Granular temperature in a gas fluidized bed*. Granular Matter, 2008. **10**(2): p. 63-73.
37. Xie, L., M.J. Biggs, D. Glass, A.S. McLeod, S.U. Egelhaaf, and G. Petekidis, *Granular temperature distribution in a gas fluidized bed of hollow microparticles prior to onset of bubbling*. Europhysics Letters, 2006. **74**(2): p. 268-274.
38. Lemieux, P.A. and D.J. Durian, *Investigating non-Gaussian scattering processes by using nth-order intensity correlation functions*. Journal of the Optical Society of America A, 1999. **16**(7): p. 1651-1664.
39. Viasnoff, V., F. Lequeux, and D.J. Pine, *Multispeckle diffusing-wave spectroscopy: A tool to study slow relaxation and time-dependent dynamics*. Review of Scientific Instruments, 2002. **73**(6): p. 2336-2344.
40. Cipelletti, L., H. Bissig, V. Trappe, P. Ballesta, and S. Mazoyer, *Time-resolved correlation: a new tool for studying temporally heterogeneous dynamics*. Journal Of Physics-Condensed Matter, 2003. **15**(1): p. S257-S262.
41. Duri, A., H. Bissig, V. Trappe, and L. Cipelletti, *Time-resolved-correlation measurements of temporally heterogeneous dynamics*. Physical Review E, 2005. **72**(5): p. 051401.
42. Zakharov, P., F. Cardinaux, and F. Scheffold, *Multispeckle diffusing-wave spectroscopy with a single-mode detection scheme*. Physical Review E, 2006. **73**(1): p. 011413.
43. Menon, N. and D.J. Durian, *Diffusing-wave spectroscopy of dynamics in a three-dimensional granular flow*. Science, 1997. **275**: p. 1920-1922.
44. Zivkovic, V., M.J. Biggs, D.H. Glass, P. Pagliai, and A. Buts, *Particle dynamics in a dense vibrated fluidized bed as revealed by diffusing wave spectroscopy*. Powder Technology, 2008. **182**(2): p. 192-201.
45. Durian, D.J., *Accuracy of diffusing-wave spectroscopy theories*. Physical Review E, 1995. **51**(4): p. 3350-3358.
46. Bissig, H., S. Romer, L. Cipelletti, V. Trappe, and P. Schurtenberger, *Intermittent dynamics and hyper-aging in dense colloidal gels*. PhysChemComm, 2003. **6**: p. 21-23.
47. Hebraud, P., F. Lequeux, J.P. Munch, and D.J. Pine, *Yielding and rearrangements in disordered emulsion*. Physical Review Letters, 1997. **78**(24): p. 4657-4660.
48. Kim, K., J.K. Moon, J.J. Park, H.K. Kim, and H.K. Pak, *Jamming transition in a highly dense granular system under vertical vibration*. Physical Review E, 2005. **72**(1).
49. Berthier, L., L.F. Cugliandolo, and J.L. Iguain, *Glassy systems under time-dependent driving forces: Application to slow granular rheology*. Physical Review E, 2001. **63**(5): p. 051302.
50. Kumaran, V., *Kinetic theory for a vibro-fluidized bed*. Journal Of Fluid Mechanics, 1998. **364**: p. 163-185.

51. Martin, T.W., J.M. Huntley, and R.D. Wildman, *Hydrodynamic model for a vibrofluidized granular bed.* Journal of Fluid Mechanics, 2005. **535**: p. 325-345.
52. Jenkins, J.T. and S.B. Savage, *A theory for the rapid flow of identical, smooth, nearly elastic, spherical-particles.* Journal of Fluid Mechanics, 1983. **130**: p. 187-202.
53. Lun, C.K.K., S.B. Savage, D.J. Jeffrey, and N. Chepurniy, *Kinetic theories for granular flow - inelastic particles in couette-flow and slightly inelastic particles in a general flowfield.* Journal of Fluid Mechanics, 1984. **140**(MAR): p. 223-256.

Chapter 6 Particle dynamics in a water-immersed vibro-fluidized bed

6.1 Introduction

Vibration is commonly present in the industrial handling and transporting of powders. The granular temperature of a dry vibro-fluidized bed has been intensively investigated experimentally, computationally and theoretically as discussed in the previous Chapter. The problem of particle dynamics in a water-immersed vibro-fluidized bed is an area of granular dynamics that has yet to be investigated. Experimental work on granular dynamics in such systems has been devoted either to investigation of interactions between a small number of spheres [1, 2] or to bulk dynamic phenomena such as heaping dynamics [3-5], convection [6], travelling waves [7] and Faraday tilting [8]. Therefore, we employed diffusing wave spectroscopy to measure for the first time granular temperature in a water-immersed vibro-fluidized bed.

The presentation here proceeds as follows. We will first outline the experimental details, such as pertain to the apparatus and the particulate material, and the experimental procedures used. This is followed by presentation of the results obtained and their discussion.

6.2 Experimental section

6.3.1 Experimental set-up

The experimental apparatus is illustrated in figure 6.1. The granular material was held in a rigidly fixed rectangular box with smooth plexiglass walls. The inner dimensions of the box were 15 x 200 mm in the horizontal plane and 500 mm in height. The measurements were carried out using semi-transparent spherical glass particles of density ρ_p = 2650 kg/m^{-3} and diameter d_p = 475 ± 25 μm[*]. The box was filled with granular material and tap water. The column was then shaken to release any air bubbles and then refilled, so than no air bubbles were contained within its volume. The mean granular bed height was h = 95 ± 1 mm, while the water level was usually set up to be h_w = 125 ± 1 mm.

The rectangular column with water-immersed granular material was subject to vertical vibrations provided by an air-cooled electromagnetic driven shaker (V721, LDS Ltd., Hertfordshire, UK). The vibrations were controlled by a Dactron COMET USB controller (LDS Ltd.) with feedback from two integrated circuit piezoelectric accelerometers (model 353B03, PCB Piezotronics Inc., NY, US) attached to the base of the column.

The dynamics of the particles in the vibro-fluidized bed were studied using DWS in transmission mode as described in Chapter 3. Both the laser and the fibre optic cable were mounted on linear stages so that different points above the base of the vibro-fluidized bed could be investigated, as can be seen on figure 6.1.

---

[*] Ballistic region was not found for 165 μm particles which force me to choose larger particles. I do not have explanation for this observation.

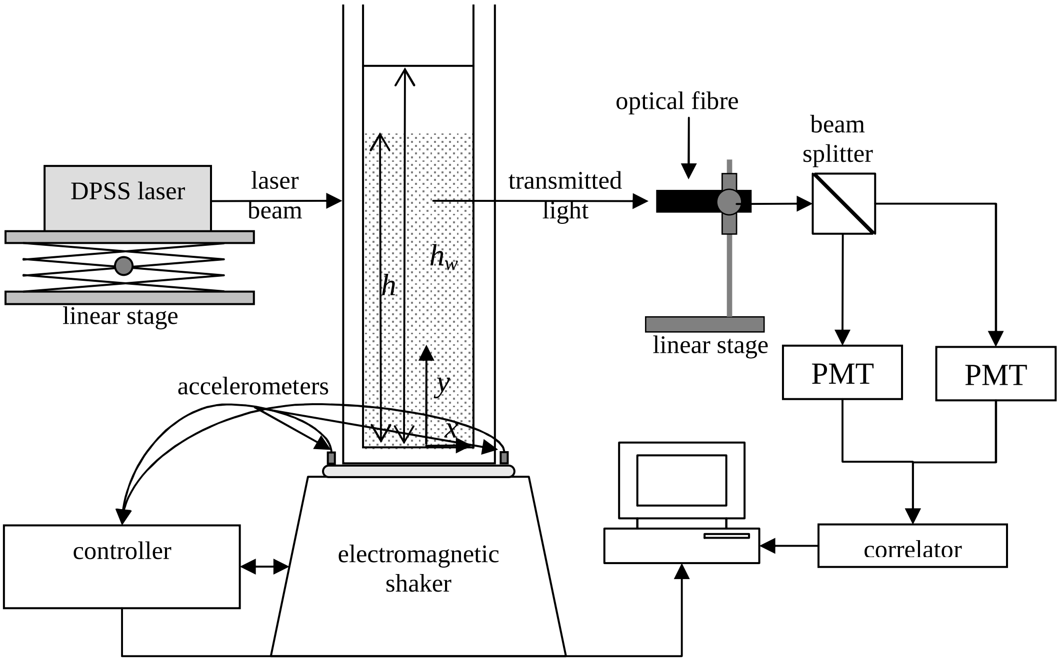

Figure 6.1. Schematic of the experimental set-up.

6.3.2 Experimental procedure

The water-immersed vibro-fluidized bed was subject to sinusoidal vibrations in all cases reported here. The vertical position of the piston at time, *t*, for such vibrational motion is governed by

$$y_p = A\sin(\omega t) \tag{6.1}$$

where *A* and $f = \omega/2\pi$ are the amplitude and frequency respectively. The associated peak vibrational velocity and acceleration of the piston are $v_p = \omega A$ and $a_p = \omega^2 A$ respectively; the latter is presented here in the non-dimensional form, $\Gamma = a_p/g$, where *g* is the acceleration due to gravity. The intensity autocorrelation functions (IACF) was determined for four different measurement points along the centreline of the vibrated bed, $x = 0$ mm, at different vertical positions $y = 40$, 50, 60 and 70 mm above the base of the box. Before each measurement the system was vibrated for at least 10 minutes, allowing the bed to reach stationary state.

The IACF were obtained by collecting and correlating ten blocks of data of 30 s long each. Each IACF was then subject to the data analysis procedure outlined in Chapter 3 to obtain granular temperature. Equation 3.14 requires knowledge of the transport mean free path, l^*, and absorption path length, l_a, at the positions and conditions considered. Because the experimental set-up meant only the $L = 15$ mm bed described above could be vibrated, a two-stage method based on the static transmission method of Leutz and Rička [9] was used to obtain the transport mean free path and absorption path length data. We used a reference sample of 0.1 vol % aqueous suspension of latex spheres (0.6 μm polystyrene, G. Kisker GbR., Germany) whose mean free path and absorption path length are $l_R^* = 2.30$ mm and $l_{aR} = 11.2 \pm 0.1$ mm respectively, and packed beds of thickness $L = 15$, 20, 25 and 30 mm.

Our previous work on air [10, 11] and water (Chapter 4) fluidized beds suggests that the absorption path length in a granular system is not particularly sensitive to spatial position or solids density even for a large degree of expansion. On this basis and taking into account that the degree of expansion experienced in the water-immersed vibrated bed considered here was negligible, we assumed that the value obtained for the packed bed was also valid for all points and condition in the granular bed; i.e. $l_a = 9.8 \pm 0.3$ mm. Further, transmitted light intensity was found to vary little with applied vibrational conditions, indicating that l^* is a function of height above the distributor only. The determined transport mean free path for four different measuring points at $y = 40$, 50, 60 and 70 mm above the base of the box was $l^* = 1.36 \pm 0.05$, 1.37 ± 0.06, 1.42 ± 0.07 and 1.48 ± 0.06 mm respectively.

6.3 Results and discussion

6.3.1 Overview of the particle dynamics observed

Figure 6.2 shows an intensity autocorrelation function (IACF), $g_2(t)$, typical of mid-range acceleration along with the electric-field autocorrelation function (FACF), $g_1(t)$, and mean square displacement (MSD), $<\Delta r^2(t)>$, obtained from the analysis outlined in Chapter 3. The example IACF, shown in figure 6.2(a), first decays from $g_2(t) \approx 1.5$ over the timescale of $10^{-6} \sim 10^{-4}$ s to an intermediate plateau of $g_2(t) \approx 1.006$ where it remains before once again decaying over the timescale of $10^0 \sim 10^1$, this time towards unity. The intercepts of the $g_2(t)$ for all considered vibrational conditions were close to 1.5, the expected value for depolarized light.

Figure 6.2(b) shows that the double decay and timescales seen in the IACF are reflected and enhanced in the FACF, as one would expect given the Siegert relationship, equation 3.3. While it is reasonable to attribute the intermediate plateau and second decay in the ACFs of figures 6.2 to caged motion of particles at intermediate time and cage breaking at longer times where particles break free of their cages only to become trapped once again in new cages nearby defined by neighbouring particles as discussed in Chapter 5, it is not possible to eliminate other possibilities like density fluctuations. A better picture of this long time behaviour would be obtained using alternative light scattering approaches [12-15].

The mean square displacement obtained from inversion of equation 3.14 using the FACF is shown in figure 6.2(c). Quantitative analysis of the ballistic region of this MSD gives a particle velocity fluctuation of $\langle \delta v^2 \rangle^{1/2} = 0.713$ mm/s. We also fit the experimental data with the purely empirical relation equation 4.6, to obtain the same value of the velocity fluctuation and a decorrelation time of $\tau_{dws} = 32.6$ μs. Although it is tempting to attribute this decorrelation time to the mean time between collisions [10, 11, 16-18], direct experimental measurements using for example high-speed video imaging are necessary to confirm this hypothesis. Additionally, the product of the granular temperature and decorrelation time obtained from figure 6.2(c) gives a length scale Δs = 23.25 nm at which we probed particle dynamics. This is only a small fraction of the mean particle diameter (0.005 % of particle diameter) and indeed of the order of the surface roughness. However, as the solid fraction for our system is very close to the random close packing limit (solid volume fraction around 0.64), it is very complicated to estimate inter-particle distance to compare it with a given length scale Δs.

The curvature of the MSD line beyond $t \approx 7$ μs may be an indication of multi-particle collisions [19]. An increase of the typical inter-particle contact lifetime from short binary to longer multi-body collisions would alter and decrease the slope of MSD on a log-log plot from the value of 2 ($<\Delta r^2> \sim t^2$) typical of the ballistic regime. Another possible explanation for this discrepancy is that the ballistic trajectories of the particles are affected by the fluid flow [20]. The computed Stokes number of $St = 2/9\rho_p d\langle\delta v^2\rangle^{1/2}/\mu \approx 3$, where μ is the fluid viscosity, means that eddies may cause significant deviations in the particle trajectory. However, in our previous study in a liquid fluidized bed (Chapter 4) with similar values of Stokes number, we did not observe this deviation from ballistic behaviour.

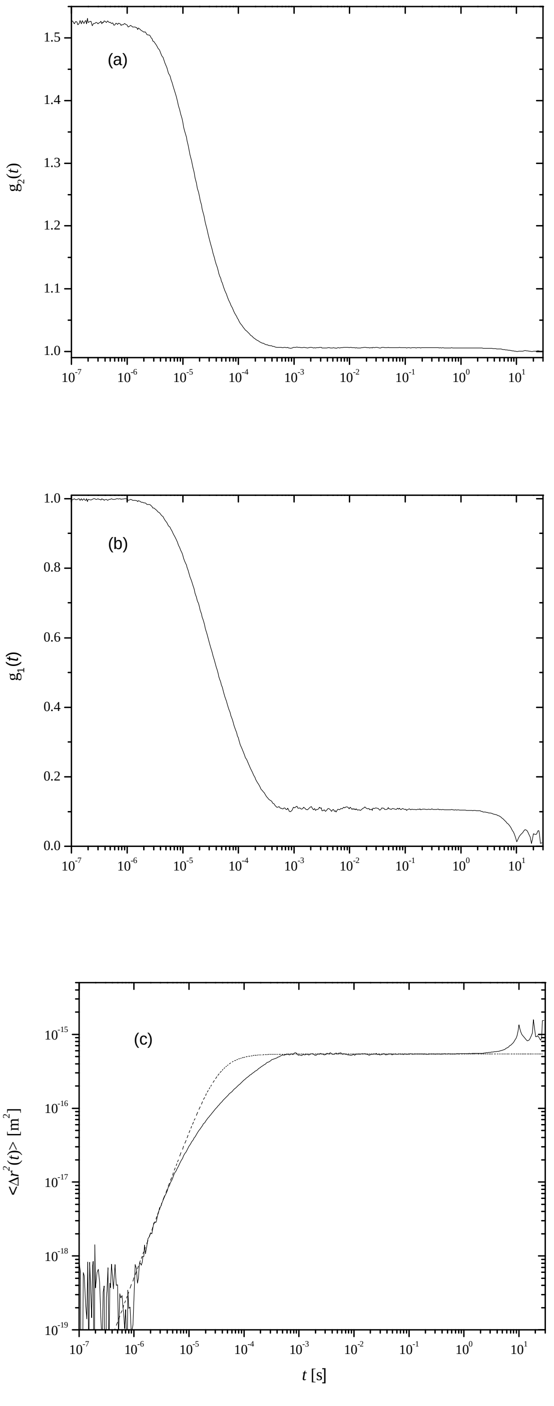

Figure 6.2. (a) The intensity autocorrelation function, $g_2(t)$, for the point $x = 0$ mm and $y = 50$ mm above the base at $\Gamma = 2$ and $f = 100$ Hz. (b) The normalized electric-field autocorrelation function, $g_1(t)$, obtained from $g_2(t)$ using the Siegert relationship, equation 3.3. (c) The mean square displacement obtained from $g_1(t)$ by inverting equation 3.14. The dashed line is a fit to the empirical formula, equation 4.6.

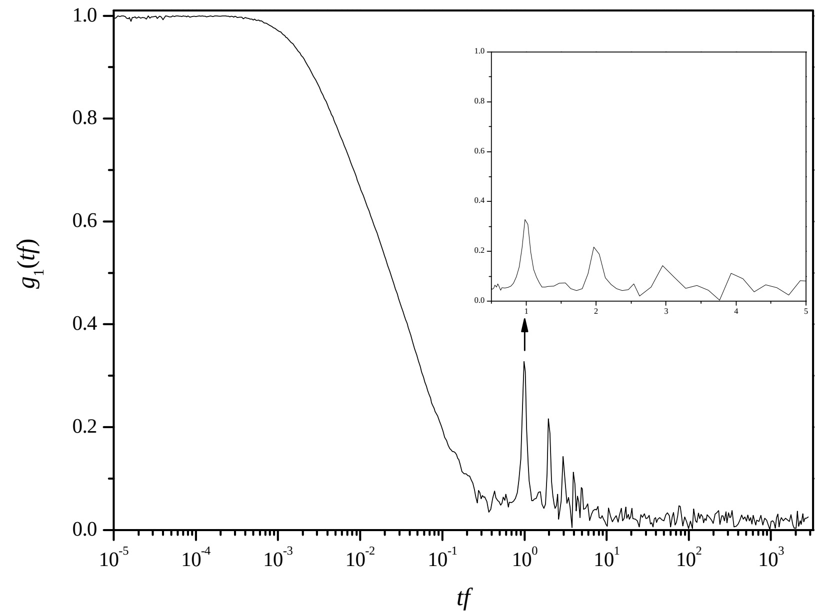

Figure 6.3. The normalized electric-field autocorrelation function, $g_1(t)$, for the point $x = 0$ mm and $y = 50$ mm above the base at $\Gamma = 0.9$ and $f = 100$ Hz. The insert shows a fraction of the oscillatory data on a linear time axis to emphasis that the period of the oscillations is the same as that of the forcing. Note the fact that the time axes have been non-dimensionalized by the forcing frequency.

Figure 6.3 shows an electric-field autocorrelation function typical of the lower accelerations considered here. The FACF exhibits an initial decay at short times followed by a finite number of decaying oscillations or echoes [21] whose period is identical to that of the forcing (see insert of this figure). For perfectly reversible periodic motion of the scatterers, the FACF will reinitialize to 1 ($=g_1(0)$) at integral multiplies of the oscillation period. However, if only a fraction of the scattering particles undergoes periodic reversible motion, with the remainder undergoing aperiodic motion, the echo heights will decay with time [21] which is the case here. This can be used to characterize the degree of fluidization and jamming transition in a highly dense vibrated granular bed [18, 22].

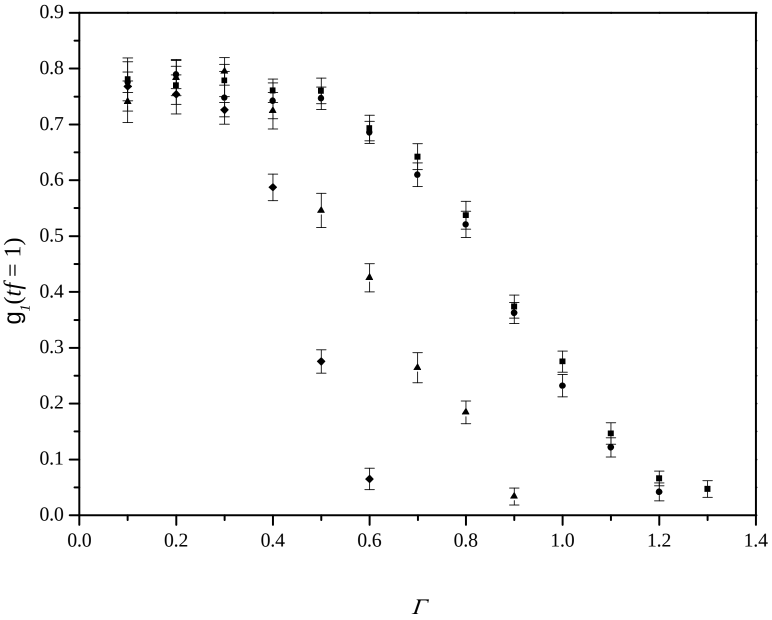

Figure 6.4. Variation of the height of the first echo in the FACF, $g_1(tf=1)$, with dimensionless acceleration, Γ, at points x = 0 mm and y = 40 mm (squares), y = 50 mm (circles), y = 60 mm (triangles) and y = 70 mm (diamonds) for the fixed frequency of f = 100 Hz.

The height of the first echo, $g_1(tf=1)$, shown in figure 6.4, decreases monotonically with dimensionless acceleration Γ for all vertical positions, y, investigated. The fraction of particles that are undergoing non-periodic irreversible motion, which is inversely related to the height of the echoes [22] and indicative of a degree of fluidization, also increases with vibrational excitation Γ in dry granular systems. Kim et al. [22] observed solid-like behaviour of a dry vibrated bed for $\Gamma < 1$ which is characterized by perfectly reversible periodic motion where the height of the echoes does not change with time and is equal to 1. However, even for very small vibrational excitations, e.g. $\Gamma = 0.1$, we did not detect perfect solidlike behaviour in our water-immersed vibrated granular system. This is probably due to higher viscous forces in our slurry system compared to the dry granular system and a complex flow pattern of water [1] which may fluidize a small fraction of particles even at minute vibrational excitations.

Moreover, at a fixed acceleration echo heights decrease with the distance above the base of the bed, at least for points above y = 40 mm, which indicates that the degree of fluidization in effect increases with height in the bed. These results are in line with experimental findings in a dry vibrated bed [22] as well as with the visual observations of Kozlov et al. [3] and Ivanova et al. [4] that only layers near the free surface are completely fluidized. At a certain critical dimensionless acceleration Γ_m, the height of the first echo completely disappears which indicates that the scattering volume become fluidized. The critical acceleration is, as expected, a function of the vertical position as in a dry vibrated bed [22] but there are two differences. The dependence is not linear as there is no significant difference between the y = 30 mm and y = 40 mm points. In addition, for the points near the free surface Γ_m is smaller than the gravitational acceleration which is considered as a threshold for fluidization in a dry system [22].

6.3.2 Granular temperature

Figure 6.5(a) shows that the fluctuation velocity, $\langle \delta v^2 \rangle^{1/2}$, is correlated very well with the vibrational acceleration whilst there is no correlation with the frequency and consequently two other associated vibrational parameters - peak vibrational velocity v_p and amplitude A. This implies that the granular temperature is scaling with the square of acceleration which is in contrast with the dry system where granular temperature is scaling with the square of the peak vibrational velocity, as theoretically predicted and experimentally verified in Chapter 5. The peak in data at f = 175 Hz is due to the resonant frequency of the whole apparatus. Using transmissibility measurements [23] we found that the resonant frequency of our experimental rig is $f_r \approx 180$ Hz as shown in the transmissibility graph, figure 6.6. This frequency is very close to the observed frequency of the maxima. Moreover, our data show weak dependence of the fluctuation velocity with frequency for higher vibrational accelerations ($\Gamma > 3.5$). This coincides with the visual observation of heaping in our system which may be the cause of this weak frequency correlation. The particles are forming one big convection roll moving down near the sidewalls and moving up in the middle of the bed. This visual observation is in line with previous observations in a similar experimental set-up [5].

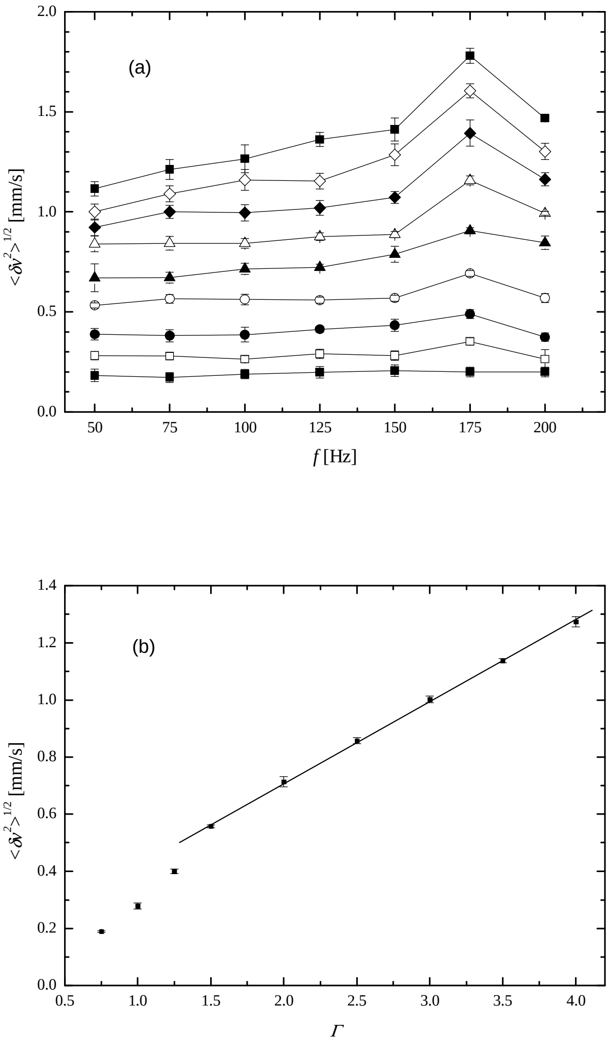

Figure 6.5. (a) Variation of the mean velocity fluctuations about the mean, $\langle \delta v^2 \rangle^{1/2}$, with the frequency, *f*, at the point *x* = 0 mm and *y* = 50 mm for various accelerations Γ = 0.75 (filled squares), 1 (squares), 1.25 (filled circles), 1.5 (circles), 2 (filled triangles), 2.5 (triangles), 3 (filled diamonds), 3.5 (diamonds) and 4 (filled squares). Lines are guide for the eye only. (b) The same data as in (a), averaged over frequencies for the different accelerations and plotted versus dimensionless acceleration, Γ. The line is a linear fit to the data.

The same frequency averaged data is plotted against the dimensionless acceleration Γ in figure 6.5(b). There are two distinguishable regions with different dependence of granular temperature on acceleration. The data above $\Gamma = 1.5$ shows linear dependence and was described very well by $\langle \delta v^2 \rangle^{1/2} = 0.289\Gamma + 0.14$ (coefficient of determination $R^2 = 0.99968$), while data below this crossover point shows non-linear dependence (jammed or solidlike region). This crossover point, Γ_c, is close to the critical acceleration Γ_{m} where echoes disappear (see the data for $y = 50$ mm in figure 6.4), suggesting that it is near the jamming point [22, 24].

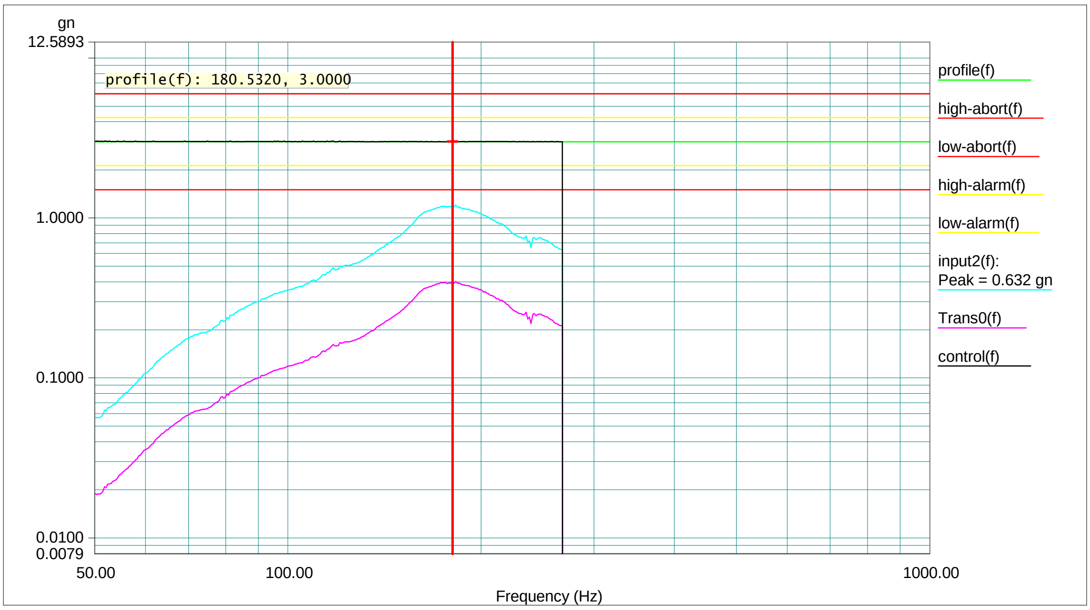

Figure 6.6. Transmissibility graph for the experimental set-up. Reference channel (profile –green line) was mounted on the base and response channel (input2 –light blue line) was mounted on the fluidized bed. The transmissibility function (pink line) which is given as a ratio of the two acceleration signals clearly show a resonant frequency around 180 Hz.

Further experiments were performed for a fixed frequency of f =100 Hz, as a mid-range frequency far away from the resonant frequency of the experimental apparatus. Variation of the velocity fluctuation with the acceleration at this fixed frequency, for various vertical positions, is shown in figure 6.7. Firstly, the granular temperature is clearly a function of position which is again in contrast withthe DWS study in a dry vibro-fluidized bed as presented in Chapter 5. In addition, table 6.1 gives a value of crossover points Γ_c, the critical accelerations Γ_m (figure 6.4) and the slope of the fully fluidized region. As this table shows, the crossover point decreases with height in a non-linear manner which is a trend observed for critical acceleration also. The slope of the fluidized region increases with height, indicating once again that the system near the free-surface is more fluidized.

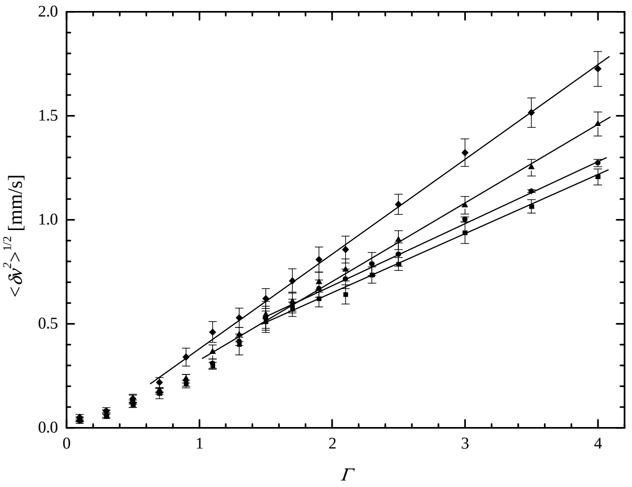

Figure 6.7. Variation of the mean velocity fluctuations about the mean, $\langle \delta v^2 \rangle^{1/2}$, with the dimensionless acceleration Γ at points x = 0 mm and y = 40 mm (squares), y = 50 mm (circles), y = 60 mm (triangles) and y = 70 mm (diamonds) for the fixed frequency of f = 100 Hz. Lines are a linear fit to the data.

Vertical position y [mm]	Γ_m	Γ_c	slope	R^2
40	1.3	1.5	0.281	0.99856
50	1.2	1.5	0.299	0.99912
60	0.9	1.1	0.368	0.99929
70	0.6	0.7	0.452	0.99912

Table 6.1. The critical acceleration Γ_m, crossover point Γ_c and slope of fully fluidized region with corresponding coefficient of determination of the fitting, as a function of vertical position y.

Figure 6.8, which shows variation of the mean velocity fluctuations about the mean with the dimensionless acceleration Γ for three different water levels h_w, suggests that the granular temperature is a strong function of the water level. The data is qualitatively the same, the crossover point is identical (Γ_c = 1.5) with non-linear dependence in the jammed region below and linear dependence in the fully fluidized region above the crossover point. The slopes of the linear part of the data for water levels of h_w = 120, 150 and 200 mm are respectively 0.300 (coefficient of determination R^2 = 0.99912), 0.490 (R^2 = 0.99952) and 0.589 (R^2 = 0.99871). Thus, the slope of the linear part is increasing monotonically with water level indicating a higher degree of fluidization. We do not as yet have an explanation for the observed behaviour.

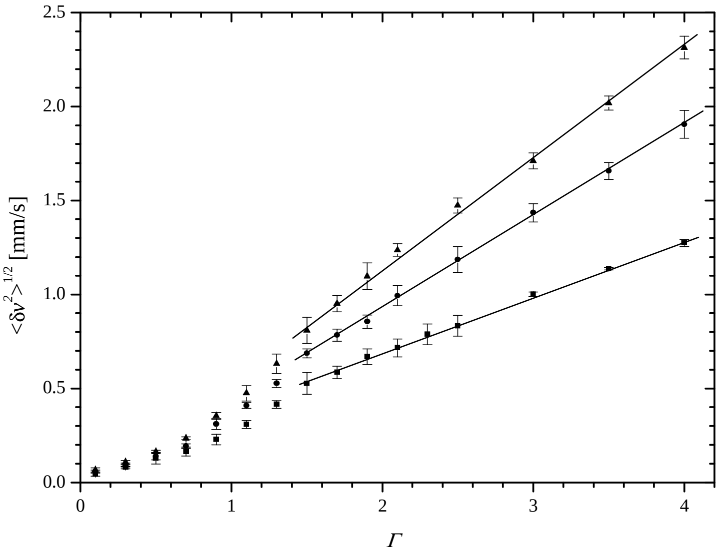

Figure 6.8. Variation of the mean velocity fluctuations about the mean, $\langle \delta v^2 \rangle^{1/2}$, with the dimensionless acceleration Γ for different water levels h_w = 120 mm (squares), h_w = 150 mm (circles) and h_w = 200 mm (triangles). Experiments performed for a fixed frequency f = 100 Hz at the point x = 0 mm and y = 50 mm. The lines are a linear fit to the data.

6.4 Conclusion

Using diffusing wave spectroscopy, we have studied the dynamics of particles in a dense three-dimensional water-immersed vibrated bed and have determined the granular temperature as a function of the vibrational conditions and height above the base of the bed.

Our results show interesting differences and similarities in granular dynamics between dry and water-immersed vibrated beds (slurry granular system). First, the granular temperature scales with the square of the vibrational acceleration in contrast to a dry vibrated bed where it scales with the square of the vibrational velocity . Secondly, we found variations of the granular temperature with height while our previous DWS study in a dry vibrated bed showed little variation with height. Moreover, we found strong dependence of the granular temperature with the water level in the box. Finally, our results indicate that near-surface regions of the water-immersed vibrated bed are fluidized even for accelerations smaller than the gravitational acceleration. In conclusion, it is obvious that the interstitial fluid effect should be taken into account in future theoretical and computational consideration of vibrated granular slurry systems.

As in the dry vibrated bed, some features of glassy dynamics and the jamming transition were also observed in a water-immersed vibrated bed. Multispeckle DWS techniques [12-15] are more appropriate for long time dynamics and can resolve these issues.

References

1. Klotsa, D., M.R. Swift, R.M. Bowley, and P.J. King, *Interaction of spheres in oscillatory fluid flows.* Physical Review E, 2007. **76**(5): p. 056314.
2. Voth, G.A., B. Bigger, M.R. Buckley, W. Losert, M.P. Brenner, H.A. Stone, and J.P. Gollub, *Ordered clusters and dynamical states of particles in a vibrated fluid.* Physical Review Letters, 2002. **88**(23): p. 234301.
3. Kozlov, V.G., A.A. Ivanova, and P. Evesque, *Sand behavior in a cavity with incompressible liquid under vertical vibrations.* Europhysics Letters, 1998. **42**(4): p. 413-418.
4. Ivanova, A., V. Kozlov, and P. Evesque, *Fluidization of a granular medium in a viscous fluid under vertical vibration.* Fluid Dynamics, 2000. **35**(3): p. 406-413.
5. Schleier-Smith, J.M. and H.A. Stone, *Convection, heaping, and cracking in vertically vibrated granular slurries.* Physical Review Letters, 2001. **86**(14): p. 3016-3019.
6. Medved, M., H.M. Jaeger, and S.R. Nagel, *Convection in a fully immersed granular slurry.* Physical Review E, 2001. **63**(6).
7. Smith, A.J., M.C. Leaper, M.R. Swift, and P.J. King, *Travelling waves in a water-immersed binary granular system vibrated within an annular cell.* Physical Review E, 2005. **71**(3): p. 031303.
8. Milburn, R.J., M.A. Naylor, A.J. Smith, M.C. Leaper, K. Good, M.R. Swift, and P.J. King, *Faraday tilting of water-immersed granular beds.* Physical Review E, 2005. **71**: p. 011308.
9. Leutz, W. and J. Rička, *On light propagation through glass bead packings.* Optics Communications, 1996. **126**: p. 260-268.
10. Xie, L., M.J. Biggs, D. Glass, A.S. McLeod, S.U. Egelhaaf, and G. Petekidis, *Granular temperature distribution in a gas fluidized bed of hollow microparticles prior to onset of bubbling.* Europhysics Letters, 2006. **74**(2): p. 268-274.
11. Biggs, M., D. Glass, L. Xie, V. Zivkovic, A. Buts, and M. Curt Koenders, *Granular temperature in a gas fluidized bed.* Granular Matter, 2008. **10**(2): p. 63-73.
12. Viasnoff, V., F. Lequeux, and D.J. Pine, *Multispeckle diffusing-wave spectroscopy: A tool to study slow relaxation and time-dependent dynamics.* Review of Scientific Instruments, 2002. **73**(6): p. 2336-2344.
13. Cipelletti, L., H. Bissig, V. Trappe, P. Ballesta, and S. Mazoyer, *Time-resolved correlation: a new tool for studying temporally heterogeneous dynamics.* Journal Of Physics-Condensed Matter, 2003. **15**(1): p. S257-S262.
14. Duri, A., H. Bissig, V. Trappe, and L. Cipelletti, *Time-resolved-correlation measurements of temporally heterogeneous dynamics.* Physical Review E, 2005. **72**(5): p. 051401.
15. Zakharov, P., F. Cardinaux, and F. Scheffold, *Multispeckle diffusing-wave spectroscopy with a single-mode detection scheme.* Physical Review E, 2006. **73**(1): p. 011413.

16. Menon, N. and D.J. Durian, *Diffusing-wave spectroscopy of dynamics in a three-dimensional granular flow*. Science, 1997. **275**: p. 1920-1922.
17. You, S.Y. and H.K. Pak, *Study of the short-time dynamics of a thick and highly dense vibro-fluidized granular system by using diffusing wave spectroscopy*. Journal of Korean Physical Society, 2001. **38**(5): p. 577-581.
18. Zivkovic, V., M.J. Biggs, D.H. Glass, P. Pagliai, and A. Buts, *Particle dynamics in a dense vibrated fluidized bed as revealed by diffusing wave spectroscopy*. Powder Technology, 2008. **182**(2): p. 192-201.
19. Campbell, C.S., *Granular material flows - An overview*. Powder Technology, 2006. **162**(3): p. 208.
20. Benavides, A. and B. van Wachem, *Numerical simulation and validation of dilute turbulent gas-particle flow with inelastic collisions and turbulence modulation*. Powder Technology, 2008. **182**(2): p. 294-306.
21. Hebraud, P., F. Lequeux, J.P. Munch, and D.J. Pine, *Yielding and rearrangements in disordered emulsion*. Physical Review Letters, 1997. **78**(24): p. 4657-4660.
22. Kim, K., J.K. Moon, J.J. Park, H.K. Kim, and H.K. Pak, *Jamming transition in a highly dense granular system under vertical vibration*. Physical Review E, 2005. **72**(1).
23. Blake, R.E., *Basic vibration theory*, in *Shock and vibration handbook*, C.M. Harris, Editor. 1996, McGraw-Hill: London. p. 2.1-2.33.
24. Abate, A.R. and D.J. Durian, *Approach to jamming in an air-fluidized granular bed*. Physical Review E, 2006. **74**: p. 031308.

Chapter 7 Conclusions and future work

7.1 Conclusions

This thesis concerns granular temperature and particle dynamics in a variety of dense fluidized beds as revealed by the non-intrusive technique of diffusing-wave spectroscopy, which has been reviewed in Chapters 2 and 3 along with other methods for study of particle dynamics in granular systems.

Chapter 4 presents the most comprehensive experimental study to date of granular temperature in a liquid fluidized bed. It reports granular temperature and solid fraction fields for a thin rectangular bed (20×200 mm cross section and 500 mm high) of glass particles (mean diameter 165 μm and density 2500 kg/m^3) fluidized by water for superficial velocities ranging from $0.05U_t$, which is approximately double the minimum fluidization velocity, to $0.49U_t$, where U_t is the particle terminal velocity estimated by fitting the Richardson-Zaki correlation to the bed expansion data. At superficial velocities below $0.336U_t$, the solid fraction and granular temperature are uniform throughout the bed. At higher superficial velocities, the solid fraction tends to decrease with height above the distributor, whilst the granular temperature first increases to a maximum before decaying towards the top of the bed. Correlation of the mean granular temperature with the mean solid fraction and the local granular temperature with the local solid fraction both suggest that the granular temperature in the liquid fluidized bed can be described solely in terms of the solid fraction, ϕ. The granular temperature increases monotonically with solid fraction to a maximum at $\phi \approx 0.18$ where it then decreases monotonically as ϕ approaches the close-packed limit.

Chapter 5 presents granular temperature data and long-time dynamics of mono-disperse glass particles (mean diameter of 950 μm and density 2650 kg/m^3) in a three-dimensional dense granular bed (14.5×196 mm cross section, 500 mm high and filled with particles up to 75 mm) subject to vertical sinusoidal vibrations over a wide range of conditions. The granular temperature of the particles was found to scale with the square of the peak vibrational velocity in line with theoretical predictions. A double decay observed in the autocorrelation functions obtained by DWS suggest that the dynamics of vibro-fluidized beds resemble the dynamics of non-equilibrium glassy systems such as viscous liquids and dense colloids; ballistic at short time scales, so-called caged dynamics at intermediate time scales, when the particles are trapped within a cage of surrounding particles, and sub-diffusive at long time scales, when the particles finally break out from their cages only to become trapped once again in new cages nearby. Following the analogy with glassy systems, by lowering temperature (energy injection) or density, the granular system can be jammed, *i.e.* ‘frozen’ in a small region of the phase space. Observed solid-like behaviour of the granular system (decaying echoes in the autocorrelation function whose period matches that of the vibrations), at very weak excitation levels, correlated very well with the vibration velocity, indicating that this jamming transition is energy driven.

Chapter 6 presents the first ever study of granular temperature in a water-immersed vibro-fluidized bed. It reports a study of the dynamics of mono-disperse glass particles (mean diameter 475 μm and density 2500 kg/m^3) in a three-dimensional dense granular bed (15×200 mm cross section, 500 mm high and filled to a depth of 75 mm with particles) immersed in water and subject to vertical sinusoidal vibrations. Our work shows there are both strong similarities and strong differences between the dry and submerged vibro-fluidized beds. For example, similar to the dry vibro-FB, a double decay in the autocorrelation function, which is an indication of caged dynamics, was also observed for a range of conditions in the submerged vibro-FB. Perhaps one of the most striking differences between dry and water-immersed vibro-fluidized bed is our observation that the granular temperature in the latter scales with the vibrational acceleration rather than the peak vibrational velocity observed for the former. In particular, we have observed that the granular temperature scales with the square of acceleration, a result that is yet to be theoretically predicted.

7.2 Future work

The first and most obvious extension of the work presented in this thesis would be to combine liquid fluidization with vibration for excitation of granular matter. DWS study of the particle dynamics and granular temperature in a liquid vibro-fluidized bed would represent the first experimental study of such a granular system. Scaling of the granular temperature with the superficial velocity, solid volume fraction, vibration peak velocity, frequency and amplitude would be very interesting to explore, especially in the light of results for a water-immersed vibro-fluidized bed. These results would also have immediate practical application in the use of vibrated liquid fluidised beds in the size/density separation of solid materials.

In this project, granular temperatures in dense rectangular fluidized beds were studied. Cody et al. [1] point out that the granular temperature in a gas fluidized bed might be sensitive to the bed geometry. Moreover, in industry, the common geometry for a fluidized bed unit is cylindrical, quite in contrast with our rectangular lab scale fluidized beds. Therefore, further DWS studies in cylindrical lab scale fluidized beds, both gas and liquid, would be very desirable. Comparison with our experimental data from a rectangular liquid fluidized bed would reveal the influence of bed geometry on granular temperature experimental results. Although the fact was not specifically emphasized in this thesis, all the published theoretical correlation function equations for DWS data analysis are for a flat experimental cell containing the sample. This is the reason why all DWS studies of granular dynamics have so far been performed in equipment of rectangular geometry. Even though geometry has been shown to have a rather negligible effect for the application of DWS [2], extension of DWS work to cylindrical beds would require theoretical or numerical [2] determination of the correlation function for this kind of experimental geometry, or at least an experimental demonstration that the difference between a flat-walled and a cylindrical cell is negligible at higher diameters.

Cody’s conclusion [1] was based on comparison of experimental data generated by the acoustic shot noise technique (circular geometry) and DWS (rectangular geometry). Another possible reason for the discrepancy between experimental results is the difference in experimental techniques and approach. Therefore, an experimental study of granular temperature in a representative granular system using all the different techniques available (acoustic shot noise, PEPT, NMR, video imaging and mechanical spectroscopy) in parallel would clarify whether the same quantity is being measured by each measurement method and validate comparisons of existing and future work. Furthermore, for example by combining DWS measurements of the granular temperature with PEPT measurement of granular temperature (though not in a dense granular system due to the latter’s low temporal resolution), velocity and concentration fields would provide comprehensive experimental data for validation of both theoretical and numerical simulation models. However, choosing appropriate particles and experimental configuration for comparing several techniques of granular temperature measurement is not a trivial task (e.g. the oil-seeded particles suitable for NMR are not suitable for DWS studies as they are strongly light absorbing particles).

Investigating mixing and segregation in granular systems is very important and topical in academic and industrial research into fluid/solid systems. In order to apply DWS to a binary particulate system to study mixing and segregation, modifications to the basic DWS methods would be necessary. There are two possibilities of achieving this goal. The first solution would be to utilize the refractive index matching technique [3] to distinguish one particle type from another. By nearly matching the refractive index of one particle type to that of the liquid phase, the scatter at the interface between solid and liquid can be eliminated thus enabling measurements of granular temperature of the other particle type. However, due to weaker scattering more scattering events would be necessary requiring thicker samples and consequently a higher power laser. The second option would be to use highly light absorbing (coloured) particles. Again, the scattered light would mostly originate from the other type of particles as the coloured particles would preferentially absorb the light instead of scattering it. This would in practice make coloured particles invisible to DWS probing, but experimental work is necessary to validate this hypothesis. Yet again higher laser power would be necessary to provide sufficient signal because of the higher light absorption. The granular temperature experimental data from binary systems obtained by such a modified DWS technique could be used to validate kinetic theory based models (for example Jenkins and Yoon [4]).

Finally, some features of glassy behaviour and the jamming transition were observed both in dry and water-immersed vibro-fluidized beds, as presented in this thesis. Elucidating these phenomena requires more detailed study of the dynamics of the jamming transition using multiple light scattering techniques that are more suited to probing slower dynamics, such as time-resolved correlation spectroscopy and speckle visibility spectroscopy. Time-resolved correlation spectroscopy is particularly suitable to quantify heterogeneous glassy dynamics [5]. Further, an interesting experimental project would be mapping a jamming phase diagram for dense granular media. A jamming phase diagram [6, 7] is a unifying concept for description of soft condensed phase matter behaviour which is important in understanding the rheological behaviour of attractive colloidal suspensions, foams, gels, spin glasses and granular matter.

Reference

1. Cody, G.D., J. Johri, and D. Goldfarb, *Dependence of particle fluctuation velocity on gas flow, and particle diameter in gas fluidized beds for monodispersed spheres in the Geldart B and A fluidization regimes.* Powder Technology, 2008. **182**(2): p. 146.
2. Vanel, L., P.A. Lemieux, and D.J. Durian, *Diffusing-wave spectroscopy for arbitrary geometries: numerical analysis by a boundary-element method.* Applied Optics, 2001. **40**(24): p. 4179-4186.
3. Chen, R.C. and L.-S. Fan, *Particle image velocimetry for characterizing the flow structure in three-dimensional gas-liquid-solid fluidized beds.* Chemical Engineering Science, 1992. **47**: p. 3615-3622.
4. Jenkins, J.T. and D.K. Yoon, *Segregation in binary mixtures under gravity.* Phys. Rev. Lett., 2002. **88**(19): p. #194301.
5. Duri, A., H. Bissig, V. Trappe, and L. Cipelletti, *Time-resolved-correlation measurements of temporally heterogeneous dynamics.* Physical Review E, 2005. **72**(5): p. 051401.
6. Liu, A.J. and S.R. Nagel, *Nonlinear dynamics: Jamming is not just cool any more.* Nature, 1998. **396**: p. 21.
7. Trappe, V., V. Prasad, L. Cipelletti, P.N. Segre, and D.A. Weitz, *Jamming phase diagram for attractive particles.* Nature, 2001. **411**(6839): p. 772.